STUDY OF NUCLEAR LEVEL DENSITY USING LIGHT PARTICLE EVAPORATION AS A PROBE

By

PRATAP ROY

Enrolment No PHYS04201304001

Variable Energy Cyclotron Centre, Kolkata

A thesis submitted to the
Board of Studies in Physical Sciences

In partial fulfillment of requirements
For the Degree of

DOCTOR OF PHILOSOPHY

of

HOMI BHABHA NATIONAL INSTITUTE

April, 2017

Homi Bhabha National Institute

Recommendations of the Viva Voce Board

As members of the Viva Voce board, we certify that we have read the dissertation prepared by **Pratap Roy** entitled "**STUDY OF NUCLEAR LEVEL DENSITY USING LIGHT PARTICLE EVAPORATION AS A PROBE**" and recommend that it may be accepted as fulfilling the dissertation requirement for the award of degree of Doctor of Philosophy.

.....**Date:**
Chairman - Dr. Sudhee Ranjan Banerjee

.....**Date:**
Guide / Convener - Dr. Chandana Bhattacharya

.....**Date:**
Member 1 - Dr. Sarmistha Bhattacharyya

.....**Date:**
Member 2 - Dr. Anjali Mukherjee

.....**Date:**
Member 3 - Prof. Rudrajyoti Palit
(External Examiner)

Final approval and acceptance of this dissertation is contingent upon the candidate's submission of the final copies of the dissertation to HBNI.

I hereby certify that I have read this dissertation prepared under my direction and recommend that it may be accepted as fulfilling the dissertation requirement.

Dr. Chandana Bhattacharya
Guide/Convener

Date:

Place:

STATEMENT BY AUTHOR

This dissertation has been submitted in partial fulfillment of requirements for an advanced degree at Homi Bhabha National Institute (HBNI) and is deposited in the Library to be made available to borrowers under rules of the HBNI.

Brief quotation from this dissertation are allowable without special permission, provided that accurate acknowledgement of source is made. Requests for permission for extended quotation from or reproduction of this manuscript in whole or in part may be granted by the Competent Authority of HBNI when in his or her judgement the proposed use of the material is in the interests of scholarship. In all other instances, however, permission must be obtained from the author.

Pratap Roy

DECLARATION

I, hereby declare that the investigation presented in the thesis has been carried out by me. The work is original and has not been submitted earlier as a whole or in part for a degree/diploma at this or any other Institution / University.

Pratap Roy

To the memory of my father

Late Pratyush Roy

Acknowledgements

"I am thankful for,

nights that turned into mornings,

friends that turned into family, and

dreams that turned into reality."

(-Anonymous)

Completing this thesis work has really been a dream come true for me. The journey to this end has never been easy, it was full of ups and down, in scientific term what we call highly non-linear. This challenging expedition could finally be ended on a successful note only because of the help and support of many people in either direct or consequential manner. I would like to take this opportunity to express my sincere gratitude to at least some of them whom I can immediately identify.

I gratefully acknowledge my sincere respects and thanks to my thesis supervisor, Prof. Chandana Bhattacharya. It has really been an enjoyable experience to work with her. She has given me all the liberty to think independently and work freely. Without her continuous support, guidance, and encouragement this thesis would not be completed. Her critical and thorough review of the thesis has helped a lot to improve its quality.

Besides my supervisor, I would like to thank the other members of my doctoral committee: Prof. S. R. Banerjee, Dr. Sarmistha Bhattacharyya, and Dr. Anjali Mukherjee for their insightful comments, and suggestions.

I would like to thank Dr. Kaushik Banerjee for his immense support to complete this work. I would particularly acknowledge his efforts to familiarize me with the nitty-gritty of the experimental techniques which were essential to carry out the experimental investigations. I have learned a lot from him and he has often played the role of a navigator in this journey through the roads full of twists and turns.

I would like to express my gratitude to our former physics group head, Prof. Sailajananda Bhattacharya for his critical remarks for the betterment of this thesis work. His efforts and suggestions towards the improvement of the quality of writing should be remembered in particular.

I should acknowledge my colleagues Dr. Samir Kundu and Dr. Supriya Mukhopadhyay for their suggestions regarding various technical issues and cherish the moments of intense physics discussions with them. With great pleasure, I would also like to thank my other collaborators Dr. Tapan Kumar Rana, Dr. Gopal Mukherjee, Dr. Tilak Kumar Ghosh, Shri Ratnesh Pandey, Shri Santu Manna, Shri Arijit Sen, Dr. Deepak Pandit, Dr.(Mrs) A. Dey, and Dr. Surajit Pal for providing necessary help and full cooperation towards me. Without their support, it could not have been possible to carry out the experiments at all.

I appreciate the efforts of Shri J K Meena, Shri Amiya Kumar Saha and Shri J. K. Sahoo for making a number of images and diagrams for the thesis apart from their regular supports in setting up the experiments. I also thank Smt. Ruchismita Mondol Saha for making most of the targets used in the experiments.

I should also take this opportunity to thank the VECC cyclotron operating staff for the smooth operation of the machine and delivering good quality beam for the experiments.

This acknowledgment will be incomplete if I fail to mention the names of the present director of VECC, Shri Amitava Roy and former director Prof. Dinesh Kumar Srivastava for providing me with the necessary permissions and assistance to continue this work. I would also like to acknowledge our Dean Academic (Physical Science), Dr. Jan e Alam, for providing necessary official supports.

On the personal note, I consider myself fortunate to have caring parents who always considered education to be most important. Particularly my father was a continuous source of inspiration and encouragement to me and always backed my decision pursue basic science. I badly miss him on this day.

I can never forget the contribution of my wife, Sampa, her moral support has always been something special. She always tried to reduce my responsibilities towards the family so that I could spend more time in achieving this goal. I also express my love and thanks to our little son, Pratyay, who has been a never ending source of energy and delight. His presence has always been the most effective element in relaxing my mind

after a long day of hard work.

I also thank my other family members and friends who supported and helped me in some way or another. I would like to acknowledge and pay my respects to all my teachers, without their vigorous efforts I could never reach up to this point. I could particularly remember my high school physics teacher Shri Bholanath Ghosh; it was him and his teaching that has triggered my love for physics at the first place.

Finally, once more I express innumerable thanks and sincere gratitude to everyone whom I have mentioned here and to all other whom I could not mention. This journey would have been much more difficult or may be impossible without the tremendous help and support of all of you.

Contents

SYNOPSIS

The decay of an excited atomic nucleus can be described in terms of the statistical model if the reaction between the participating nuclei proceeds via a succession of intermediate states of the so-called compound nucleus (projectile + target) so that the input reaction channel has no specific influence on the relative widths of the decay channels. Such an intermediate system is considered to be equilibrated in all degrees of freedom (*e.g.* energy, shape, isospin) and expected to have no memory of the way by which it was formed. In the statistical approach to study the average behaviour of an excited equilibrated compound nucleus and its decay, the most significant quantity is nuclear level density (NLD), ρ. An accurate determination of NLD is essential for the quantitative description of several important physical phenomena like particle evaporation, fission, multifragmentation, spallation *etc*. Moreover, the knowledge of NLD is of fundamental interest as it can provide interesting tests of different microscopic approaches of nuclear structure commonly used to calculate level densities. NLD is a characteristic property of every nucleus and it is expected to vary grossly exponentially with excitation energy. However, the exact value of NLD at a given excitation energy critically depends on various key nuclear factors like angular momentum, deformation, shell correction, parity, and isospin. It is extremely important as well as quite interesting to understand the exact nature of variation of NLD as a function of these factors. Theoretically the simplest and most frequently used analytic expression for NLD [$\rho \sim \sqrt{a}\ exp(2\sqrt{aE})$] is obtained under the framework of Fermi-gas (FG) model [1]. In the FG description of NLD, the most important factor is the level density parameter (a) which is directly related to the density of single-particle states around the Fermi energy. It may be noted that the simplest FG description of NLD does not incorporate important nuclear properties such as pairing correlations, shell and collective effects. These effects can be incorporated in an exact manner in the microscopic level density calculations. However, such rigorous calculations are extremely involved requiring large computation time, which severely limits their applications to the analysis of experimental data. Therefore, in most of the statistical model codes, the level

density is approximated by simple Fermi gas (FG) type analytic expression and important factors like shell effects, pairing, collectivity etc. are incorporated in completely phenomenological manner through a number of adjustable parameters (either in ρ or in a). Although the study of nuclear level density is quite an old subject, it is still an active area of research in nuclear physics. Several interesting but conflicting experimental results have come up in recent times that demand to revisit our understanding of the properties of nuclear level density. The aim of the present thesis is to experimentally investigate the excitation energy and angular momentum dependence of NLD and thereby refine our knowledge on key aspects of NLD such as spin dependence, damping of shell effect and collective enhancement which is of great significance in terms of the present status of the subject.

The thesis contains three parts which deal with three particularly important features of NLD (1) Angular momentum dependence, (2) Damping of shell effect in NLD and temperature dependence of the level density parameter and (3) role of collectivity in NLD. Three independent experimental investigations have been carried out to improve and/or extend our understanding on these aspects from the measurement of light particle evaporation spectra at different nuclear mass regions. Although there are several other experimental ways to determine NLD, the study of light particle evaporation spectra has been the most effective and widely used tool to investigate NLD over a wide range of excitation energy and angular momentum. The first experiment was performed to study the angular momentum dependence of NLD by measuring angular momentum gated light-particle (n, p, α-particles) evaporation spectra in two different reactions. In the second experiment excitation energy dependence of the level density parameter and damping of shell effects with increasing excitation energy was studied for nuclei in the doubly magic ^{208}Pb region. In the third part of the thesis, the effect of collectivity on nuclear level density and its correlation with deformation has been investigated by measuring neutron evaporation spectra from different compound nuclei having different ground-state deformations.

Angular Momentum Dependence of Level Density:

In the phenomenological descriptions of NLD, the spin (angular momentum) dependence is generally incorporated through the spin and deformation dependent rotational energy. There is no further dependence of the level density parameter *a* on angular momentum or deformation. This prescription was mostly tested with inclusive particle spectra and found to be reasonable to explain the experimental data. However, a number of recent data from exclusive measurements with respect to angular momentum have not been properly explained by the available prescriptions of the spin dependence of nuclear level density. In measurements of angular momentum gated proton and α-particle spectra from ^{12}C,^{16}O + ^{93}Nb and ^{89}Y reactions Mitra *et al.* observed broad bump-like structures which could not be explained by the standard level density prescriptions [2,3]. Although the origin of such feature was not clear, a specific *J*-dependent enhancement in NLD was suggested by the authors to explain the experimental data. Angular momentum dependence of the inverse level density parameter (k=A/$\tilde{a}$, where A is the nuclear mass number and $\tilde{a}$ is the asymptotic value of the level density parameter) was studied by Gupta. *et al.* for several nuclei in $A \sim$180 and $A \sim$120 mass regions through α-particle measurements. Although the results in the $A \sim$180 region showed a constant nature of the inverse level density parameter as a function of the angular momentum (J) [4], a strong variation (increase) of k with increasing J was observed for a number of nuclei in the $A \sim$120 region [5]. On the other hand in a recent measurement of angular momentum gated neutron evaporation spectra for nuclei with $A \sim$118, excitation energy $E^* \sim$ 31 and 43 MeV and in an angular momentum $J\sim$10 - 20 $\hbar$, the inverse level density parameter was observed to decrease with increasing angular momentum [6]. It is thus evident that even after these experimental efforts the understanding on the angular momentum dependence of NLD is not conclusive and demands further investigations in this area. Moreover, it will also be interesting to observe the variation of nuclear level density parameter as a function of J estimated from different light-particle measurements simultaneously which will be useful to understand the spin dependence of NLD in a consistent manner. With

this aim, we have measured the light-particle (n, p and α) evaporation spectra in the ^{4}He + ^{93}Nb and ^{4}He + ^{58}Ni reactions at the excitation energy E^{*} ~36 MeV. In the present experiment, populated angular momenta were estimated from the measured γ-ray multiplicity using a 50 element BaF_2 detector array, in coincidence with the emitted light particles. The charged particles and neutrons were detected at the backward angles by using a three element detector telescope [Si Strip-Si Strip-CsI(Tl)] and a number of liquid scintillator based neutron detectors, respectively. Theoretical analysis of the experimental data using the statistical model code CASCADE [7] has been carried out to extract the value of the inverse level density parameter at different angular momentum regions, corresponding to different γ-multiplicities. From the analysis of the angular momentum gated particle spectra, it was observed that the k-value decreases consistently with increasing $< J >$ for all three types of particle emissions. The experimental data indicates a relative enhancement in level density at higher angular momenta, which was taken care of by the additional J dependence of the level density parameter. The current trend of the data could not be explained by the available phenomenological NLD models with standard spin dependence. Microscopic calculations for the specific systems may enlighten on the origin of the observed phenomenon.

Excitation energy dependence of the level density parameter:

Like many other nuclear phenomena shell structure of atomic nuclei are observed to have important consequences in NLD too. The strong departure of the level density parameter from its standard low-energy value of ~A/8 is very well known for nuclei in the vicinity of closed shells. However, shell effects are strongly excitation energy dependent, expected to be damped and finally washed out at higher excitation energies. In the phenomenological descriptions of NLD, shell effect is incorporated using an excitation energy (U), and shell correction (ΔS) dependent parameterization of the level density parameter [$a = \tilde{a}\{1 + (\Delta S/U)(1 + exp(-\gamma U)\}$] as suggested by Ignatyuk [8]. The rate of depletion of shell effect with energy is determined by the shell damping parameter (γ). Although there have been a few early theoretical estimates on the value of γ [8,9], experimental information is quite limited. The value of the shell damping

factor has very recently been determined experimentally by Rout *et al.* by measuring neutron evaporation spectra followed by transfer-induced fusion (used to populate low excitation energies) of ^{7}Li on ^{205}Tl populating particle unbound states in ^{208}Pb [10]. However, the extracted γ-value ($0.060^{+0.01}_{-0.02}$ MeV^{-1}) differs somewhat from the value (0.079 ± 0.007 MeV^{-1}) estimated earlier from neutron resonance data [11]. It is interesting to mention at this point that apart from the discussed variation of the level density parameter due to shell effect (as determined by γ), the asymptotic (or smooth) value of the level density parameter ($\tilde{a}$, expected when there is no shell effect) is also observed to show interesting variation as a function of excitation energy (temperature). A reduction in the value of asymptotic level density parameter with increasing temperature, from $\sim A/8$ at zero temperature to $\sim A/13$ at $T \sim 5$ MeV was reported in several experimental studies, particularly in the $A \approx 160$ mass region [12 - 16]. However, a constant nature or rather a weak dependence of $\tilde{a}$ on T were reported in many cases for lighter systems [17 - 19]. Moreover, there is a large discrepancy among the experimental results on the temperature dependence of $\tilde{a}$ particularly in the $A \sim 200$ mass region [20 - 22]. Given the scarcity of experimental data on the shell damping factor and disparity among various experimental results on the temperature dependence of $\tilde{a}$, we planned to study the temperature dependence of the level density parameter and the damping of shell effects with excitation energy in the $A \sim 210$ region using light ion induced reactions (suitable for population of low excitation energy). With this aim, we have carried out a measurement, in which neutron evaporation spectra have been measured from two different compound nuclei ^{212}Po and ^{213}At close to the doubly magic ^{208}Pb nucleus having large ground-state shell corrections. The experiment was carried out using the ^{4}He-ion beams of incident energies 28, 31, 35, 40 and 60 MeV from the K130 cyclotron at VECC. The experimental neutron spectra measured at backward angles were compared with statistical model predictions. The value of the shell damping factor ($\gamma = 0.052 \pm 0.018$ MeV^{-1}) has been extracted from the lowest energy data (which had the highest sensitivity over this parameter). The extracted γ-value is in good agreement with the earlier estimates. The temperature dependence of

the asymptotic level density parameter has been studied in a temperature range T~0.7 - 1.4 MeV and compared with the Thomas-Fermi (TF) model calculations [23]. An overall decrease of the level density parameter with increasing temperature was observed in agreement with the TF prediction. The experimental results were also shown to be very well explained by a linear increase of the inverse level density parameter with excitation energy, with the empirical relation, k(U)= 7.8 + 7.5 (U/A).

Collective enhancement and its fadeout:

Another major issue in the area of nuclear level density which is yet to be resolved is the inter-relationship between collective excitations and nuclear level density as a function of excitation energy (or temperature). In nuclei, collective rotation and vibration involving several nucleons couple to the single-particle excitations. It is thus expected that the contribution of the collective excitations would appear as an enhancement in NLD. For nuclei with appreciable ground-state deformations, the main contribution to the collective enhancement comes from the rotational excitations, whereas in the case of spherical nuclei the collective enhancement is likely to be due to vibrational excitations. The collective enhancement in NLD is expected to die out at high energies due to the gradual damping of long-range correlations which are mainly responsible for the collective enhancement. It has been suggested in several theoretical studies that the fadeout energy (or temperature) strongly depends on the ground-state deformation of the nucleus [24 - 26]. In the recent past, only a few experimental attempts have been made to look for the collective enhancement in nuclear level density and its subsequent fadeout at higher excitation energies. In one of such attempts, Junghans *et al.* [27] studied the yields of nuclei produced in the fragmentation of relativistic Pb and U projectiles. Although they found some evidence for the loss of collectivity of nuclear excitations as a function of nuclear temperature, the damping of the collective enhancement in the nuclear level density was observed to be independent of nuclear deformation which is in contrast to the theoretical picture. On the other hand, Komarov *et al.* [28] attempted to extract information on collective enhancement and its fadeout by studying α-particle evaporation from the strongly deformed ^{178}Hf compound nucleus

produced in the heavy-ion fusion reaction. However, they did not find any convincing evidence of the existence of collective enhancement and its fadeout in their data. The nature of the controversy among the existing results warrants new measurements to independently verify the status of collective enhancement. So with the aim to see the effect of ground state deformation and subsequent collectivity on nuclear level density we have measured the neutron evaporation spectra from three different compound nuclei (^{169}Tm, ^{185}Re and ^{201}Tl) having different ground state deformations, at two different excitation energies around the predicted fadeout region. The neutron spectra measured at backward angles were compared with statistical model calculations. The values of the level density parameter, extracted at these excitations from the theoretical fits to the experimental data were observed to increase substantially at the lower excitation energy (~26 MeV) for nuclei having large ground state deformation (residues of ^{185}Re, and ^{169}Tm); whereas for near spherical nuclei (residues of ^{201}Tl*), the *a* value remains unchanged at the two energies. The increase in *a* at the lower excitation energy for the deformed systems amounts to a relative increase in nuclear level density, indicating a collective enhancement. To understand the phenomenon in more detail the measurement has been extended to wider excitation energy range (~25 - 55 MeV) in small energy intervals for three compound nuclei (^{173}Lu, ^{185}Re and ^{201}Tl). Statistical model analysis of the experimental data was carried out to extract the values of the inverse level density parameter at different excitation energies. It was observed that the gross variation of k with energy is in agreement with prediction given by the standard empirical relation [k(U) =$k_0 + \kappa$ (U/A)]. However, there is sharp reduction in the value of k (or enhancement in a) around E^{*} ~30 MeV for the deformed systems (^{173}Lu and ^{185}Re) compared to the near spherical system (^{201}Tl). The current observation provides a strong signature of collective enhancement of NLD at low excitation energies which are expected for the deformed systems due to the collective rotation. The data also suggest a correlation between collective enhancement and ground-state deformation and indicate a fadeout energy of collective enhancement in between E^{*} ~30 - 35 MeV for the current systems, which may be linked with a shape phase transition of the above

nuclei from deformed to spherical shape around that excitation.

References:

1. H. A. Bethe, Phys. Rev. **50**, 332 (1936); Rev. Mod. Phys. **9**, 69 (1937).
2. A. Mitra *et al.* Nucl. Phys. **A 707**, (2002) 343.
3. A. Mitra *et al.* J. Phys. **G 36**, (2009) 095103.
4. Y. K. Gupta *et al.* Phys. Rev. **C 78**, 054609 (2008).
5. Y. K. Gupta *et al.* Phys. Rev. **C 80**, 054611 (2009).
6. K. Banerjee *et al.* Phys. Rev. **C 85**, 064310 (2012).
7. F. Puhlhofer, Nucl. Phys. **A 280**, 267 (1976).
8. A.V. Ignatyuk, *et al.* Sov. J. Nucl. Phys. **21**, 255 (1975).
9. K. H. Schmidt *et al.* Z. Phys. **A 308**, 215-225 (1982).
10. P. C. Rout *et al.* Phys. Rev. Lett. **110**, 06250 (2013).
11. S. F. Mughabghab and C. Dunford, Phys. Rev. Lett. **81**, 4083 (1998).
12. G. Nebbia *et al.*, Phys. Lett. **B 176**, 20 (1986).
13. K. Hagel *et al.* Nucl. Phys. **A 486**, 429 (1988).
14. M. Gonin, *et al.* Phys. Lett. **B 217**, 406 (1989).
15. M. Gonin *et al.* Phys. Rev. **C 42**, 2125 (1990).
16. R. Wada *et al.* Phys Rev. **C 39**, 497 (1989).
17. A. Chbihi *et al.*, Phys Rev. **C 43**, 666(1991).
18. G. Nebbia *et al.* Nucl. Phys. **A 578**, (1994) 285.
19. K. Yoshida *et al.*, Phys. Rev. **C 46**, 964 (1992).
20. B. J. Fineman *et al.* Phys. Rev. **C 50**, 1991 (1994).
21. D. Fabris *et al.* Phys. Rev. **C 50**, 1261(R) (1994).
22. A. L. Caraley *et al.* Phys. Rev. **C 62**, 054612 (2000).
23. S. Shlomo and J. B. Natowitz, Phys. Rev. **C 44**, 2878, (1991).
24. S. Bjornholm, A. Bohr and Mottelson, in Proceedings of the International Conference on the Physics and Chemistry of Fission, Rochester, New York, 1973 (IAEA,

Vienna, 1974) Vol. **1**, p. 367.

25. G. Hansen and A. S. Jensen, Nucl. Phys. **A 406**, 236 (1983).
26. C. O. Zen, Y. Alhassid and H. Nakada, Phys. Rev. Lett. bf 110, 042502 (2013)
27. A. R. Junghans *et al.* Nucl. Phys. bf A 629, 635 (1998).
28. S. Komarov *et al.*Phys. Rev. **C 75**, 064611 (2007).

List of Figures

List of Tables

Chapter 1

Introduction

"By convention there is color,
By convention there is sweetness,
By convention there is bitterness,
But in reality there are atoms and space."

-Democritus (400 BC)

1.1 The nucleus and nuclear physics

Some of the longest standing questions that have guided the progress of natural science are perhaps: *what is the universe made up of, what holds it together and how it came to existence, in its present form?* These questions have always enthralled the intrinsically curious minds of human beings and their endeavor to find answers to these questions has started with the beginning of human civilization itself. To know what the universe is constituted of, people have been looking for its fundamental building blocks. By fundamental building blocks we understand objects or entities that are simple, structureless and not made up of anything smaller. The idea that all matter in the world are made up of some small discrete units which further cannot be divided was

found to exist even in the ancient civilizations. It was the Greek philosopher Democritus (~400 BC) who first introduced the word *atom* (meaning *indivisible*) as the elementary constituent of matter. But even before that (probably around 600 BC), the Indian philosopher Kanada introduced the concept of *Anu* as the smallest and indestructible particle of matter. However all these ideas were completely abstract as they were based on philosophy rather than empirical evidences. It was only in the early 1800s when the idea of atom was accepted by scientists and refined into an evidence-based theory. For an enormous time period spanning more than 22 centuries atoms were known to be indivisible and fundamental constituent of matter. The belief that atoms are indivisible and ultimate particles of matter was overturned with the discovery of electron by British Physicist J. J. Thomson (1897), who showed that electrons are negatively charged particles and are part of every atom. As an atom is electrically neutral it must contain some entities with positive charges in order to neutralize the negative charges of electrons. Accordingly Thomson proposed a model of the atom in which the negatively charged electrons were distributed in a uniform soup of positive charges. This is known as the *"plum pudding model"*. During 1906 - 1911 Geiger and Marshden under the direction of Ernest Rutherford performed a series of experiments to look into the inside of the atom and to test the validity of the plum pudding model by bombarding a thin gold foil with energetic α-particles. They observed that most of the incident α-particles traversed almost undeviated while a small fraction of them were deflected at very large angles. Such huge deflections could not be explained by Thomson's model of the atom, where positive charges were uniformly distributed throughout the atom. For such large deflections all positive charges had to be concentrated in a very small region having a mass much greater than the mass of the α-particles. Thus the interpretation of the experimental data led to the idea of an atom having a small (less than 10^{-12} of the atomic volume) dense *nucleus* at the center containing most of the atom's mass with a surrounding cloud of light electrons.

In subsequent years it was realized that the nucleus is made up of positively charged *protons* and neutral *neutrons* called together as *nucleons*. Thus an atom was found to

be made up of neutrons, protons, and electrons. Atoms join together to form molecules and molecules join together to make the different macroscopic form of matter. At this point, the immediate question that comes to one's mind is that, whether neutron and proton (and also the electron) are fundamental particles? In fact, physicists have tried to probe the inside of the proton in the same way as Rutherford did to probe inside of the atom, by throwing energetic particles into it. Such experiments were carried out in the late sixties using high energy electron beams. The results of such experiments were remarkably similar to that of Rutherford's, as the most of the incident particles pass right through the proton while only a few bounced back sharply. This means that the positive charge inside the proton is concentrated in small lumps, just as Rutherford's result indicated that the positive charge in an atom is concentrated in the nucleus. However, in the case of the proton, the evidence suggested three such lumps instead of one. Thus it was discovered that the proton (and also the neutron) are made up of three more elementary particles named as *quarks*, which are held together inside the nucleons by *gluons* (mediator of the strong force). As we know it today *quarks* and *leptons* (electrons along with μ, τ and ν) are point-like particles and fundamental building blocks of the universe. However, quarks (and gluons) do not exist in nature freely. They always remain absolutely confined inside the nucleons (or *hadrons* in general). According to the present cosmological models, the quarks and gluons were free in the form of *quark-gluon plasma* only at the very initial time, a few microsecond after the *Big-Bang* (beginning of the universe) when the temperature of the universe was about 150 MeV. It took a few microseconds further for the universe to cool down to a temperature when the quarks permanently got confined to hadrons. Thus the existence of quarks and their influence in nuclear dynamics can only be observed in very high energy ($\approx$ 1 GeV/A) nuclear collisions. Therefore even if nucleons contain quarks, the ground-state or moderately excited states of nuclei can safely be viewed as ensembles of interacting nucleons instead of interacting quarks. Since quarks and gluons always remain bound inside the nucleons we can safely consider nucleons as the effective elementary constituents of nuclei. Similarly, quantum chromo dynamics (*QCD*) which

is the elementary theory to describe the fundamental interaction between quarks and gluons, can also be safely replaced by an effective interaction between the nucleons. Physics of nuclei in the vicinity of their ground state is thus a physics of nucleons interacting via the nucleon-nucleon interaction [1]. Such a picture of nuclei as sets of interacting nucleons constitutes the basis of most studies devoted to the understanding of the structure and dynamical properties of nuclei. In our immediate environment, atomic nuclei exist only in their ground state, so they affect the world in which we live only by their charge and mass and not by their dynamical properties. All the interesting nuclear phenomena thus can be observed only in energetic collisions generated in our laboratories using the particle *accelerators*. However, the universe has its own natural laboratories, the centers of all stars where nuclear reactions are going on, which are the sources of our energy supply on earth. Understanding the nuclear dynamics is thus essential for energy production in the earth using nuclear reactors. But nuclear physics is even more important for us from the point of view of understanding history of the universe. The composition of matter as we see it today is the product of nuclear reactions which have taken place a long time ago in the stars or in stellar explosions. Today within our accelerating machines we try to simulate the conditions for those reactions to occur, in a very microscopic way. An accurate determination of different nuclear reaction rates is essential in order to understand exact processes of nucleosynthesis and to reproduce the observed abundances of different elements in the universe. Moreover, the atomic nucleus is a perfect example of a finite (and isolated) quantum many-body system. So, study of nuclear structure and dynamics helps us to refine our ideas of several areas of fundamental physics such as quantum mechanics, statistical mechanics, many body physics.

Although the existence of the atomic nucleus was established more than 100 years ago and the substructure of its constituents was discovered experimentally more than 40 years ago, many of the structural and dynamical properties of the nucleus are still unknown or poorly known. Moreover, with the advent of modern accelerators delivering *radioactive ion beams (RIB)* and sophisticated radiation detectors, many new direc-

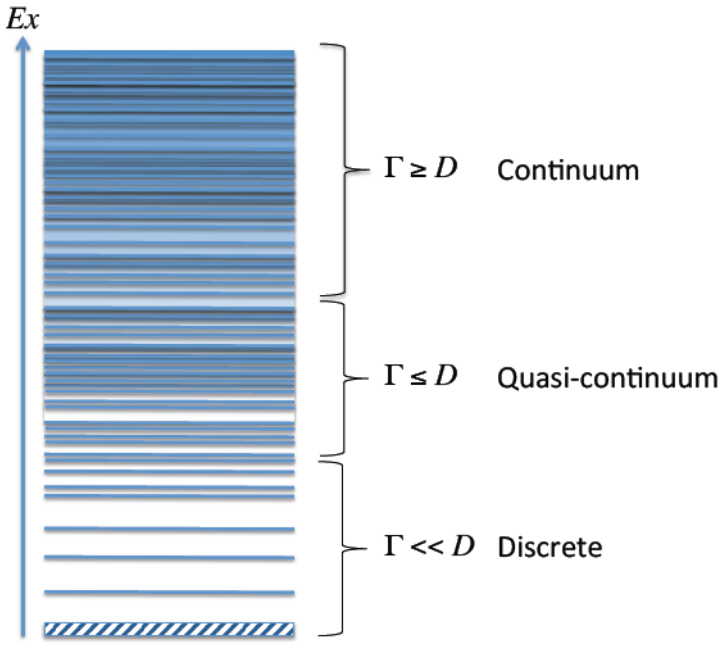

Figure 1.1: *A schematic diagram of energy level distribution of a typical nucleus.*

tions in nuclear physics research have opened up in last one or two decades. It will not be exorbitant to say that modern accelerators and detectors have given a rebirth of nuclear physics. With the existing and coming large scale RIB facilities along with the highly developed detector arrays one could reach out to those areas of the nuclear landscape which were previously inaccessible. So currently we are standing at a time when the arena of nuclear physics is expanding at a rapid rate and many new surprises in this field are expected to astonish us.

1.2 The notion of nuclear level density (NLD)

The atomic nucleus is a perfect example of a finite quantum many-body system. Like every quantum mechanical system nucleus also exhibits a discrete energy spectrum *i.e.* it can exist only in certain allowed energy levels. However, the individual description of excited nuclear levels is possible only for the low excitation energies where the excited levels are small in number, well separated and rather simple in struc-

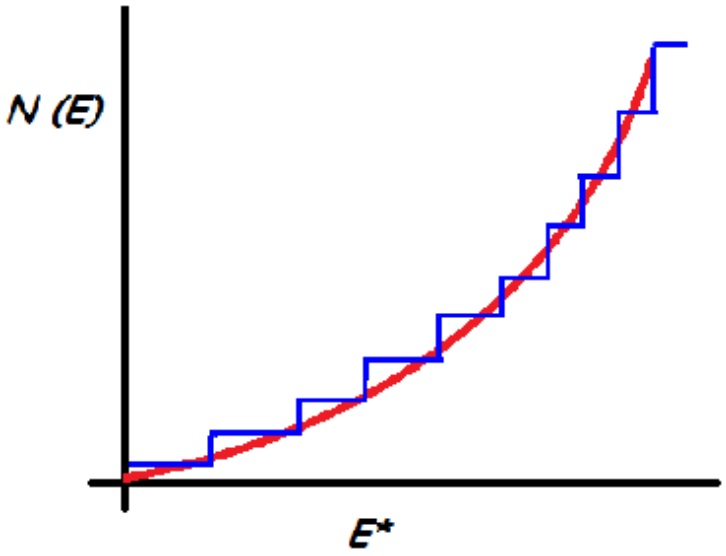

Figure 1.2: *Schematic variation of cumulative number of energy level with energy. The smooth (red) line represents its average behavior.*

ture. In this region, the excited states are analyzed using the spectroscopic approach. However, with the increase in excitation energy, the spacing between the energy levels (D) become narrower and the nature of excitations become very complicated. In fact, for excitation energy more than a few MeV, the energy levels become almost overlapping and it is impossible to distinguish them experimentally. The energy spectrum of a typical (heavy) nucleus has been schematically shown in Fig. 1.1. The spectrum can be divided grossly into three regions. In the low energies where the width (Γ) of individual levels are significantly lower compared to the spacing between energy levels (*i.e.* $\Gamma \ll$ D); we have the discrete energy region. As the energy is increased the widths become comparable to the spacings ($\Gamma \lesssim$ D), leading to the quasi-continuum region. If the energy is further increased the widths become larger than the level spacings ($\Gamma \geq$ D). In this scenario, the individual description of the excited levels is no longer possible and it has to be replaced by a global description in terms of a **level density** function. Correspondingly, the spectroscopic approach is substituted by the statistical approach which allows a more comprehensive description of the average behavior of the excited nucleus and its decay. The *nuclear level density* (NLD) which is the most relevant quantity describing the statistical properties of the nucleus, is expressed as a

function of various constants of motion, e.g. excitation energy, angular momentum, the number of particles, parity, isospin *etc*. NLD [$\rho(E)$] is a characteristic property of every nucleus and it is defined as the number of levels per unit energy at a certain excitation energy,

$$\rho(A, E) = \frac{dN(A, E)}{dE} \tag{1.1}$$

where $N(E)$ is the cumulative number of levels up to an energy E. The variation of the function $N(E)$ is shown schematically in Fig. 1.2. Although N(E) is a step function its average behavior can always be represented by a smooth function as shown by the red line in Fig. 1.2. The level density as defined in Eqn. 1.1 is related to the number of different ways in which individual nucleons can be placed in the various *single-particle* orbitals such that the excitation energy lies in the range between E and $E + dE$.

1.3 Theoretical Methods for the determination of NLD

1.3.1 The combinatorial method

The basic principle of the combinatorial method for the calculation of nuclear level density is quite straightforward and it follows automatically from the definition of NLD itself. In this approach, the level density is determined by finding the number of ways in which the nucleons can be distributed among the available single-particle energy levels for a given energy of the nucleus [2]. The single-particle energy eigenfunctions and eigenvalues up to some reasonably high energy are determined quite accurately using the shell model where each nucleon is assumed to move independently in the average potential created by the other A-1 nucleons. Important nucleon-nucleon interactions such as the paring force can also be included in the calculations. A very large set of nuclear wave functions representing the ground state and many excited states are generated from the permutations of A nucleons into the single-particle eigenfunctions with proper anti-symmetrization required for the fermionic system. The energy E_α for

a particular configuration α is given by the sum of the eigenvalues (ϵ_i) of the occupied single-particle orbitals

$$E_\alpha = \sum_i \epsilon_i \tag{1.2}$$

and the excitation energy is given by

$$\mathcal{E}_\alpha = E_\alpha - E_g \tag{1.3}$$

where E_g is the energy of the ground state. The configurations are generated by cycling the occupation of each of the single-particle levels over all its allowable values. The calculation of level density is then reduced to just finding a large (10^6 or so) number of E_α values and sorting them in terms of particle number, energy, angular momentum and other possible quantum numbers. The main advantage of this method is that the level density is calculated numerically by counting the exact number of levels and no drastic mathematical approximation is required as compared to other methods. Moreover, important nuclear properties like shell and pairing effects are automatically included in this method and it allows to obtain the distribution of NLD in terms of angular momentum, parity *etc*. The combinatorial method has been used to calculate NLD by several authors in the recent times [3, 4, 5, 6, 7, 9, 8, 10]. The major disadvantage of this procedure arises from the fact that the number of nuclear levels becomes extremely large even at moderate excitations, specifically for heavy nuclei. Therefore, such calculations can be performed only with large computers and limited to low excitation energies only.

1.3.2 The partition function method

The partition function method, also known as the statistical method, is by far the most widely used technique for calculating level density particularly in view of its ability to provide simple analytical formula. In this approach the average level density of a nucleus can be calculated under the assumption that the system can reasonably be described in terms of independent particle motion (IPM) of its constituents. The

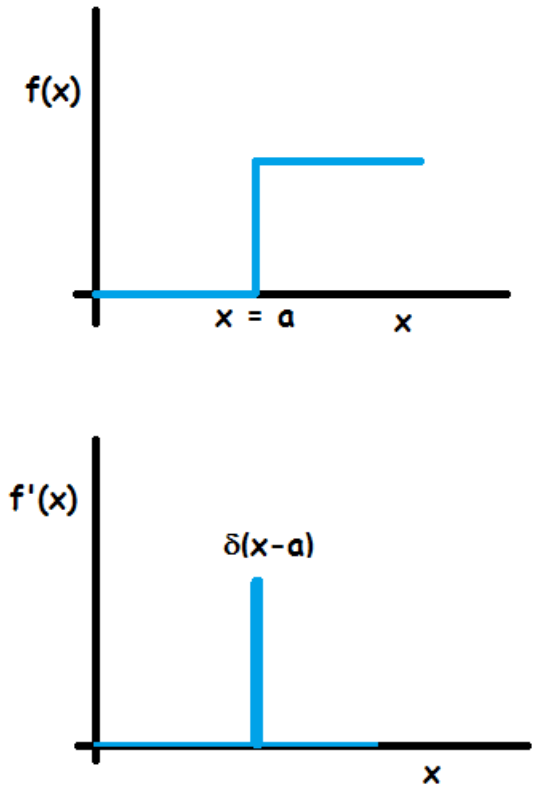

Figure 1.3: *Schematic representation of a step function (f(x)) and it's derivative (f'(x)).*

density of level as a function of energy and particle number is given by [11],

$$\rho(A,E) = \sum_{n,i} \delta(A-n)\delta(E-E_i(n)) \tag{1.4}$$

where $E_i(n)$ is the energy of the i^{th}-quantum state of the n-particle system. The relation 1.4 follows from the definition of ρ(E) as given in Eqn. 1.1, and the fact that N(E) in Eqn. 1.1 is a step function (See Fig. 1.3 for illustration).

Now, under the independent-particle approximation, one can write

$$\begin{aligned} n &= \sum_{\nu} n(\nu)_i \\ E_i &= \sum_{\nu} n(\nu)_i E(\nu) \end{aligned} \tag{1.5}$$

Here $n(\nu)_i$ is the occupation number of the single-particle state ν in the i^{th} quantum state of the n-particle system. For fermionic systems, as per the Pauli's exclusion principle, $n(\nu)_i$ can be either 0 or 1. It can be seen that the Eqn. 1.4 has singularities at

each eigen values given by Eqns. 1.5. However, it is the average value of the function integrated over an interval in A and E is the quantity of interest. It is suggestive from the additive nature of the relations 1.5 that, it is convenient to work with the Laplace transform of Eqn. 1.4 given by,

$$\begin{aligned} \mathcal{Z}(\alpha,\beta) &= \int_0^\infty \int_0^\infty \rho(A,E) exp(\alpha A - \beta E) dA dE \\ &= \sum_{n,i} \exp(\alpha n - \beta E_i(n)) \end{aligned} \tag{1.6}$$

where α and β are the Lagrange multipliers associated with nucleon number and energy. The quantity $T = 1/\beta$ is known as the statistical temperature. The function $\mathcal{Z}(\alpha,\beta)$ can readily be identified as the grand-canonical partition function for the system. Inserting Eqn 1.5 into Eqn 1.6 and considering the fact that $n(\nu)_i$ can only be either 0 or 1, the partition function can be written as

$$\mathcal{Z}(\alpha,\beta) = \prod_\nu (1 + exp(\alpha - \beta\epsilon(\nu)) \tag{1.7}$$

In each factor, the term 1 comes from n(ν) = 0, and the exponential term comes from n(ν) = 1. In order to evaluate the product (Eqn. 1.7) in terms of a sum over the single-particle states, we take the logarithm,

$$\begin{aligned} ln\mathcal{Z}(\alpha,\beta) &= \sum_\nu ln(1 + exp(\alpha - \beta\epsilon(\nu))) \\ &= \int_0^\infty g(\epsilon) ln(1 + exp(\alpha - \beta\epsilon) d\epsilon \end{aligned} \tag{1.8}$$

The function g(ϵ) describes the density of single-particle states

$$g(\epsilon) = \sum_\nu \delta(\epsilon - \epsilon(\nu)) \tag{1.9}$$

Having determined $\mathcal{Z}$, the calculation of level density reduces to the evaluation of the inverse Laplace transformation,

$$\rho(A,E) = \frac{1}{(2\pi i)^2} \int \int_{-i\infty}^{+i\infty} \mathcal{Z}(\alpha,\beta) exp(-\alpha A + \beta E) d\alpha d\beta \tag{1.10}$$

The inverse Laplace transformation is generally determined under the *saddle point approximation* (SPA), which is based on the fact that the integrand in Eqn. 1.10 is a rapidly varying function of α and β, and has significant contribution only in a small region around a saddle point (α_0, β_0) where the integrand is stationary. The conditions that determine the saddle point are given by

$$\frac{\partial ln\mathcal{Z}}{\partial \alpha} - A = 0$$
$$\frac{\partial ln\mathcal{Z}}{\partial \beta} + E = 0 \tag{1.11}$$

Under the saddle point approximation (Eqn. 1.11), the level density expression for a nucleus with A nucleon and excitation energy E can be obtained by using Eqn. 1.10 [11] as,

$$\rho(A, E) = \frac{exp(S)}{2\pi\sqrt{D}} \tag{1.12}$$

Where the entropy S of the system given by,

$$S = ln\mathcal{Z}(\alpha_0, \beta_0) + \beta_0 E - \alpha_0 A \tag{1.13}$$

and

$$D = \begin{vmatrix} \frac{\partial^2 ln\mathcal{Z}}{\partial \beta^2} & \frac{\partial^2 ln\mathcal{Z}}{\partial \beta \partial \alpha} \\ \frac{\partial^2 ln\mathcal{Z}}{\partial \beta \partial \alpha} & \frac{\partial^2 ln\mathcal{Z}}{\partial \alpha^2} \end{vmatrix} \tag{1.14}$$

1.4 Simplest analytic description of NLD in terms of Fermi gas model

Historically, the first analytic expression of NLD was determined under the framework of Fermi gas model with the additional assumptions that the single-particle states are uniformly distributed (Fig. 1.4) and the Fermi gas is highly degenerate [12]. The level density for a nucleus with mass number A and excitation energy E under the Fermi gas approximation can be obtained using Eqn. 1.12 - 1.14 as [11],

$$\rho(A, E) = \frac{exp(2\sqrt{aE})}{4\sqrt{3}E} \tag{1.15}$$

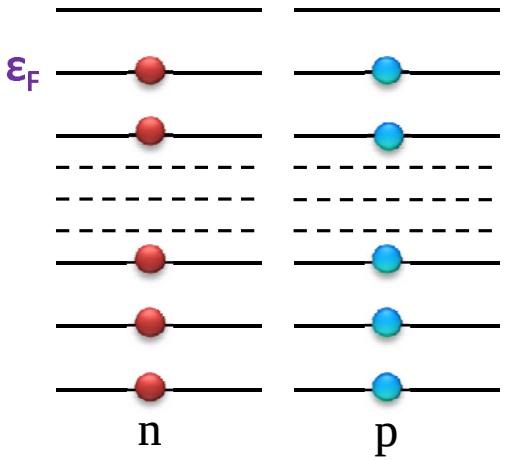

Figure 1.4: *Equidistant energy levels of a degenerate Fermi gas*

where the level density is mostly determined by the **level density parameter (LDP)** a, which is related to the density of single-particle states near the Fermi energy by the relation $a = \frac{\pi^2}{6} g(\epsilon_F)$. Now in the Fermi gas model, the density of single-particle states is given by $g(\epsilon_F) = \frac{3A}{2\epsilon_F}$, where ϵ_F is the Fermi energy. Therefore, we can write

$$a = \frac{\pi^2}{4}\frac{A}{\epsilon_F}. \tag{1.16}$$

In the case where Z protons and N neutrons of the nucleus are distinguished we have

$$\rho(N, Z, E) = \frac{\sqrt{\pi}}{12}\frac{exp(2\sqrt{aE})}{a^{1/4}E^{5/4}}, \tag{1.17}$$

with,

$$a = \frac{\pi^2}{6}(g_\pi(\epsilon_F) + g_\nu(\epsilon_F)), \tag{1.18}$$

where g_π and g_ν are proton and neutron single-particle densities respectively. In deriving the expression 1.15 (or 1.17) several mathematical approximations have been incorporated, which put a few restrictions on the applicability of this expression.

1. The first restriction is that,

$$g(\epsilon_F)E \gg 1. \tag{1.19}$$

This condition simply reflects the fact that the average level density ρ is not defined until we come to excitation energies E, large compared to the energy of the first excited

state. (There must be many excited levels in order that the average level density is defined.)

2. The second condition is,

$$E \ll \epsilon_F A^{1/3}. \tag{1.20}$$

This limit results from the fact that the single-particle level spacing g(ϵ) has been considered as constant, although for a Fermi gas it varies approximately as the square root of the particle kinetic energy ($g(\epsilon) \propto \epsilon^{1/2}$). This variation can be accounted in the calculations, however, then the level density becomes a more complicated function of the excitation energy (non-degenerate Fermi gas). Thus the expressions 1.15 and 1.17 can only be considered as the zeroth order approximation of a Fermi gas. An estimate of the value of the level density parameter can be obtained by putting $\epsilon_F \approx$38 MeV in Eqn. 1.16 which gives $a \approx \frac{A}{15}$. However, the average value of *a* at low energies as suggested by experimental observations corresponds to a much larger value of *a* close to *A*/8. The disagreement is not very surprising as the real single-particle spectrum of a nucleus is considerably complicated than the simple equidistant Fermi gas picture. Therefore in most of the phenomenological descriptions of NLD, *a* is treated as a free parameter which is adjusted to match the experimental data. It may be mentioned here that although there is a large discrepancy between the experimental value of *a* at low energies (~A/8) and its Fermi gas prediction (~A/15); the inconsistency is somewhat removed at high energies where the experimental value of *a* is observed to approach towards its Fermi gas limit. This will be discussed in more detail in *Chapter* **3** where the excitation energy (temperature) dependence of *a* will be presented.

1.4.1 Spin dependence of NLD

In the framework of Fermi gas model it is also possible to determine dependence of the level density ρ on the angular momentum projection M. Several different methods have been employed to obtain $\rho(E, M)$, all of which provide the following result [11],

$$\rho(A, E, M) = \rho(A, E)\frac{exp(-M^2/2\sigma^2)}{\sqrt{2\pi\sigma^2}} \tag{1.21}$$

where σ is known as the spin cut-off parameter which is given by $\sigma^2 = g < m^2 > T = \mathcal{I}T/\hbar^2$. Here $< m^2 >$ is the average of the square of the single-particle spin projections, $\mathcal{I}$ is the moment of inertia and T is the nuclear temperature. The dependence of level density on the total angular momentum (spin) can be obtained from Eqn. 1.21 in the following manner. Let us consider nuclear states with total angular momentum J and spin projection M; and write them as | J M>. Since M can have values from +J to -J, the level density $\rho(E, M)$ contains all states with magnetic quantum number M and total angular momentum J≥ M. Let us consider $\rho(E, M = J)$ and $\rho(E, M = J + 1)$ in particular. $\rho(E, M = J)$ contains states like | J J>, | J+1 J>, | J+2 J> ... *etc.* Whereas $\rho(E, M = J + 1)$ contains states such as | J+1 J+1>, | J+2 J+1>, | J+3 J+1> ... *etc.* In the absence of any external magnetic field we can observe all states with different J only, not those with different M. Therefore states like | J+1 J> & | J+1 J+1> and | J+2 J> & | J+2 J+1> will be degenerate. So, the difference $\rho(E, M = J)$ - $\rho(E, M = J + 1)$ gives contribution only from the states | J J>, *i.e.*, states with different J each counted only once. Thus,

$$\rho(E, J) = \rho(E, M = J) - \rho(E, M = J + 1) \tag{1.22}$$

This difference can be approximated by taking the first derivative of $\rho(E, M)$ with respect to M, calculated at M =J+1/2.

$$\begin{aligned} \rho(E, J) &= \frac{d\rho(E, M)}{dM} \Big|_{M=J+1/2} \\ &= \rho(E)\frac{2J+1}{\sqrt{8\pi}\sigma^3} exp\left(\frac{-(J+\frac{1}{2})^2}{2\sigma^2}\right) \qquad (1.23) \\ &\simeq \rho(E)\frac{2J+1}{\sqrt{8\pi}\sigma^3} exp\left(\frac{-(J(J+1))^2}{2\sigma^2}\right) \qquad (1.24) \end{aligned}$$

The spin dependence of NLD will be discussed further in detail in the next chapter where the results of our experimental investigation on the spin dependence of NLD will be presented.

1.5 NLD beyond independent particle model

The mathematical formulations described above provide level densities under the independent particle picture of the nucleons. The independent particle motion of the nucleons reflects the existence of a nuclear mean field. However, correlations (both short range and long range) among the nucleons beyond the mean field are observed to have important effects on nuclear properties. Two main aspects of the effects beyond IPM in NLD are (i) pairing correlations (short range) that account for the tendency of the like nucleons to be in pairs and (ii) collective properties (rotation and vibrations) that involve coherent excitations of the nucleons (long range correlations). These effects can be taken care of in sophisticated microscopic NLD calculations using realistic Hamiltonians, which try to account for the coupling between these properties. However, these calculations are highly complicated and time-consuming. Therefore, in most practical cases these properties are considered phenomenologically using some adjustable parameters in simple analytic NLD expressions (such as the one obtained using the FG model).

1.5.1 Pairing effects in NLD

As already mentioned, that the pairing effect reflects the tendency of the fermions to be coupled as pairs. In terms of NLD, the pairing effects imply that for a given excitation energy and in a narrow mass range, the level density of an even-even nucleus is generally lower than that of an odd-even nucleus which in turn is lower than the level density of an odd-odd nucleus. The reason is that before exciting the fermions of the nucleus, pairs (when they exist) have to be broken which requires an additional energy. Thus the pairing effects can be accounted to a good extent by reducing the excitation energy in the Fermi gas expression by an amount equal to the pairing energy

correction (Δ) used in the semi-empirical mass formula to take care of the odd-even effect, $\rho(E) \longrightarrow \rho_{IPM}(E - \Delta)$.

1.5.2 Collective effects

Additional contributions to NLD beyond independent particle model can arise from the collective rotation and/or vibration of the nucleons. For example, if we have a deformed nucleus, then for each single-particle configuration, one can consider collective rotations. In addition, both spherical and deformed nuclei can have collective vibrational motions. These collective motions give rise to rotational and vibrational bands enhancing the level density above the single-particle value. This is termed as the collective enhancement of NLD which is expressed as,

$$\rho_{tot}(E, J) = K_{coll}(E)\rho_{IPM}(E, J), \tag{1.25}$$

$$K_{coll}(E) = K_{rot}(E) \times K_{vib}(E) \tag{1.26}$$

where $K_{coll}(E)$ is known as the collective enhancement factor, and K_{rot} & K_{vib} are its rotational and vibrational components, respectively. The collective enhancement is expected to be damped and finally washed out ($K_{coll}(E) \rightarrow 1$) at higher excitation energies. The collective enhancement in NLD and its fadeout with excitation energy will be discussed in *Chapter* **4**.

1.6 Phenomenological descriptions of NLD

As we have already mentioned that the simple analytic expression for the nuclear level density derived from the basic Fermi gas model does not incorporate important nuclear properties such as pairing correlations, shell and collective effects. Therefore this elementary formulation gives only a global and qualitative description of level density. On the other hand, microscopic calculations including the key nuclear effects

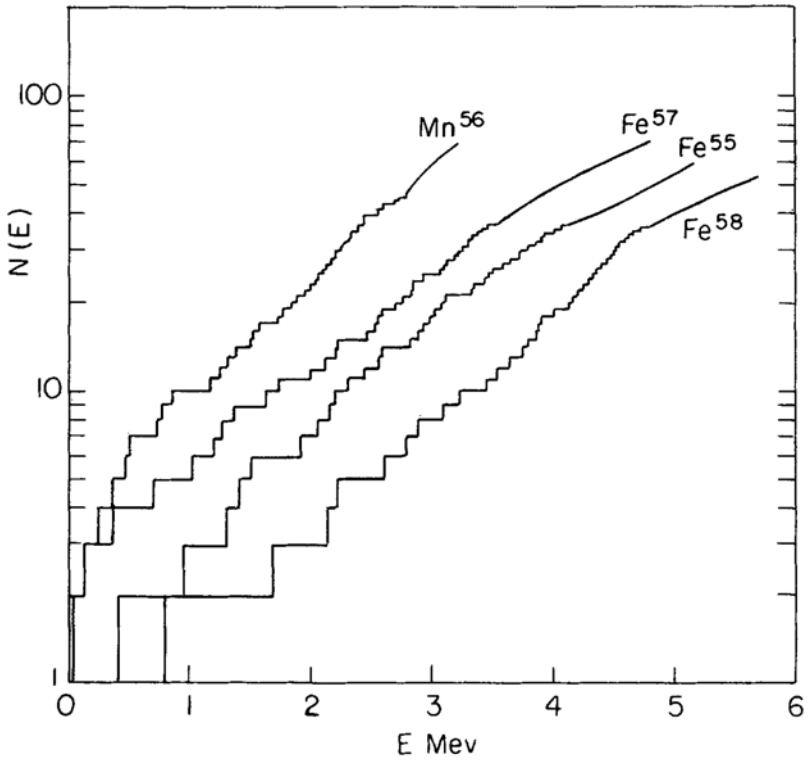

Figure 1.5: *The total number of states up to excitation energy E for* ^{55}*Mn,* ^{56}*Fe,* ^{57}*Fe and* ^{58}*Fe vs. E, taken from Ref. [13]*

provide a much accurate description of NLD for individual nuclei. However, rigorous microscopic calculations are extremely involved and in most of the cases don't provide analytic expressions. These severely limit their application to the analysis of experimental data. Therefore in most of the statistical model codes, one starts with a Fermi gas type level density expression; and the shell, pairing, deformation and collective effects are incorporated in a completely phenomenological manner through a number of adjustable parameters. The most widely used phenomenological level density prescriptions can be differentiated mainly into two approaches (1) the Back-Shifted Fermi Gas (BSFG) approach and (2) the Gilbert-Cameron (GC) approach.

1.6.1 Back-Shifted Fermi Gas Level Density

It is known from the observed nuclear masses that the binding energy of nuclei with even number of proton or neutron is more compared to the neighboring odd-Z or odd-N nuclei by an amount equal to the pairing energy. Similarly these nuclei have level spacing (at least up to the neutron resonance region) larger than the nearby odd-Z or odd-N nuclei. So, the pairing effects have important consequences on nuclear level density, particularly at lower excitation energies. A direct demonstration of this effect is shown in Fig. 1.5 by the comparison of the number of levels as a function of excitation energy for neighboring nuclei of odd and even character in the iron region [13]. The odd-even effect seems mainly to cause a shift of the effective excitation energy between the odd and even nuclei. The magnitude of this shift is close to the value of the pairing energy as determined from nuclear binding energies in this region. This odd-even effect can be some what taken care by replacing the energy E in the level density formula of Eqn. 1.17 by an effective energy $E - \Delta$, where Δ is the shift in the energy (ground state) which is approximately equal to the pairing energy. Thus $\rho(E)$ is given by,

$$\rho(E) = \frac{\sqrt{\pi}}{12} \frac{exp(2\sqrt{a(E-\Delta)})}{a^{1/4}(E-\Delta)^{5/4}} \tag{1.27}$$

The exact value of the pairing energy depends on the individual nucleus, however, the average value of Δ can be approximated by the relation $\Delta = 12A^{-1/2}$, (as shown by the continuous line in Fig. 1.6). In general one can write,

$$\Delta = n\frac{12}{\sqrt{A}} \tag{1.28}$$

where n = -1, 0 and 1 for odd-odd, odd-A, and even-even nuclei. This approach is known as shifted Fermi gas model. Later, this energy correction was found to be too large to explain experimental data. Hence the shift was somewhat back-shifted again, resulting in the back-shifted-Fermi-gas (BSFG) formula [11]. In the BSFG model both a and Δ are taken as adjustable free parameters to match the experimental data. In this case Δ is given by,

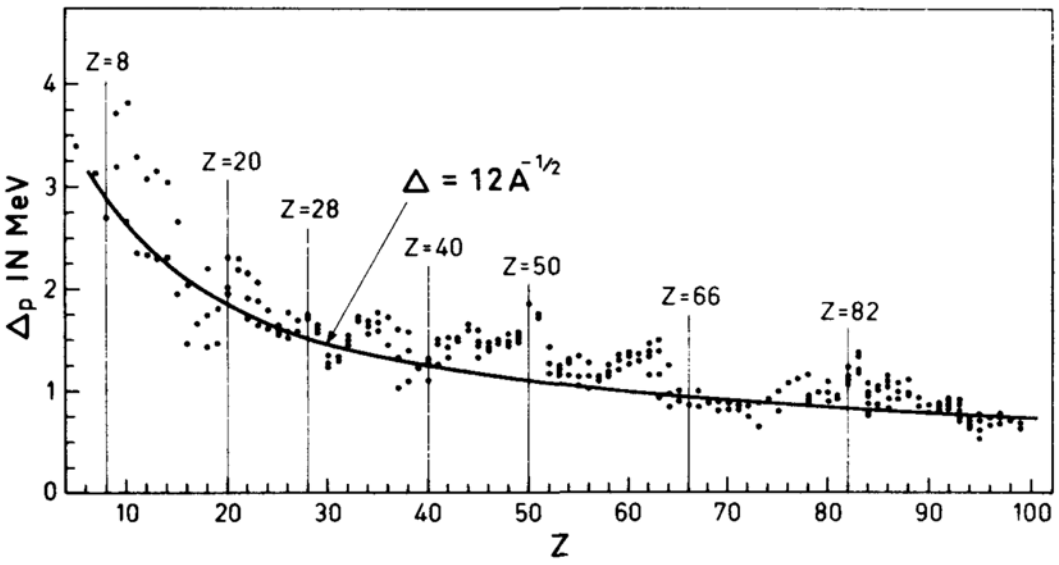

Figure 1.6: *The odd-even mass differences for protons from Ref [11].*

$$\Delta = n\frac{12}{\sqrt{A}} + \delta \tag{1.29}$$

where δ is the free parameter adjusted to fit experimental data for each nucleus. The back-shifted Fermi-gas model has been very popular and most common description of nuclear level densities for decades.

1.6.2 Gilbert-Cameron prescription

It has been observed that the cumulative number of levels $N(E)$ at the lower excitation energies (discrete energy level region) is well represented by the relation,

$$N(E) = exp\left(\frac{E - E_0}{T_0}\right) \tag{1.30}$$

which gives a level density

$$\rho(E) = \frac{dN(E)}{dE} = \frac{1}{T_0} exp\left(\frac{E - E_0}{T_0}\right) \tag{1.31}$$

this is known as the constant temperature formula, where the energy shift E_0 and the constant temperature T_0 are treated as adjustable parameters to fit the experimental data. Although Eqn. 1.31 does provide a better representation of nuclear levels at

low energy; it fails at higher energies. On the other hand, the level density prescription given by the back-shifted Fermi gas model (Eqn. 1.27) works reasonably well at higher energies, but it could not explain the variation of cumulative number of levels at the lower excitation energies. So Gilbert and Cameron [14] have suggested to use two different level density formulations in the two different energy regions. In the high energy regions (usually above 10 MeV or so) the level density expression is given by Eqn. 1.27, whereas in the low energy (discrete energy level) region the level density is given by Eqn. 1.31. The two prescriptions should match together smoothly at a transition energy U_x. This is ensured if both level density and its first derivative (related to nuclear temperature) is continuous at $U = U_x$. The actual value of the transition energy depends on the individual nucleus. However one can assign an average value of U_x given by [14],

$$U_x = 2.5 + 150/A. \tag{1.32}$$

In the GC approach there are four free parameters E_0, T_0, a, and Δ which are extracted by fitting experimental data in both energy regions.

1.7 Shell effect in NLD

Shell structure in atomic nuclei is evident through a large number of phenomena such as the enhanced binding energy of the *magic nuclei*, the occurrence of fission isomers, asymmetric mass distribution of fission fragments, the existence of super-deformed nuclei *etc*. Shell effects are observed to have important consequences in NLD too. Because of the large single-particle energy spacing around the Fermi energy the shell closed (magic) (or near shell closed) nuclei, are observed to have a lower (by considerable amount) level density as compared to nearby non-magic nuclei at the same energy. This phenomenon is very well demonstrated by Moretto *et al.* [15] through the level density calculation in the framework of Nilson shell model for a

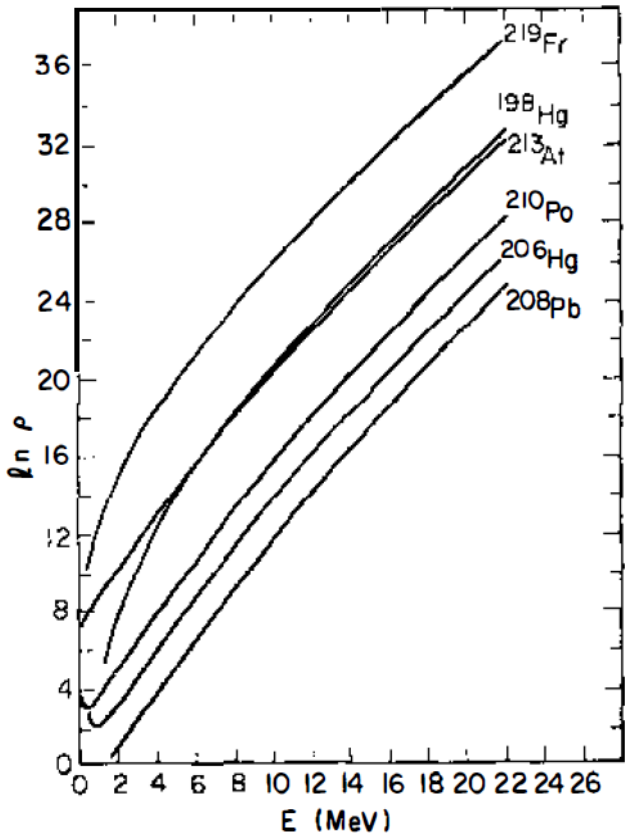

Figure 1.7: *Theoretical level densities as a function of excitation energy for nuclei in the neighborhood of the* ^{208}*Pb doubly closed shell [15].*

number of nuclei in the vicinity of doubly magic ^{208}Pb. The calculated level densities by Moretto *et al.* as a function of excitation energy has been shown in Fig. 1.7. The shell effect is clearly evident from the figure as the most magic nucleus, ^{208}Pb, has the lowest level density, and the level densities increase for nuclei which are farther and farther away from the double closed shell. Different excitation energy dependences of the level densities of different nuclei (particularly at the low excitations) are also apparent from the figure. The shell effect can also be evident from the observed variation of the level density parameter as a function of nucleon number as shown in Fig. 1.8 where the level density parameter around the neutron binding energy has been extracted from the experimental data (the neutron resonance spacings and the cumulative numbers of low-lying levels) using the BSFG prescription [16]. While the average variation of *a* with the mass number (*A*) can be represented by a smooth dependence

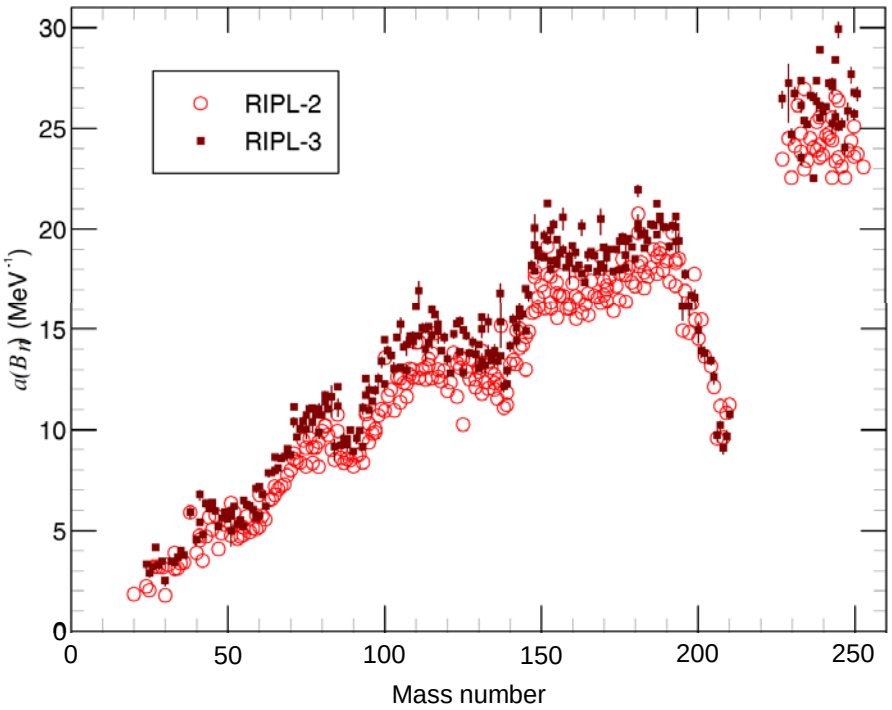

Figure 1.8: *Level density parameter around neutron binding energy for different nuclei as obtained from RIPL compilations [16]*

corresponding to $a \approx A/8$ at low energies, large deviation from this average value can be observed for nuclei around shell closure. In previous sections, we have mentioned that important properties beyond IPM like pairing correlations and collective effects can be taken care of phenomenologically by using certain adjustable parameters in the Fermi gas type level density formulations. A similar strategy is followed for the shell effect which is also unaccounted in the Fermi gas model of NLD but observed to have important consequences. The shell effect depends strongly on the excitation energy and is expected to die out beyond a critical energy. Shell effect in nuclear level density is generally incorporated through an excitation energy-dependent nuclear level density parameter as proposed by Ignatyuk *et al.* [17],

$$a = \tilde{a}[1 + \frac{\Delta S}{U}\{1 - \exp(-\gamma U)\}] \qquad (1.33)$$

The prescription incorporates the effect of nuclear shell structure in a at low excitation energy and goes smoothly to the liquid drop value ($\tilde{a}$) at higher excitation energy. Here ΔS is the shell correction obtained from the difference between the experimental and the liquid drop model masses and γ is the shell damping parameter, which determines the rate at which shell effects are depleted with the increase in excitation energy. In the present thesis work the shell damping parameter has been determined experimentally for nuclei close to the doubly magic ^{208}Pb, which will be presented in *Chapter* **3** along with the observed temperature dependence of $\tilde{a}$ for nuclei in this region.

1.8 Experimental sources of information on NLD

1.8.1 Counting of levels at low excitation energy

Nuclear level density can be computed directly by counting nuclear levels up to a given excitation energy [18, 19, 20, 21]. Of course, this can be done at low energies where the levels can be resolved and counted. Several nuclear reactions and detection techniques are employed to identify the individual nuclear levels. For example, various charged particle reactions along with magnetic spectrograph are used to get a resolution of the order of $\Delta E \approx 10$ keV. Measurement of neutron spectrum using the time of flight method, form different reactions such as (p, n) or (d, n) can give resolution ~ 5 keV. Even better resolution can be obtained by measuring γ-rays from the capture or other reactions, where it can provide useful information about nuclear level density. Several nuclear reactions such as (p, p'), (n, n'), (α, α'), (p, α), (d, p) (d, t) and (^{3}He, α), have been employed to study levels at low energies. However, if this technique is to be used for accurate level density information, one must be assured that levels of all angular momenta are excited. This technique has limited application particularly for heavy nuclei where the levels tend to overlap even at very low excitation energy. The

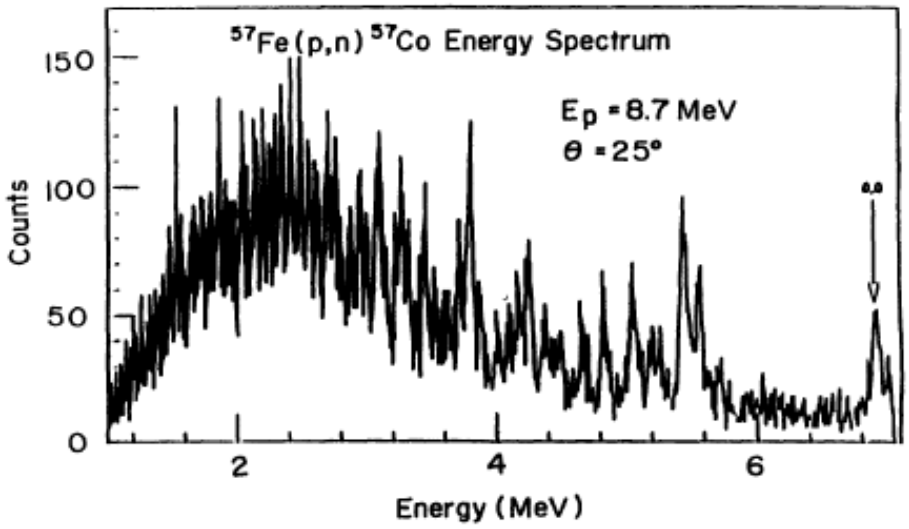

Figure 1.9: *Neutron spectrum from the ^{57}Fe(p, n)^{57}Co reaction at a bombarding energy of 8.7 MeV and an angle of 25^0 taken from Ref. [21].*

experimental spectra for the ^{57}Fe$(p, n)^{57}$Co reaction [21] showing the discrete energy levels is shown in Fig. 1.9.

1.8.2 Counting of neutron (and charged particle) resonances

Most substantial information about NLD comes from the study of neutron resonances. In these type of measurements resonance in the total cross-section is observed around an energy close to the neutron binding energy (B_n) and the number of levels is counted by counting the number of resonances for a given neutron energy interval. It is necessary for such experiments that the width Γ of each level be less than the level spacing D and that the experimental resolution is good enough to resolve individual levels. In the past several such studies have been carried out using low energy neutrons. In this case, the resonances are mostly of *s*-wave (*i.e.* partial waves with ℓ=0) in nature. The mean spacing of the observed resonances can be directly related to the level density of the compound nucleus at excitation energies close to B_n by the relation,

$$\frac{1}{D_0} = \frac{1}{2}[\rho(B_n + \Delta E/2, I_t + \frac{1}{2}) + \rho(B_n + \Delta E/2, I_t - \frac{1}{2})] \quad \text{for} \quad I_t \neq 0 \quad (1.34)$$

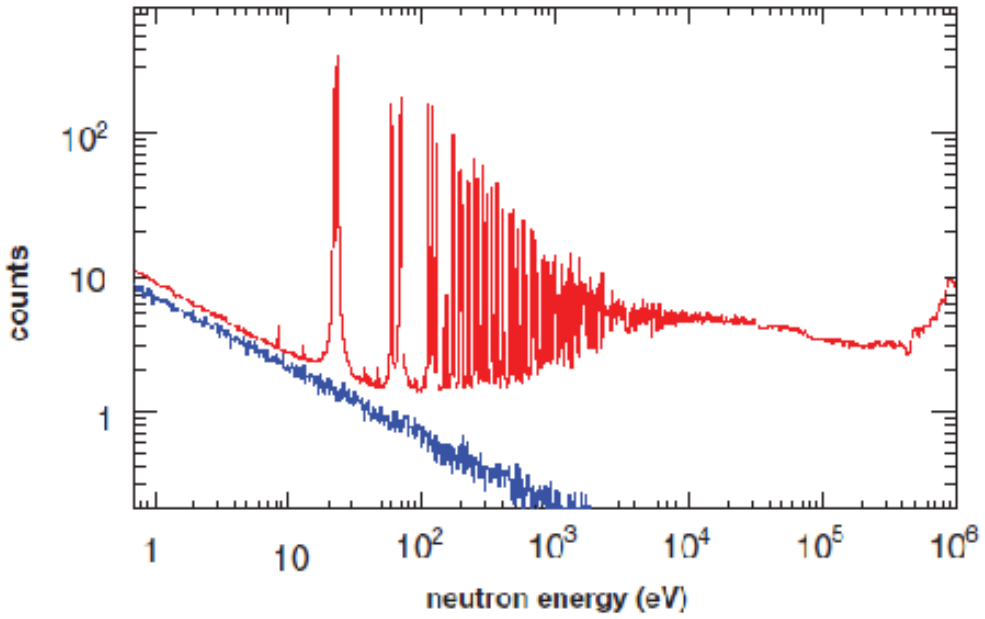

Figure 1.10: *The unweighted spectrum of the thorium sample showing the resonance structure. The constant radioactive background, well below the time-of-flight spectrum, is shown in blue. Taken from the Ref. [26]*

$$= \frac{1}{2}\rho(B_n + \Delta E/2, \frac{1}{2}) \qquad \text{for} \quad I_t = 0$$

where B_n is the neutron binding energy, ΔE is the energy interval for which the resonances are being examined, I_t is the spin of the target nucleus and the factor $1/2$ before the sum takes into account the fact that *s*-neutrons form resonances only of a particular parity. If required, resonances for *p*-neutrons can also be accounted in a similar manner. The level density is extracted from the measured D_0 values, using standard level density formulations. The major advantages of this approach are that the level densities can directly be related to experiments in a model independent manner and the procedure is applicable for almost all nuclei in the nuclear chart. Level spacing information has already been obtained from slow-neutron-resonance (*s*-wave) data for about 200 nuclei. Several compilations on experimental resonance spacing are available from many authors [14, 22, 23, 24, 25]. The notable drawbacks or errors of this techniques are (a) difficulty in detecting all the *s*-wave resonances in a given energy region as the strengths of resonances of a particular spin and parity vary greatly from

one resonance to another (b) possibility of mixing of *p*-wave resonances with *s*-wave. Typical neutron resonance structure for the ^{232}Th(n,γ) reaction as measured by n_TOF collaboration [26] is shown in Fig. 1.10.

Information on the nuclear level density can also be obtained from the charged-particle capture resonance studies in a manner similar to that of the neutron-capture resonance. However, the charged-particle resonance data are restricted to light and medium nuclei due to the existence of Coulomb barrier. The charged-particle resonance studies are particularly useful for nuclei which cannot be studied by neutron resonance spectroscopy. A compilation of such data for a number of light nuclei has been published by Endt and Van der Leun [27].

1.8.3 Measuring excitation functions of isolated levels

It was first pointed out by Ericson [13] that the absolute cross sections for formation of isolated residual levels in compound nuclear reactions can be used to determine nuclear level densities. Measurements of the absolute cross sections for isolated final levels as a function of bombarding energy have been used to determine the energy dependence and absolute values of the level densities of a number of residual nuclei (^{56}Fe, ^{52}Cr, ^{59}Co) [28] populated through the reactions of proton and α-particles with ^{55}Mn, ^{56}Fe, ^{59}Co, and ^{62}Ni targets. The excitation function of the single level (or levels) is fitted with different forms of the level density (*e.g.* BSFG or CT models) in order to obtain reasonable agreement between experiment and theory. Although this technique has some intrinsic advantages and gives an absolute measure of the level density, it suffers from the exponentially decreasing cross section with the energy of a single level and the possible admixture of direct reaction particles. Improvement in statistical accuracy can be attained by examining the energy dependence of the cross section of many final levels [29, 30]. However, other uncertainties in the analysis may offset the advantage gained by better statistics.

1.8.4 Fluctuation width analysis

Nuclear reaction cross section at a compound nuclear excitation energy region where the average level width Γ is larger than the average spacing D between compound nuclear levels, is observed to fluctuate remarkably as a function of projectile energy. Such fluctuating cross sections, when analyzed in terms of statistical theory, can be used to get a measure of level density. The level width Γ obtainable from correlation functions of the fluctuating cross sections can be used together with the information on the exit channels known from other measurements, to obtain the level density of the compound nucleus at an excitation energy of approximately 20 MeV [28, 31, 32, 33, 34]. For a long time, this method known as the *Ericson fluctuation width* technique has been the only method to extract NLD at high excitation energies ($\gtrsim$20 MeV).

1.8.5 The Oslo Method

As discussed in the previous sections, level densities can be extracted directly by counting the number of levels only up to a few MeV (particularly for medium or heavy nuclei). On the other hand, neutron resonance counting provides level density information close to the neutron binding energy ($\sim$ 8 - 10 MeV). So, there is a region where there is no source of experimental information on the NLD, and it can at best be estimated by extrapolating data obtained from the above two techniques. The Oslo method [35] is particularly useful to extract level densities in the region between the discrete level and neutron resonances. By this method, both level density and γ-ray strength function can be extracted up to the particle emission threshold, from a single experiment. In this technique nucleus is excited to an energy below the particle emission threshold by means of transfer reaction (*e.g.* (p,d), (p,t) (d,p) $(^3He,\ ^4He)$) or inelastic scattering (p,p'), (d,d'), $(^3He,\ ^3He')$), then the all the γ-rays emitted during the sequential γ-transitions cascading down to the ground state are measured by the

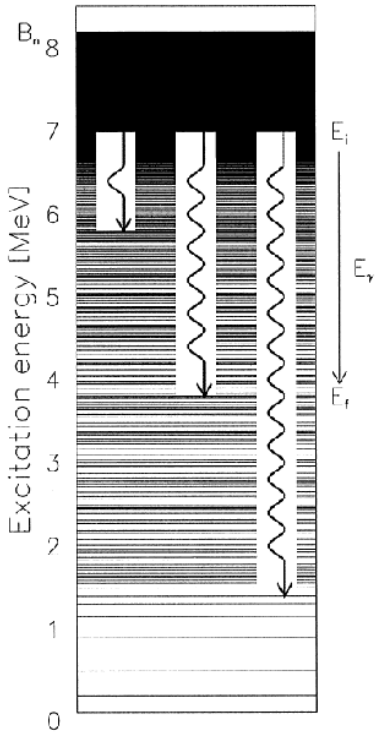

Figure 1.11: *The γ decay probability from an initial excitation energy E_i in the statistical region is proportional to the level density at the final excitation energy E_f and the γ strength function at the γ energy $E_\gamma = E_i - E_f$.*

total absorption technique in coincidence with the out going charged particle (ejectile). The excitation energy (E_i) is obtained from the measured ejectile energy using known Q-value and reaction kinematics. From the particle-γ coincidence measurement the matrix $F_p(E_i, E_\gamma)$, which is a two-dimensional matrix of the excitation energy of the nucleus and the energy of the *primary* γ-rays (E_γ) is generated. In the experiment, all the γ-rays emitted in a cascade are detected and it is not possible to identify which among those were emitted in the first chance (called as the primary γ-rays). The primary γ-rays are extracted at each excitation energy (energy bin) from the total cascade using the experimentally measured matrix $F(E_i, E_\gamma)$, by a subtraction technique developed in Refs. [36, 37]. If the primary γ-ray spectrum is normalized to unity for each excitation energy bin,

$$\sum_{E_\gamma = E_\gamma{}^{min}}^{E_i} F_p(E_i, E_\gamma) = 1 \qquad \text{for each} \qquad E_i \tag{1.35}$$

then the first generation matrix $F_p(E_i, E_\gamma)$ will represent the decay probability from $E_i \rightarrow E_f = E_i - E_\gamma$. Now the γ decay probability from an initial excitation energy E^* in the statistical region is proportional to the level density at the final excitation energy E_f and the γ strength function at the γ energy E_γ (see Fig. 1.11 for illustration). In this case, one can write,

$$F_p(E_i, E_\gamma) \propto T(E_\gamma)\rho_f(E_i - E_\gamma), \tag{1.36}$$

where T is the γ-ray transmission coefficient, and ρ_f is the level density at excitation energy E_f after the first γ-ray emission. The ρ and T functions can be determined by an iterative procedure [36], where each data point in the two functions is adjusted until a global χ^2 minimum with the experimental $F_p(E_i, E_\gamma)$ matrix is reached. The Oslo technique has been extensively used in recent times to extract information on NLD [37, 38, 39, 40, 41, 42, 43, 44, 45].

1.8.6 Spectrum of evaporated particles

Study of evaporation spectra of particles emitted from a hot compound nucleus provides useful information on the nature of nuclear level density. Although the technique does not provide an absolute measure of ρ, it is one of the most useful methods to understand the variation of NLD over a wide range of excitation energy and angular momentum. The method is particularly suitable at higher excitation energies where the other methods like direct level counting or measurement of neutron resonance spacing fail because of the presence of densely overlapping nuclear levels in this region. A large variety of nuclei can be studied by this technique through judicious choice of target and projectile combination. The process of particle evaporation from an excited nucleus can be described by the statistical theory of compound nuclear reactions developed originally by Weisskopf and Ewing [46]. The cross section for emitting a light particle with kinetic energy ϵ can be simplistically given as,

$$\sigma(\epsilon) \propto T_l(\epsilon)\,\frac{\rho_d(E^* - \epsilon - B_\beta)}{\rho_{CN}(E^*)} \tag{1.37}$$

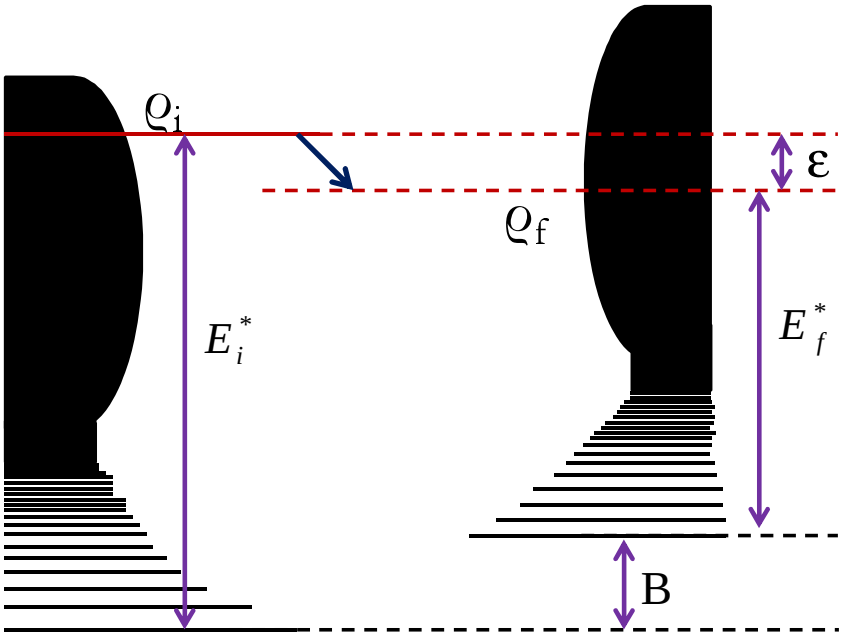

Figure 1.12: *A schematic of the evaporation process.*

Here, ρ_d and ρ_{CN} are the level densities of the daughter and compound nucleus, and $T_l(\epsilon)$ is the transmission coefficient or barrier penetration factor for the emission of the particle; B_β is the separation or binding energy of the emitted particle. Thus the kinetic energy spectra of the evaporated particle (particularly the high energy part (slope) of it) are highly sensitive to the variation in level density of the daughter nucleus. So this part of the experimental spectra is compared with theoretical calculations (statistical model) to extract information about nuclear level density. A possible drawback of this technique arises from the fact that the spectrum of evaporated particles is a sum total of a multi-step decay process, thus sampling various nuclei at different steps. Therefore, the extracted level densities (or rather the rate of change of level density) may not correspond to a specific nucleus but averaged over a few neighbouring nuclei. However, the extracted information can still be of high significance. A number of recent experimental investigations can be found in literature [47, 48, 49, 50, 51, 52, 53, 54, 55, 56, 57, 58, 59, 60, 61, 62] that utilized this technique to extract information on the chracteristics of NLD. In the current thesis, experimental information on various aspects of NLD has been extracted by studying

light particle (proton, α-particles and/or neutron) evaporation spectra using of ^{4}He-ion induced reactions on several target nuclei. The evaporation process is schematically shown in the Fig. 1.12.

1.9 Motivation and structure of the present thesis

Understanding the properties of nuclear level density and its accurate determination is of prime importance in nuclear physics, as it can provide interesting tests of different microscopic approaches of nuclear structure used to calculate NLD. Apart from this fundamental interest, study of NLD is even more important as it serves as an essential ingredient in various theoretical models used for quantitative explanation of a number of related physical phenomena in nuclear physics (yields of evaporation, fission, multifragmentation, spallation), astrophysics (thermonuclear reaction rates for nucleosynthesis) and reactor technology (fusion-fission cross sections). It has already been mentioned that nuclear level density depends on various important nuclear factors like excitation energy (temperature), angular momentum (spin), parity, pairing correlations, shell effects, iso-spin, and collectivity. Although nuclear level density has been a matter of investigation (both theoretically and experimentally) over a long time, it is still an active area of research. In recent years a number of interesting but conflicting observations have been made on the dependence of level density on energy, angular momentum, and collectivity. These investigations demand to revisit our understanding of the properties of nuclear level density and prompted us to carry out new investigations. Thus the aim of the present thesis is to improve and extend experimental information on the variation of NLD on key nuclear factors and try to resolve some of the open questions (discussed in subsequent chapters) in these areas. The present thesis particularly focuses on the three aspects of NLD; (i) spin dependence (iii) damping of shell effect and temperature dependence of level density parameter and (iii) collective enhancement and its fadeout. A series of experiments have been performed under the thesis work. Experimental information on the variation of NLD was obtained from the

measured light particle evaporation spectra which are the most effective and widely used tool to investigate NLD over a wide range of excitation energy and angular momentum. For the present measurements, we have chosen light-ion (^{4}He ion) induced reactions which have a number of advantages as compared to the heavy-ion (HI) route. Firstly, the contribution from the incomplete fusion events (e.g. transfer or breakup induced fusion) is expected to be less due to the high binding energy of the projectile. Secondly, the numbers of effective decay channels are also less compared to the HI reactions; therefore, the extracted level density correspond more closely to those of the nuclei of interest and not averaged over a large number of nuclei. The present thesis is divided into five complete chapters.

1. **Chapter 1** presents a brief introduction to the subject of nuclear level density. An overview of the different theoretical and experimental techniques employed to determine NLD has been presented.

2. **Chapter 2** deals with the angular momentum (spin) dependence of NLD. Experimental results on the spin dependence of NLD obtained from our measurement of angular momentum gated light-particle spectra in the case of ^{4}He + ^{58}Ni, and ^{93}Nb reactions are presented. Details of the experimental setup, data analysis technique, and statistical model calculation is also discussed.

3. **Chapter 3** speaks about the excitation energy (temperature) dependence of the level density parameter. Experimental results of the neutron evaporation study in the case of ^{4}He + ^{208}Pb, and ^{209}Bi reactions in a wide excitation energy range have been described. The physical interpretation of the data has been provided in terms of existing theoretical picture.

4. **Chapter 4** discusses about role of collective excitations in nuclear level density. Results of our investigation on the collective enhancement in NLD and its fadeout in the case of nuclei having large ground-state deformation have been presented. And finally,

5. **Chapter 5**, gives a summary and conclusions to the present thesis work along with an outlook for the future.

Chapter 2

Angular momentum dependence of NLD

2.1 Introduction

The angular momentum (spin) dependence of nuclear level density can be obtained theoretically using the simplest Fermi gas picture, as shown in section 1.4. In this case, the spin dependence was introduced in the total level density by a multiplicative Gaussian function ($exp\frac{-(J+1/2)^2}{2\sigma^2}$) [Eqn. 1.23], where the width of the Gaussian is determined by the temperature (T) dependent spin cut-off factor σ. In most of the phenomenological descriptions of NLD, however, the angular momentum dependence is incorporated through the spin and deformation dependent rotational energy [11],

$$E_{rot} = \frac{\hbar^2}{2\Im_{eff}} J(J+1) \tag{2.1}$$

with,

$$\Im_{eff} = \Im_0(1 + \delta_1 J^2 + \delta_2 J^4). \tag{2.2}$$

Here $\Im_{eff}$ and $\Im_0$ are the effective and rigid body moments of inertia of the system, and δ_1 & δ_2 known as the deformability coefficients, are adjustable parameters that provide

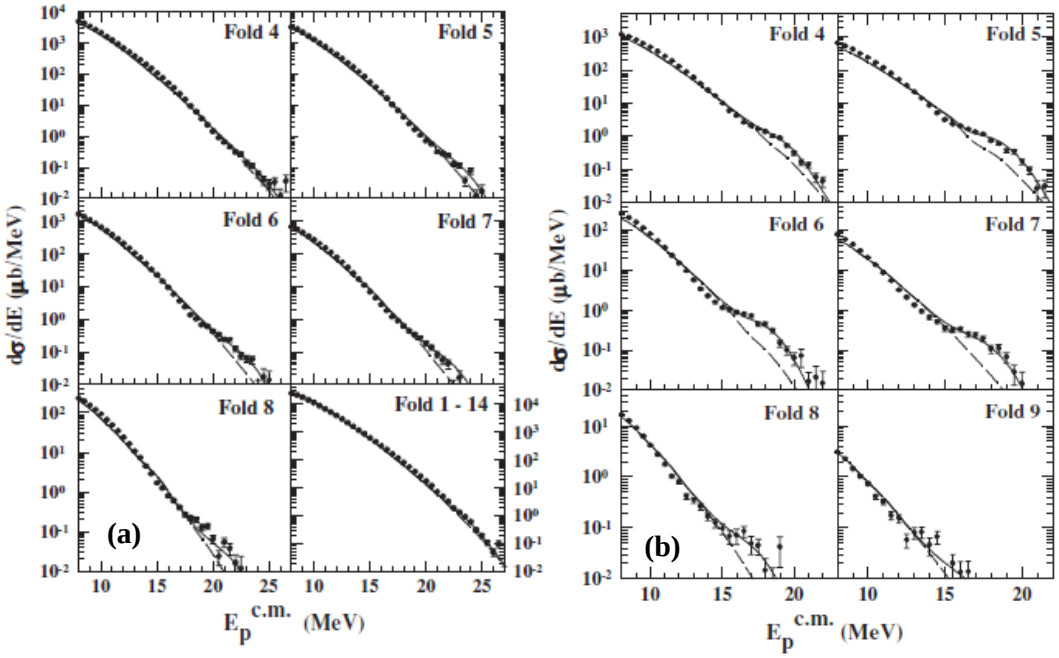

Figure 2.1: *Experimental α-particle spectra in the center-of-mass (c.m.) in case of (a) ^{12}C + ^{93}Nb and (b) ^{12}C + ^{89}Y (closed circles) reactions for different fold (angular momentum) windows, taken from Ref. [52].*

a range of choices for the spin dependence of the level density [63]. The rotational energy is subtracted from the excitation energy and the effective energy ($E^* - E_{rot}$) is used for the evaluation of NLD using the standard level density formula (Eqn. 1.17). The phenomenological description of spin dependence becomes equivalent to the Fermi gas formulation at high excitation energies (*i.e.* for $E^* \gg E_{rot}$). In these approaches, the spin dependence in NLD have been incorporated independently (in ρ) and there is no additional dependence of the level density parameter on angular momentum or deformation. On the experimental side, information on the spin dependence of NLD can be obtained by measuring evaporation spectra of particles emitted from an excited compound nucleus, in coincidence with the low energy γ-rays of different multiplicities, which is directly related to the angular momentum populated in the nucleus. It has been possible to carry out such measurements only in recent times [51, 52, 53, 54, 55] using advanced γ-ray multiplicity detector arrays. In a number of such exclusive measurements with respect to angular momentum, the experimental data have not been prop-

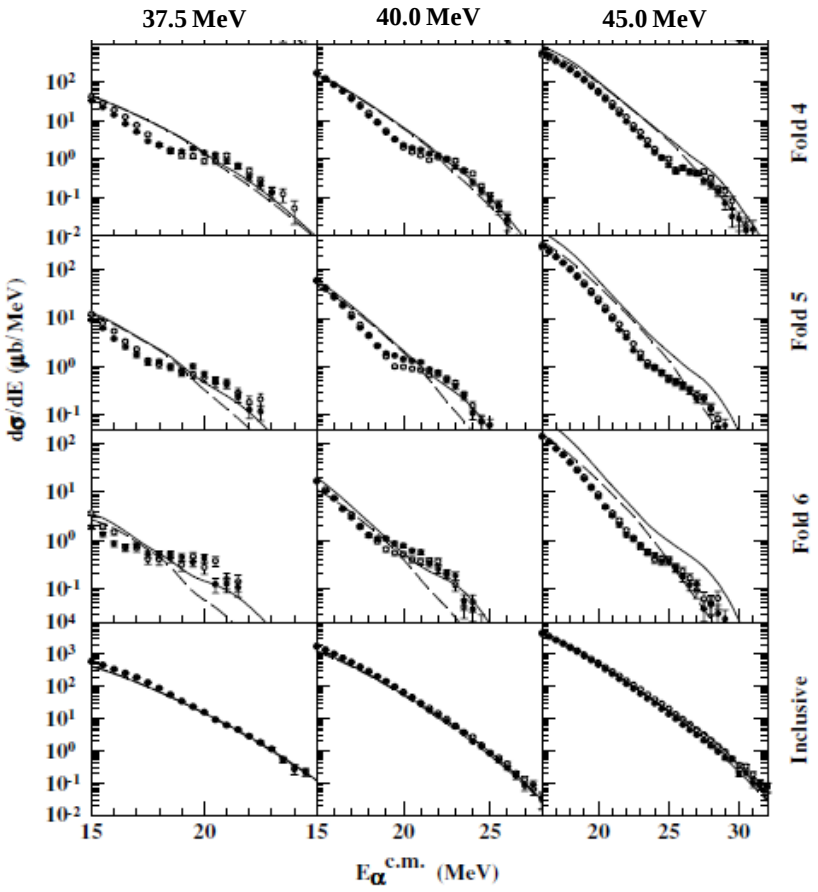

Figure 2.2: *Experimental proton spectra in the c.m. in case of* ^{12}C + ^{93}Nb *(closed circles) reaction for different fold (angular momentum) windows, taken from Ref. [52].*

erly explained by the available prescriptions of the spin dependence of nuclear level density. In these cases, additional dependence on angular momentum was required, which in some instances were incorporated through the variation of the level density parameter with angular momentum. Recently, angular momentum gated charged particle (proton and α-particles) spectra from the ^{12}C, ^{16}O + ^{93}Nb and ^{89}Y reactions were measured by Mitra *et al.* [51, 52]. The authors observed broad bump-like structures in the measured angular momentum gated particle spectra (Figs. 2.1 & 2.2), which could not be explained by the standard level density prescriptions. Although the origin of such feature was not clear, a specific J dependent enhancement in NLD was suggested by the authors to explain the multiplicity gated data. However, contributions of massive cluster transfer from the projectile to target and other direct processes could not be

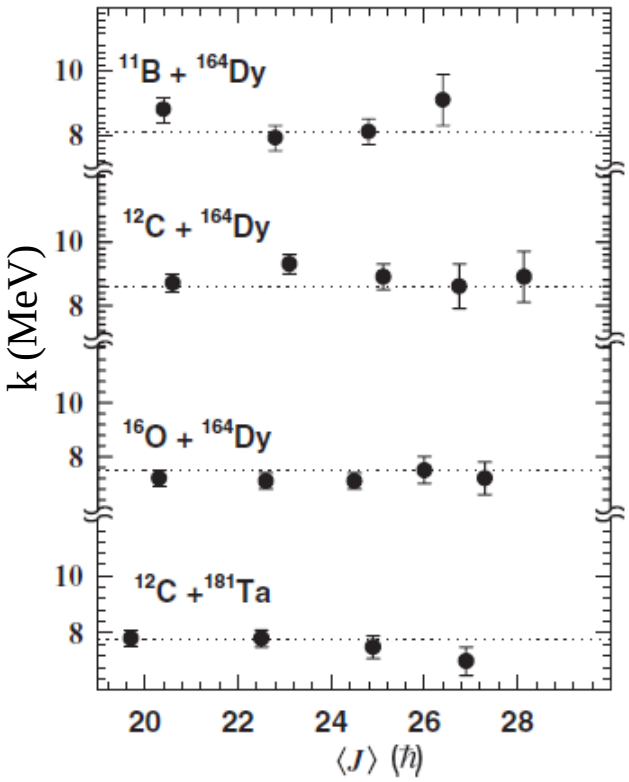

Figure 2.3: *Experimental k values at different angular momentum for nuclei with A~180 [53].*

fully ruled out from the data of Mitra *et al.* In a couple of recent experiments by Gupta *et al.* [53, 54], angular momentum dependence of NLD were studied by analyzing the α-particle evaporation spectra emitted from various compound systems. The variation of level density parameter (rather the inverse level density parameter, k = A/$\tilde{a}$) as a function of angular momentum were studied in the A ~180 and ~120 mass regions. For nuclei with A ~180, E^*~ 56 - 59, $< J >$ ~ 15 - 30 $\hbar$, the measured k values were found to remain constant within the statistical errors (Fig. 2.3). The observation is in agreement with the standard spin dependence of NLD, where the level density parameter is not expected to depend explicitly on angular momentum. However, in another experiment by Gupta *et al.* at A ~ 120, E^* ~60 MeV, J ~10 - 20 $\hbar$, rather irregular variation of the inverse level density parameter was observed [54]. For Z_R = 49, 50, and 51, (Z_R is the atomic number of the evaporation residue) k was found to be almost constant while for the other systems it was observed to increase significantly with increasing angular momentum (Fig. 2.4). On the other hand, Agarwal and Kailas [64]

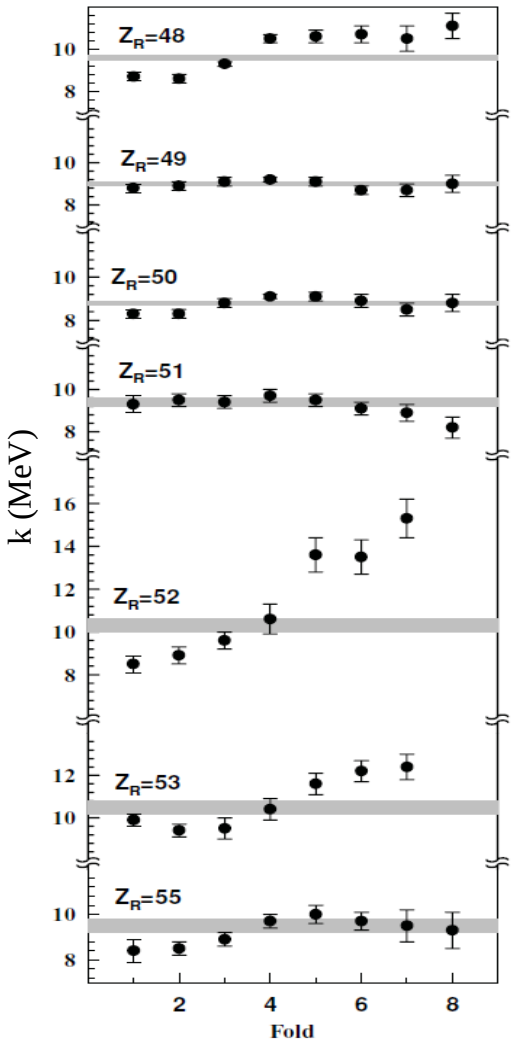

Figure 2.4: *Experimental k values at different folds for systems with A~120, taken from Ref. [54].*

had carried out a theoretical calculation based on deformed shell model to investigate the angular momentum dependence of the level density parameter for similar systems in the A ~120 region that was experimentally studied by Gupta *et al.* [54]. The calculation showed a smooth increase of the inverse level density parameter with increasing angular momentum for all the systems in this region as shown in Fig. 2.5. However, in a recent measurement of angular momentum gated neutron evaporation spectra for nuclei with A ~ 118, excitation energies E^*~31 and 43 MeV and angular momentum J ~10 - 20 $\hbar$, the inverse level density parameter was observed to decrease consider-

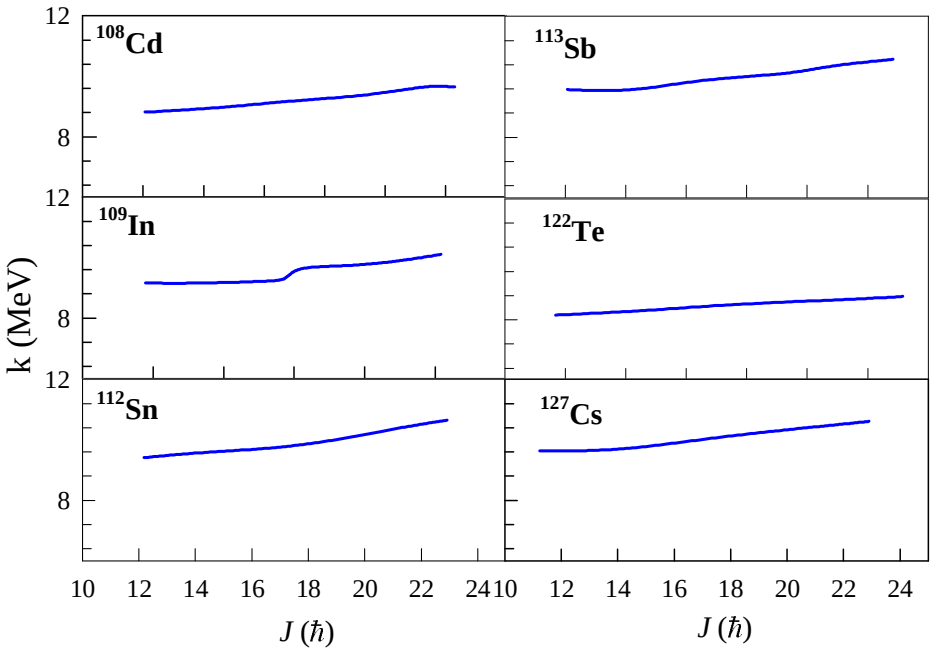

Figure 2.5: *Variation of the inverse level density parameter as a function of angular momentum from Ref. [64].*

ably with increasing angular momentum [55].

So, from the above discussion it is evident that our understanding of the variation of NLD as a function of angular momentum is not conclusive, there is disagreement between theory and experiment; moreover, the experimental results from neutron and charged-particle measurements are different in some cases. Therefore, further investigations in this area will certainly be useful. It will also be interesting to observe the variation of the level density parameter as a function of J estimated from different light particle measurements simultaneously. Such a measurement to our knowledge has not been carried out in the past. So, with this aim, we have measured light-particle (n, p, and α) evaporation spectra along with the γ-multiplicity in the ^{4}He + ^{93}Nb and ^{4}He + ^{58}Ni reactions. Simultaneous analysis of different particle spectra in the same experiment will be useful to understand the angular momentum dependence of NLD in a consistent manner.

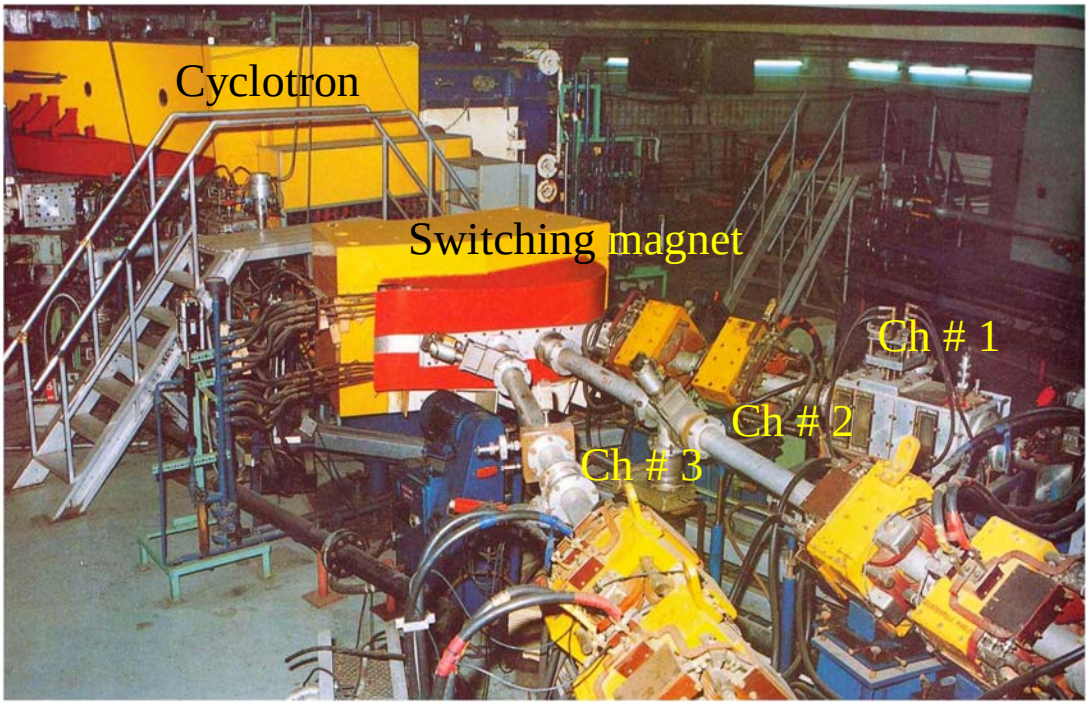

Figure 2.6: *K130 variable energy cyclotron.*

2.2 Experiment

The experiment was performed using 35 MeV ^{4}He-ion beam from the *K130* cyclotron at the Variable Energy Cyclotron Centre, Kolkata. It is an azimuthally varying field (*AVF*) cyclotron with a pole diameter of 224 cm. Fig. 2.6 shows the view of the cyclotron with the switching magnet and different beam lines. The current experiment (and the other experiments for the present thesis work) has been performed in the third beam line (Ch #3), which is dedicated to the studies involving detection of neutrons and γ-rays. A small and compact cylindrical stainless steel reaction chamber having very thin walls (wall thickness $\sim$ 3 mm), was used for the experiment. This is particularly suited for measurements involving neutron and/or γ-rays. Fig. 2.7 shows an actual photograph of the experimental setup, and various detector systems used in the experiment are shown in Fig. 2.8. In the present experiment two self-supporting foils of ^{93}Nb and ^{58}Ni (99.9% enriched) with thicknesses$\sim$1 mg/cm^2, were used as targets. The targets were prepared at VECC by rolling thin metallic foils of the elements. The

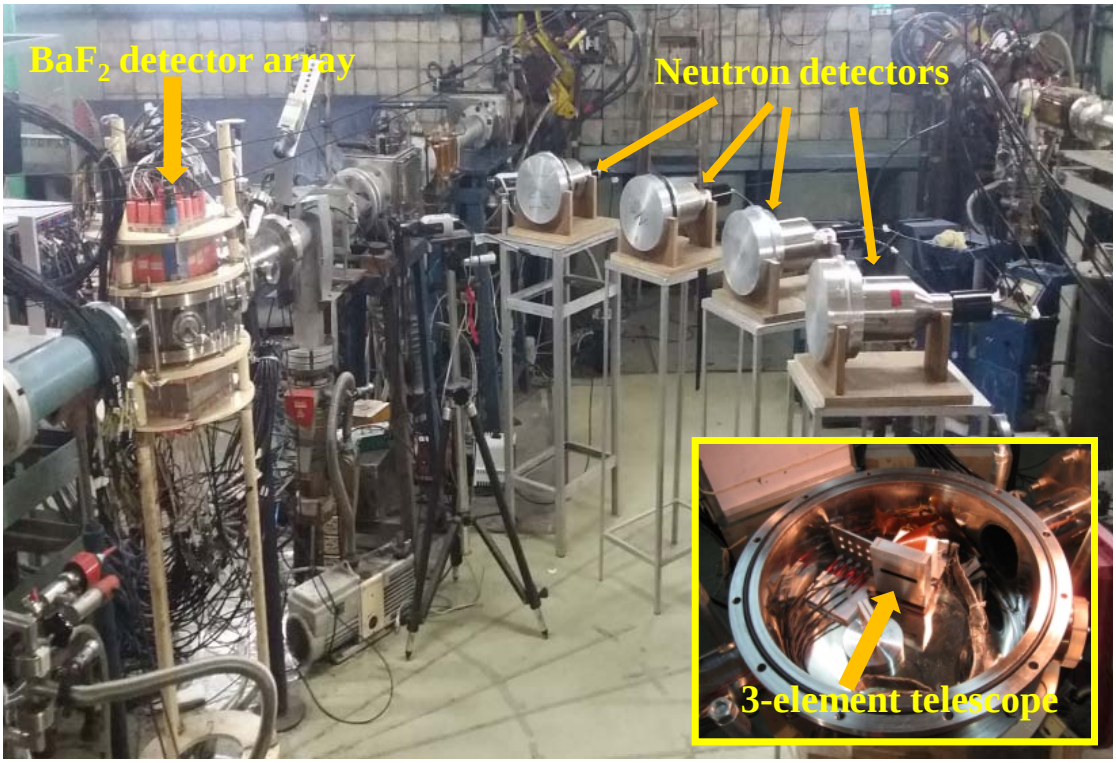

Figure 2.7: *Experimental setup*

compound nuclei ^{97}Tc* (^{4}He + ^{93}Nb) and ^{62}Zn* (^{4}He + ^{58}Ni) were populated by complete fusion reactions at an excitation energy of 36 MeV. The charged particles emitted in these reactions were detected and identified using a 3-element detector telescope consisting of a 50 μm single-sided silicon strip detector (16 channels), 500 μm double-sided silicon strip detector (16 $\times$ 16 channels) and two CsI(Tl) detectors (thickness 4 cm) at the back. The charged particle detector telescope was mounted at a mean angle of 147° covering an angular range of ±17.5°. While taking data from the 16×16 strip detectors, only 4 central horizontal (Y) strips were kept open and data of the three consecutive vertical (X) strips were added together to increase the statistics. Emitted neutrons were detected using six liquid-scintillator (BC501A) based neutron detectors, each covering a solid angle ~ 5.63 mSr. The neutron detectors were placed outside the scattering chamber at angles 45°, 75°, 90°, 100°, 120° and 150° with respect to the beam direction, at a distance of 150 cm from the target. The neutron detection thresholds were kept at 100 KeVee by calibrating the detectors with standard γ-ray sources

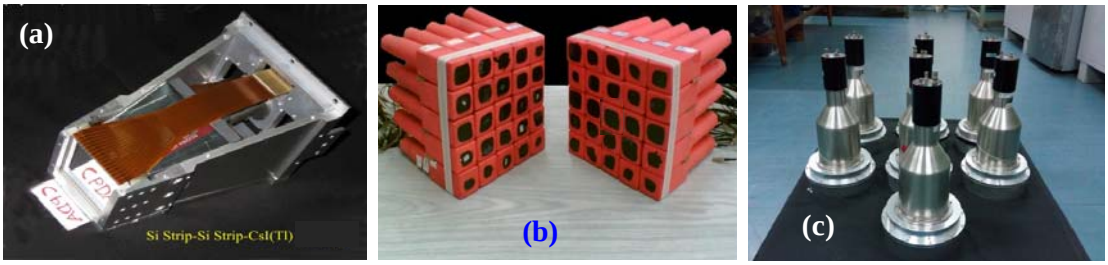

Figure 2.8: *Different detector systems used in the experiment, (a) the 3 element detector telescope, (b) BaF_2 detector array and (c) neutron detectors.*

(see Apendix A). The energy of the emitted neutrons has been measured using the time of flight (TOF) technique where a common start for the TOFs was taken from the γ-ray trigger generated using a 50-element BaF_2 detector array placed very close to the targets. The neutron-γ discrimination was achieved by using both pulse shape discrimination (PSD) and time of flight methods. The beam dump has been kept at a distance of ~3 m from the target position and shielded on all sides with layers of lead and borated paraffin to minimize the contribution of background neutrons coming from the beam dump. The scattered neutron contribution was estimated by blocking the neutrons from the target reaching the detectors with the help of 30 cm thick high-density plastic (HDP) blocks placed in between the target and the neutron detectors. In the present experiment, populated angular momenta were estimated by measuring the multiplicity of low energy γ-rays, using the 50-elements BaF_2 detector array; developed recently at VECC [65]. The array is made up of 50 individual square shaped BaF_2 crystals having cross-section 3.5×3.5 cm^2, and 5 cm in length (Fig. 2.8b). The multiplicity filter was split into two blocks of 25 detectors each and was placed on the top and bottom of the reaction chamber in a staggered castle type geometry. Typical solid angle coverage of the multiplicity filter was about ~33%. The filter records the number of detectors fired simultaneously (designated as *fold*, *F*) in each event in coincidence with the detected light-particles. The experimentally measured fold is directly related to the multiplicity of low energy γ-rays which in turn proportional to the populated angular momentum.

2.2.1 Electronic setup

Standard analog readout electronics have been used for processing and acquisition of the detector signals. The signals from the Si-strip detectors have been fed to the 16-channel pre-amplifiers (Mesytec MPR-16) [66]. The energy and timing outputs (from E detector only) of all pre-amplifiers have been fed to the input of 16 channel combined Shaper, Timing Filter, and Discriminator module (MSCF-16) [67]. The signals from the combined CsI(Tl)-PIN diode detectors have been directly fed to the integrated preamplifier and then connected to the spectroscopic amplifiers (ORTEC 572A). Outputs of the amplifiers have been fed to the inputs of the analog to digital converter (ADC). The logic outputs of the discriminators (CFD) have been fed to gate and delay generator (ORTEC GG8020) and then to a coincidence unit (PS 756) to extract logic OR output. The signal from each neutron detector was connected to a splitter to divide the anode pulse into two equal parts without any cable reflection. One of the splitter outputs was connected to the leading edge discriminator (LED, Phillips Scientific 710) and the other output was connected to the neutron-gamma discriminator module (Mesytec MPD-4) [68]. This module (MPD-4) provides simultaneously the pulse height (PH), timing trigger (using a CFD) and the zero cross over (ZCO) outputs. The CFD outputs were connected to the TDC (range 400 nS) as the STOP signals to get neutron time of flight information. The PH and ZCO were connected to the ADC to get the pulse height and the pulse shape information. The discrimination between the neutron and the γ-rays was achieved by using ZCO and TOF outputs. The LED outputs of the six neutron detectors were connected to the coincidence unit to extract logic OR output. A layout of the electronic setup used in the experiment has been shown in Fig. 2.9. A trigger from the BaF_2 multiplicity filter was generated when any two out of 50 detectors fired in coincidence over a detection threshold of 250 keV. The signals from the multiplicity filter were fed to constant-fraction-discriminators (CFD) (CAEN C808) and the output currents (1 mA per hit) were summed in a Linear-Fan-in module. The summed output was fed into a QDC (CAEN VME792) and integrated for a gate duration of 30 ns to generate, on the event-by-event basis, the experimental fold

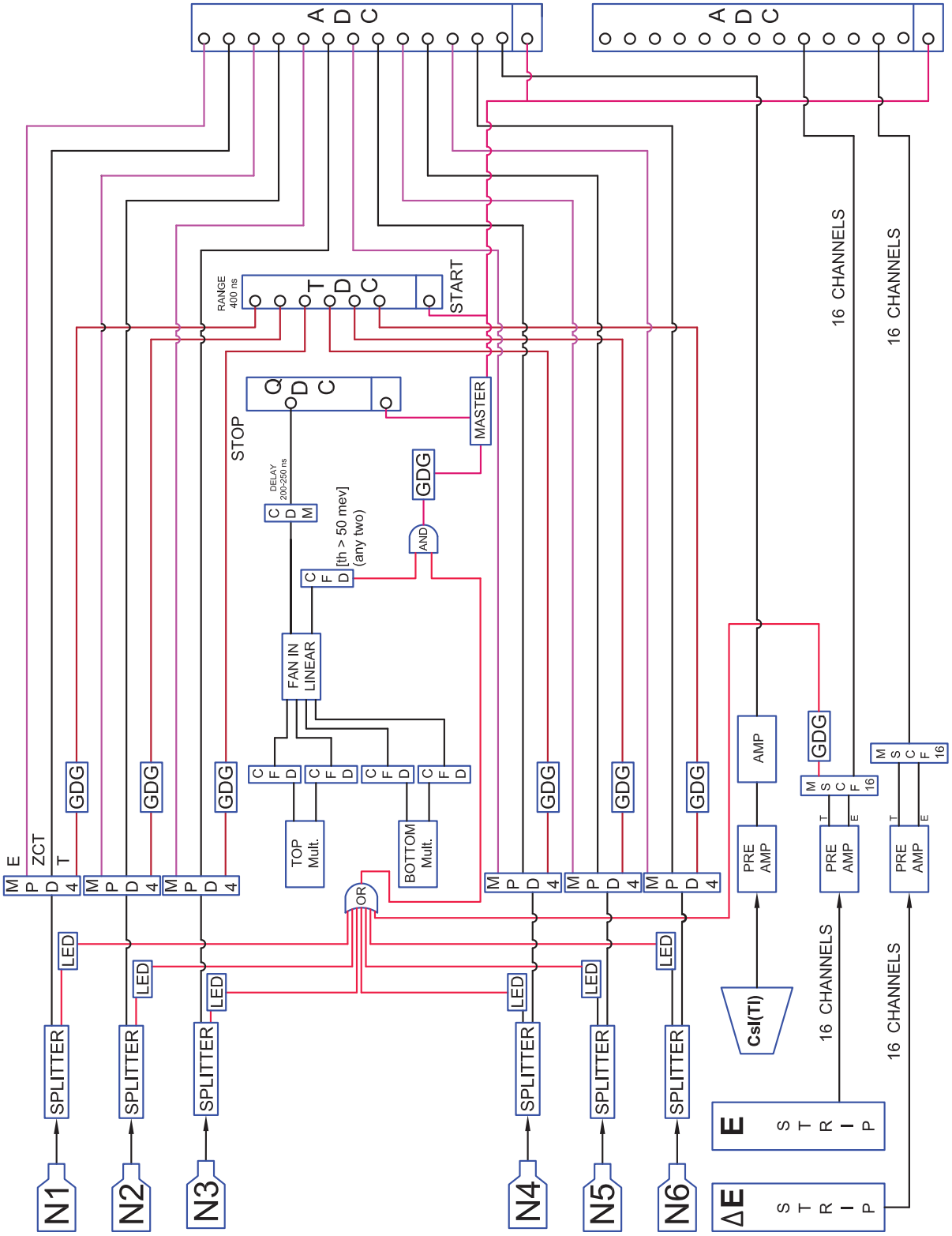

Figure 2.9: *A Layout of the electronics setup*

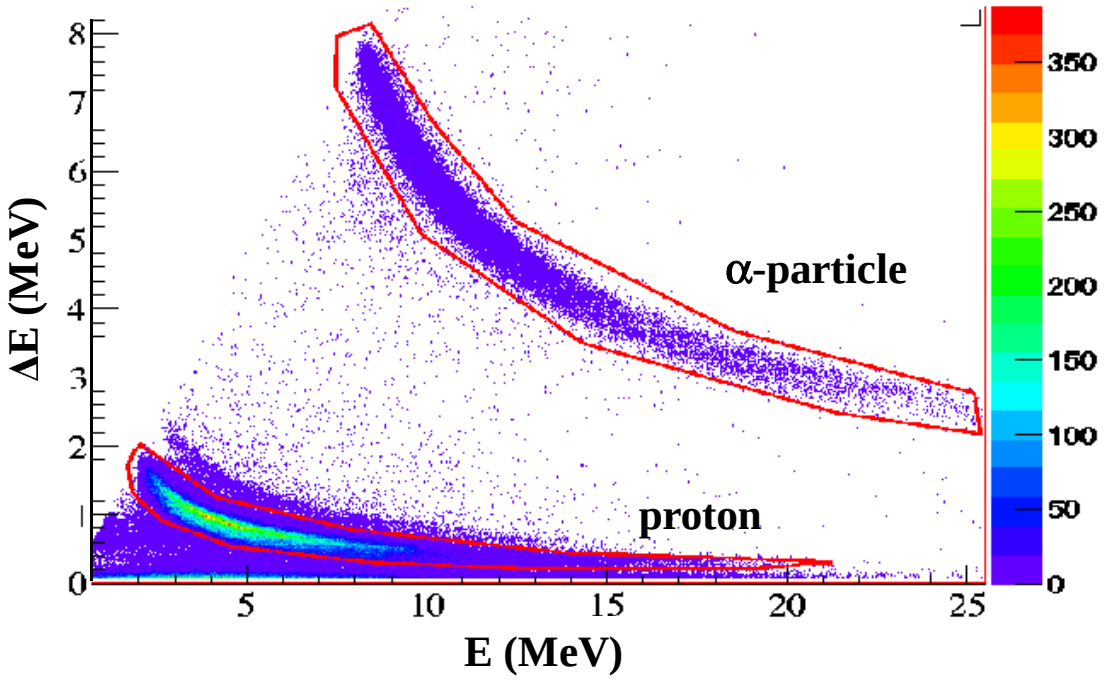

Figure 2.10: *A typical 2-dimensional ΔE - E plot.*

(F) distribution with condition ($F \geq 2$). The final master trigger was generated when at least two of the multiplicity detectors fired in coincidence with any one of the six neutron detectors OR charged particle detectors. This master trigger was connected to the STROBE inputs of the ADC, QDC and common start trigger of the TDC. A VETO signal was generated by connecting the BUSY outputs of the ADCs, TDC, and QDC in parallel. The master trigger was vetoed by this signal. This is essential to ensure event correlation between ADC, TDC, and ODC in a VME based data acquisition system. The experimental data were recorded in the event-by-event mode using a VME based data acquisition program (VECC VME-DAQ) developed at VECC. The detail of the off-line analysis of the data has been described in the following section.

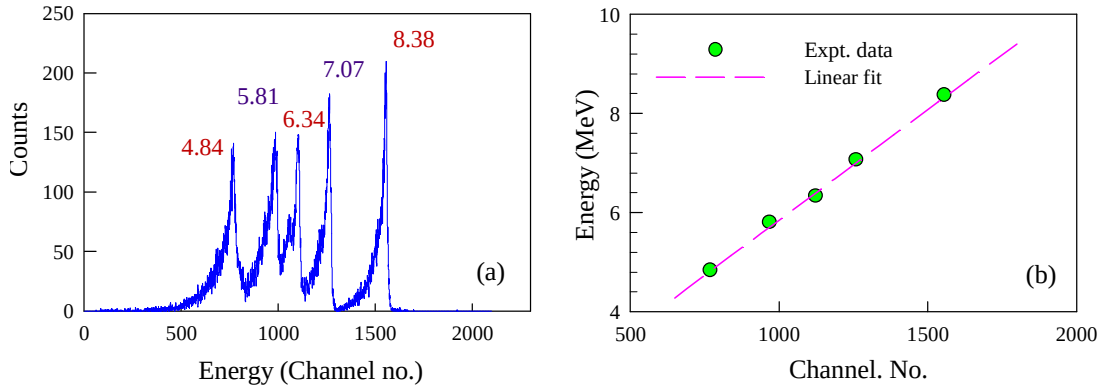

Figure 2.11: *(a) Energy spectra of the ^{229}Th α-particle source, the energy values (in MeV) have been indicated above each peak. (b) Calibration for the Si strip detector.*

2.3 Data analysis technique

2.3.1 Analysis of charged particles

As mentioned in the last section, the charged particles have been detected using a 3-element detector telescope. Different charged particles were identified from the ΔE - E_R correlation plot as shown in Fig. 2.10 for the ^{4}He + ^{58}Ni reaction. Proton and α-particle bands can be clearly identified from the plot. Energy calibration for the Si detectors was performed using standard ^{229}Th α-particle source. The energy spectra of the α-particles emitted from the ^{229}Th source and the calibration of the Si-detector are shown in Fig. 2.11. The CsI(Tl) detectors were calibrated (for proton) using the ΔE - E_R correlation plot, where ΔE is the energy lost in the two strip detectors (50 + 500 μm) and E_R is the remaining energy that is deposited in CsI(Tl). The ΔE values were calculated using the calibrations of the Si-detectors, and the E_R values corresponding to a given ΔE were estimated from the energy loss calculation performed using the SRIM software [69]. The calibration for CsI(Tl) is best represented by a quadratic relation given by

$$E = A \times (Channel \quad no)^2 + B \times (Channel \quad no.) + C \tag{2.3}$$

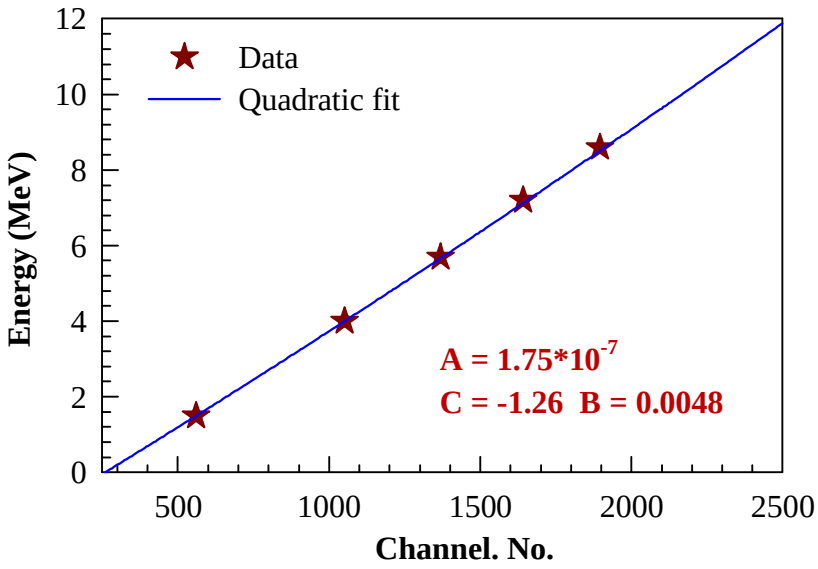

Figure 2.12: *Calibration for CsI(Tl) detector.*

The calibration curve for one CsI(Tl) detector is shown in Fig. 2.12. The kinetic energy spectra of the α-particles and protons were obtained by taking the projection of the 2-dimensional ΔE-E_{tot} plot applying suitable particle gates.

2.3.2 Analysis of neutron data

The energy of the neutrons was measured by the time of flight technique. The TOF spectra were obtained by taking projection of the 2-dimensional ZCO vs. TOF spectra (Fig. 2.12) into the TOF axis using two-dimensional gate as shown by the red contour in Fig. 2.12. Energy of the neutron is related to the flight time by the simple (non-relativistic) relation,

$$E_n = \frac{1}{2} m_n \left(\frac{l}{t_n} \right)^2 \qquad (2.4)$$

Where, m_n is the mass of the neutron, l is the flight path, and t_n is the neutron time of flight. The observed TOF spectra were transformed into energy spectra incorporating proper Jacobian for the transformation. The Jacobian ensures that the number of events (counts) remains conserved during the course of transformation from the time domain

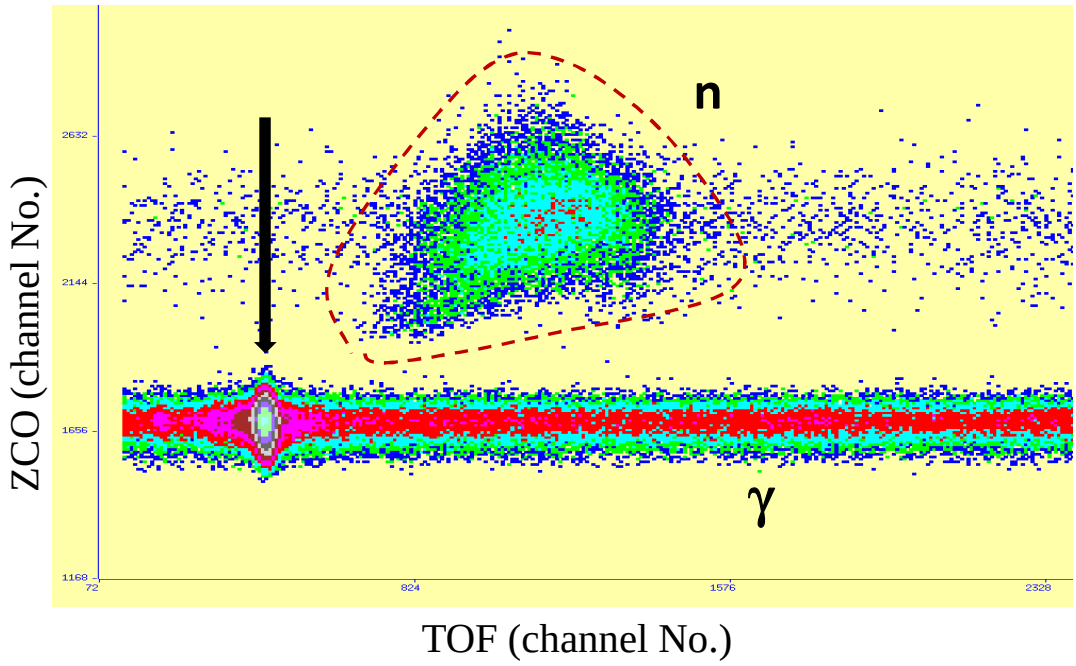

Figure 2.13: *A typical 2-dimensional ZCO vs. TOF plot.*

to the energy domain, *i.e.*

$$N(E) \cdot \delta(E) = N(t) \cdot \delta(t) \tag{2.5}$$

$$N(E) = N(t) \cdot \left| \frac{\delta t}{\delta E} \right| \tag{2.6}$$

where, N(t) is the number of event in a time bin δt, and N(E) is the corresponding number of events in the energy bin δE. Therefore, the Jacobian for the current transformation is given by (using Eqns. 2.4 and 2.6),

$$\left| \frac{\delta t}{\delta E} \right| = \frac{t}{2E}. \tag{2.7}$$

Proper time calibration of the TDC is absolutely essential in order to measure the neutron energy through the time of flight method accurately. The time calibration was performed using a precision time calibrator (ORTEC 462). Time calibration graph of a typical neutron detector is shown in Fig. 2.11. In converting the neutron TOF to neutron energy, the prompt γ peak in TOF spectra (indicated by the thick arrow in Fig. 2.12) was used as the time reference.

The energy dependent detection efficiency [ε(E)] of a neutron detector, which is a very

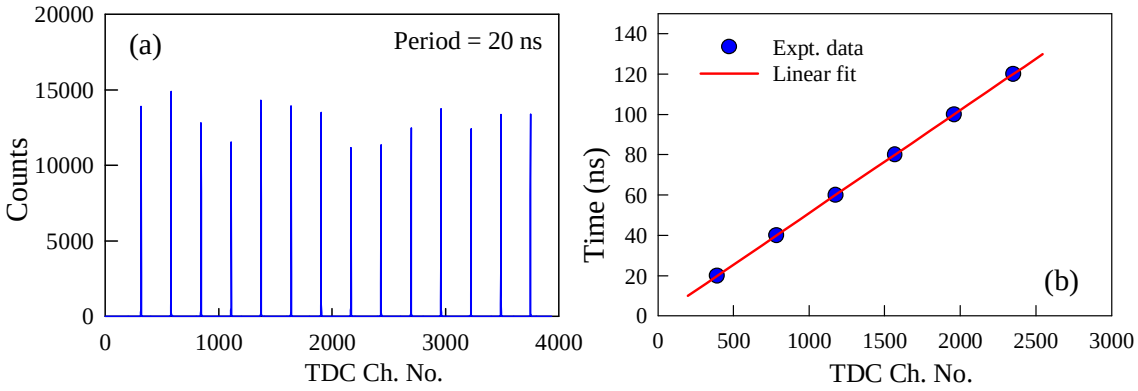

Figure 2.14: *TDC time calibration.*

crucial quantity, has been measured in the in-beam condition using a ^{252}Cf fission neutron source. The detector efficiency is determined by dividing the neutron energy spectrum per fission by the expected energy distribution for ^{252}Cf which is given by [70],

$$N(E) = \frac{2\sqrt{E}exp(-E/T)}{\sqrt{\pi}(T)^{3/2}} \tag{2.8}$$

The ideal and measured neutron energy spectra of ^{252}Cf is shown in Fig. 2.15(a). The detection efficiency as a function of neutron energy was also calculated with the Monte Carlo based NEFF simulation [71]. The Fig. 2.15(b) shows the experimental (symbol) and simulated efficiency (line) for a typical detector. Reasonable agreement between the measured and simulated efficiencies are obtained for all the detectors.

The proper estimation and reduction of the background contribution is very important for neutron measurements. In this case the background consists of neutrons which reach the detectors after being scattered from various parts (*e.g.* beam dump, floors, walls, other materials) of the experimental area. The background neutron contribution have been measured by putting 30 cm thick blocks of high density plastic in between the target and detectors. This stops the neutrons coming from the target and only the scattered neutron could reach up to the detector. The background spectrum has been measured in this way and subtracted from the data to get the background corrected spectra. The measured background spectrum along with the background corrected and background uncorrected spectrum in the case of ^{4}He + ^{93}Nb reaction has been shown in Fig. 2.16.

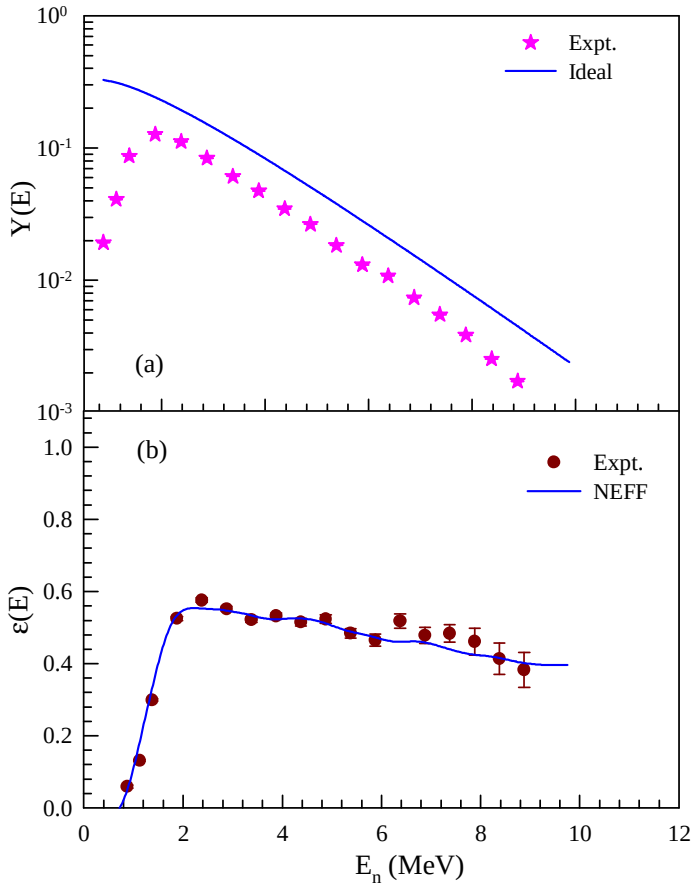

Figure 2.15: *(a) Measured (symbol) and theoretical neutron spectra for ^{252}Cf, (b) Measured (symbol) and simulated (line) efficiency of the neutron detector.*

2.3.3 Fold to angular momentum conversion

In the process of de-excitation of an excited compound nucleus formed at an excitation energy E^* and angular momentum J, the excitation energy is primarily reduced by the emission of one or more light particles (*e.g.* neutron, proton and α-particles). However, during the particle emission process, the angular momentum is almost retained in the nucleus as very little angular momentum (on the average) is carried away by the emitted particles. Once the excitation energy of the decaying nucleus becomes less than the particle emission threshold (typically 8 MeV above the *yrast* line which refers to the minimum excitation energy for a given angular momentum) emission of particle is no longer possible, and the nucleus cools down to the ground state ($E^* = 0$,

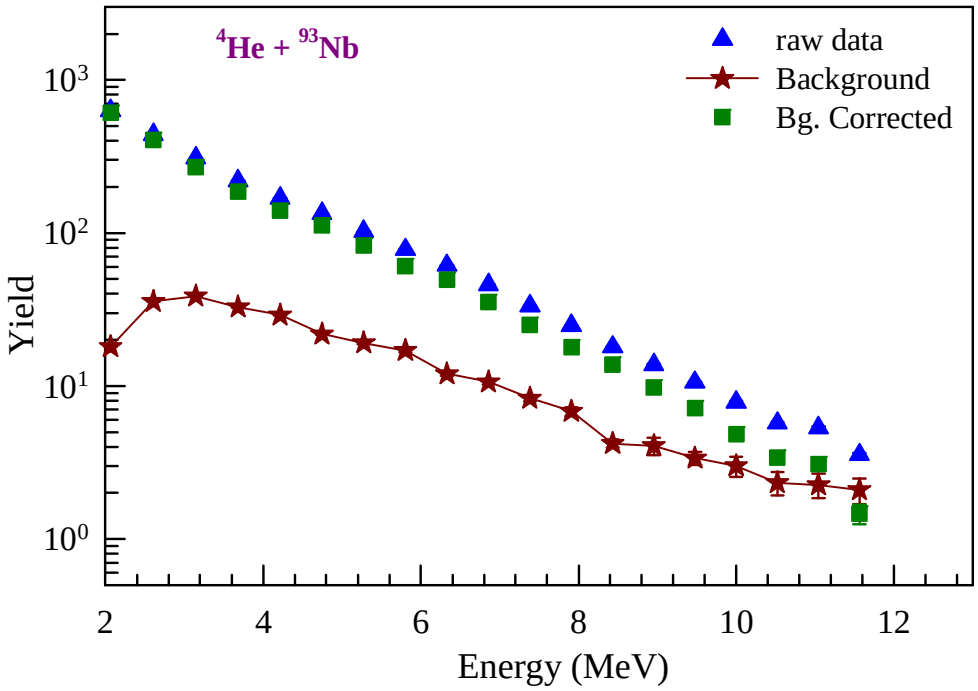

Figure 2.16: *The measured background spectrum (circle) along with the background corrected (square) and background uncorrected (triangle) spectrum in the case of* ^{4}*He +* ^{93}*Nb reaction.*

$J = J_{g.s.}$) losing the residual energy and most of its angular momentum by emitting low energy γ-rays (also known as the multiplicity γ-rays). Most of the emitted γ-rays in this region are E2 in nature (with some small mixture of M1 type transitions), known as the *stretched* E2 transitions. Therefore, the number of emitted low energy γ-rays (γ multiplicity, M_γ) is directly proportional to the angular momentum of the residual nucleus ($M_\gamma \approx J_{res}/2$). Different angular momentum region in the residual nucleus was selected by experimentally measuring the fold (F) distributions using the BaF_2-array. The F distributions can be converted to the M_γ distributions by using the F to M_γ response of the BaF_2 setup which was simulated using a *Monte Carlo* based GEANT3 toolkit [65]. Realistic experimental conditions such as detector threshold, trigger condition, cross-talk probability were taken care of in the simulation. Two blocks of 25 detectors arranged in 5× 5 arrays were kept on the top and bottom of the scattering chamber at a distance of 5 cm from the target position, similar to the experimental condition. The different input multiplicities of the low energy γ-rays were obtained by

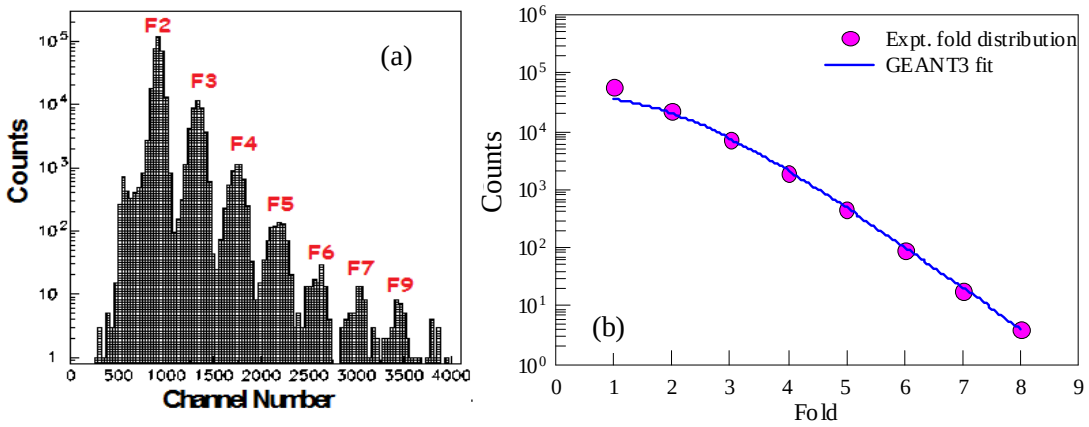

Figure 2.17: *(a) Measured fold distribution (b) Integrated (area under each fold) fold distribution along with GEANT 3 simulation.*

creating a random number according to the multiplicity distribution P(M) given by,

$$P(M) = \frac{2M+1}{1+exp(\frac{M-M_{max}}{\delta m})} \tag{2.9}$$

Low energy gamma rays having randomly generated multiplicity obtained from the above relation, were thrown isotropically from the target centre and the corresponding fold was recorded for that event. A very large number of such events were generated to record the final simulated fold distribution. The simulated fold distribution is then compared and matched with the experimental fold distribution by varying the parameters M_{max} and δm. The measured fold distribution along with the corresponding GEANT3 fit for the ^{4}He + ^{58}Ni reaction are shown in Fig. 2.17. After the simulated fold distribution is matched with the experimental one, the constraint multiplicity distributions for different folds were generated by gating on the events with folds = 2, folds = 3 and folds ≥ 4, respectively. Finally, the angular momentum distributions corresponding to different folds as shown in Fig. 2.18 were obtained from the constrained multiplicity distributions using the relation, $J_{res} = 2M_{\gamma}$ + c, where c is an adjustable parameter.

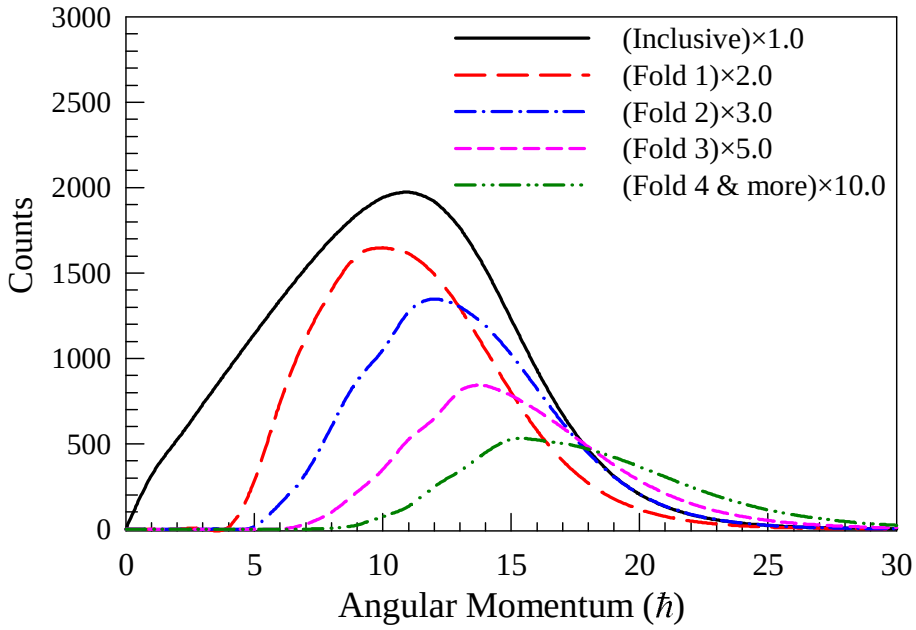

Figure 2.18: *Angular momentum distributions corresponding to different folds as obtained from the GEANT3 simulation in case of the* $^{4}He + {}^{58}Ni$ *reaction.*

2.4 Statistical model calculation

The experimental results (kinetic energy spectra of the emitted light-particles) have been compared with the theoretical prediction obtained using the statistical model code CASCADE [72]. The fundamental basis of describing the decay of an excited nucleus in terms of statistical theory is the *compound nuclear hypothesis* (also known as the *independence hypothesis*) initiated by Niels Bohr [73]. According to the compound nuclear picture the reaction between a target and a projectile nucleus is assumed to occur through two *independent* steps:

1. The formation of an intermediated and equilibrated compound nucleus (CN).

2. The disintegration of the CN into a residual nucleus and a ejectile particle (or into fission fragments) .

A compound nuclear reaction can be symbolically represented as,

$$a + A \longrightarrow [B^{*}] \longrightarrow C + c$$

where the excited CN (B^*), formed due to the collision of the projectile a with the target nucleus A, decays subsequently emitting a particle c (or γ-ray), leaving a residual nucleus C. According to the Bohr hypothesis the intermediate CN is considered to be equilibrated in all degrees of freedom (*e.g.* energy, shape, isospin) and expected to have no memory of the way by which it was formed, so that the process of formation (fusion) of CN and its subsequent decay (evaporation or fission) can be treated independently. This essentially means that the cross section for the desired reaction ($a + A \rightarrow B^* \rightarrow c + C$) is given by

$$\sigma_{\alpha,\beta}(E^*) = \sum_{J,\pi} \sigma_\alpha(E^*, J, \pi) P_\beta(E^*, J, \pi) \tag{2.10}$$

where α and β represents the entrance ($a + A$) and the exit channels ($c + C$), respectively. σ_α is the formation cross-section of the compound nucleus and P_β is the decay probability through the specific exit channel β. The partial cross section for formation of a compound nucleus of spin J and parity π from a projectile and a target nucleus (spins J_P, J_T) at a c.m. energy E is given by

$$\sigma_\alpha(J, \pi) = \pi \lambda^2 \frac{2J + 1}{(2J_P + 1)(2J_T + 1)} \sum_{S=|J_P - J_T|}^{|J_P + J_T|} \sum_{L=|J-S|}^{|J+S|} T_L(E) \tag{2.11}$$

The transmission coefficients T_L are assumed to depend only on the energy and the orbital angular momentum L. Here $S = J_P + J_T$ is the channel spin. The summation over L is restricted by the parity selection rule $\pi = \pi_P \pi_T (-1)^L$. The transmission coefficient is generally approximated by the simple Fermi distribution,

$$T_L = \frac{1}{1 + exp[-(L - L_0)/d]}, \tag{2.12}$$

the parameters L_0 and d are fixed by reproducing the measured fusion cross section. The decay probability (P_β) can be written as the ratio of the partial decay width (through the channel β) to that of the total decay width

$$P_\beta = \frac{\Gamma_\beta}{\sum_\beta \Gamma_\beta} \tag{2.13}$$

The partial decay widths (Γ_β) for light particle evaporation have been calculated according to the Hauser-Feshbach (HF) formalism [74],

$$\Gamma_\beta = \frac{1}{2\pi\rho_{CN}(E^*, J_{CN})} \int d\epsilon \sum_{J_d=0}^{\infty} \sum_{J=J_{CN}-J_d}^{J_{CN}+J_d} \sum_{l=J_d-S_\beta}^{J_d+S_\beta} T_l(\epsilon)\rho_d(E^* - B_\beta - \epsilon, J_d) \qquad (2.14)$$

Here, J_d is the spin of the daughter nucleus. S_β, J, l, ϵ and B_β are the spin, total angular momentum, orbital angular momentum, kinetic energy and binding energy of the emitted particle, respectively. ρ_d and ρ_{CN} are the level densities of the daughter and compound nucleus. $T_l(\epsilon)$ is the transmission coefficient or barrier penetration factor for the evaporated particles. The transmission coefficients were calculated (actually for the inverse reactions, *i.e.* scattering of c on C at various energies) using optical model (OM) [75, 76, 77], where the OM potentials for neutron, proton and α-particle were taken from the prescriptions of Wilmore and Hodgson [78], Perey [79], and Huizenga and Igo [80], respectively. The nuclear level density (ρ) has been evaluated using the phenomenological BSFG formulation (Eqn. 1.25) with the spin dependence incorporated through the rotational energy, *i.e.*,

$$\rho(E, J) = \frac{\sqrt{\pi}}{12} \frac{exp(2\sqrt{aU})}{a^{1/4}U^{5/4}} \qquad (2.15)$$

where,

$$U = (E - \Delta - E_{rot}). \qquad (2.16)$$

E_{rot} is defined through the Eqns. 2.1 and 2.2. The quantity U is nothing but the thermal excitation energy which is related to the temperature (T) by the relation, $T \simeq \sqrt{U/a}$. The shell effect in NLD has been incorporated through the parametrization of the level density parameter, a as given by Eqn. 1.33. However, it should be mentioned that for the current systems the shell corrections are small. Therefore, in the studied excitation energy region level density parameter is mostly determined by its asymptotic value (*i.e.* $a \approx \tilde{a}$). The asymptotic level density parameter is estimated as $\tilde{a} = A/k$, where the inverse level density parameter k is treated as a free parameter which is determined by

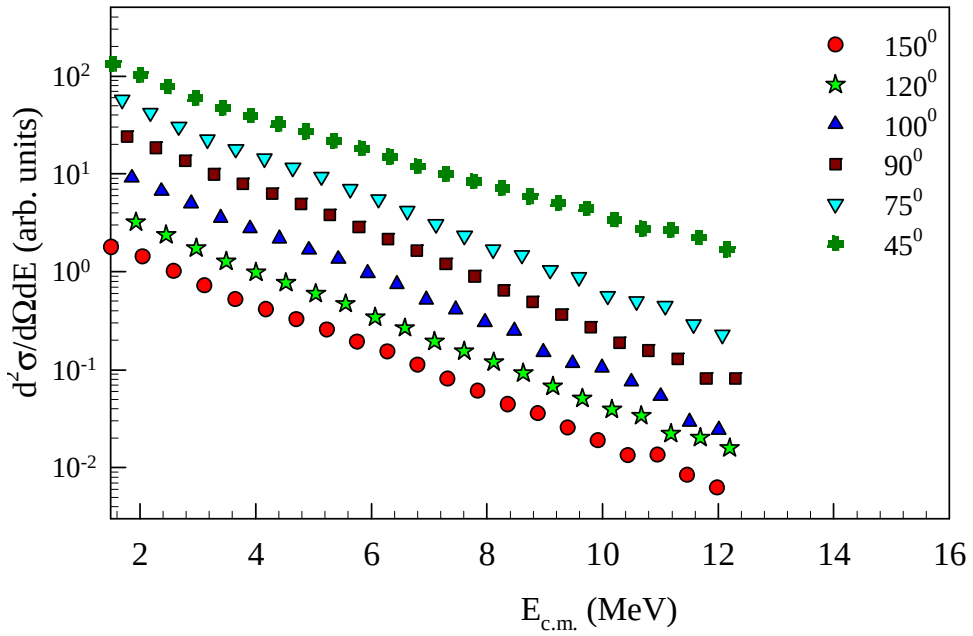

Figure 2.19: *Neutron energy spectra at different angles.*

fitting the experimental data. The experimentally determined angular momentum distributions corresponding to different γ-folds (as shown in Fig. 2.18 for the ^{4}He + ^{58}Ni reaction) were used as inputs in the CASCADE calculations to compare with the experimental fold gated energy spectra.

2.5 Results and discussions

Fold gated neutron, proton and α-particle kinetic energy spectra were generated from the raw data using proper calibrations and efficiency corrections (for the neutron detectors) as described in the last section. The energy spectra measured at various laboratory angles, were transformed to the compound nucleus center-of-mass frame. In the c.m. frame, the spectra measured at different angles (particularly at the backward angles) were found to be almost overlapping, indicating that the spectra originated from an equilibrated compound nuclear source. The neutron energy spectra measured

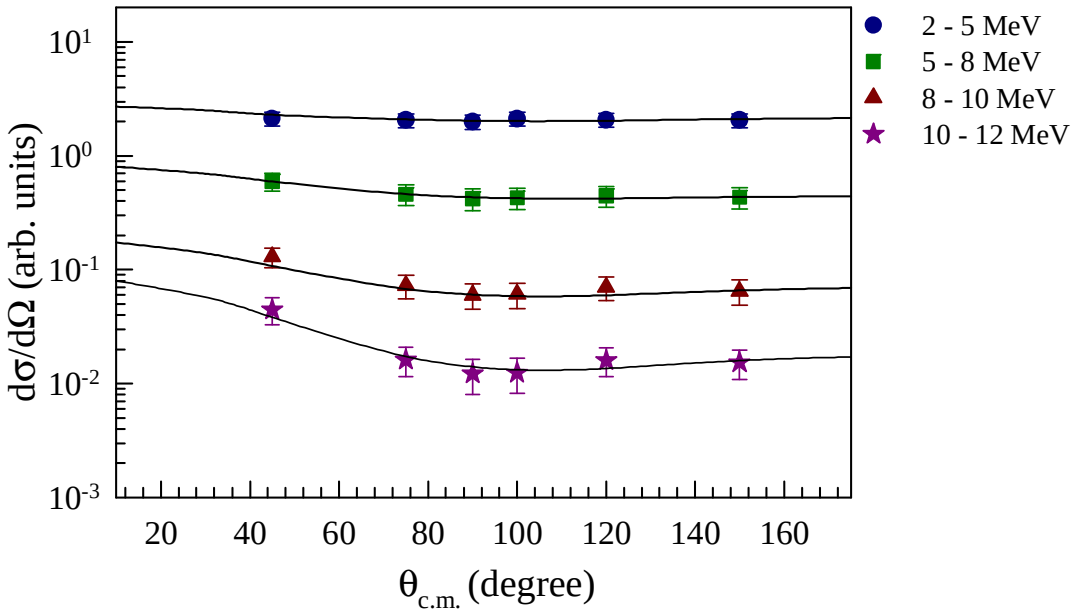

Figure 2.20: *Experimental neutron angular distributions (symbols) at different energy bins. Continuous lines are phenomenological fits using Eqn. 2.17*

at different angles are shown in Fig. 2.19. The angular distribution of the neutrons were extracted for four neutron energy bins (2 - 5, 5 - 8, 8 - 10 and 10 - 12 MeV) which are plotted in Fig. 2.20. The measured angular distributions were compared with the phenomenological Kalbach formula [81] given by,

$$\sigma(\theta) = C[exp(a_d cos\theta) + R\{exp(a_c cos\theta) + exp(-a_c cos\theta)\}], \qquad (2.17)$$

which takes into account contributions due to both compound and direct reaction mechanisms. The first term in Eqn. 2.17 describes the forward peaked component (direct) and the second one with the relative contribution R is related to the symmetric (compound) component of the angular distribution. Parameters a_d and a_c describe the steepness of the slope for both direct and compound components, respectively. It has been observed from the phenomenological fits of the neutron angular distributions (continuous lines in Fig. 2.20), that the contribution of the direct component is small (less than 10% for neutron energy up to 10 MeV). Experimental neutron, proton and α-particle spectra for different Folds (corresponding to different angular momentum regions) are shown in Figs. 2.21, 2.22 and 2.23, respectively. The experimental spectra

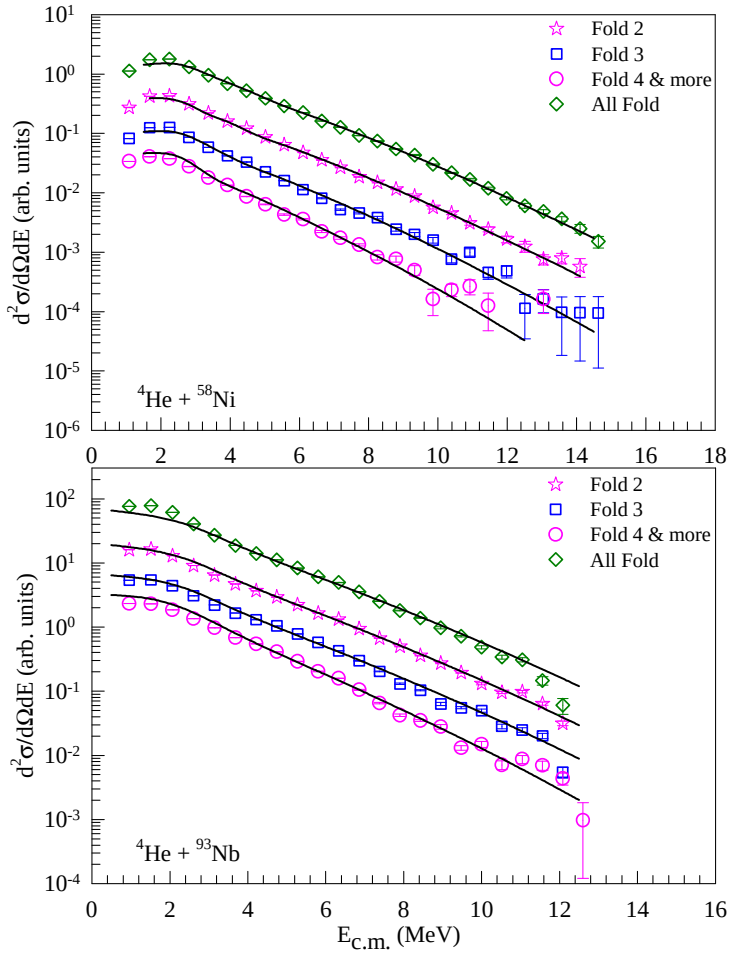

Figure 2.21: *Experimental neutron energy spectra for different folds (symbols) along with the theoretical fits (continuous lines) using statistical model code CASCADE for the* ^{4}*He +* ^{58}*Ni and* ^{4}*He +* ^{93}*Nb reactions.*

were compared and reproduced by the CASCADE calculation. It was found that variation in the OM parameters, thus in the transmissions coefficients had very little effect in determining the shape of the kinetic energy spectra (particularly the high eregy tail part), which were mostly determined by the value of the level density parameter. The role of the deformability parameters (δ_1 and δ_2) (in Eqn. 2.2) was also found to be insignificant for the neutron and proton spectra for both ^{4}He + ^{58}Ni, and ^{4}He + ^{93}Nb reactions. However, the shape of the α-particle spectra showed appreciable change with the variation of δ_1 and δ_2 in case of ^{4}He + ^{58}Ni system, although for ^{4}He + ^{93}Nb system role of δ_1 and δ_2 were still insignificant. Fig. 2.24 shows the

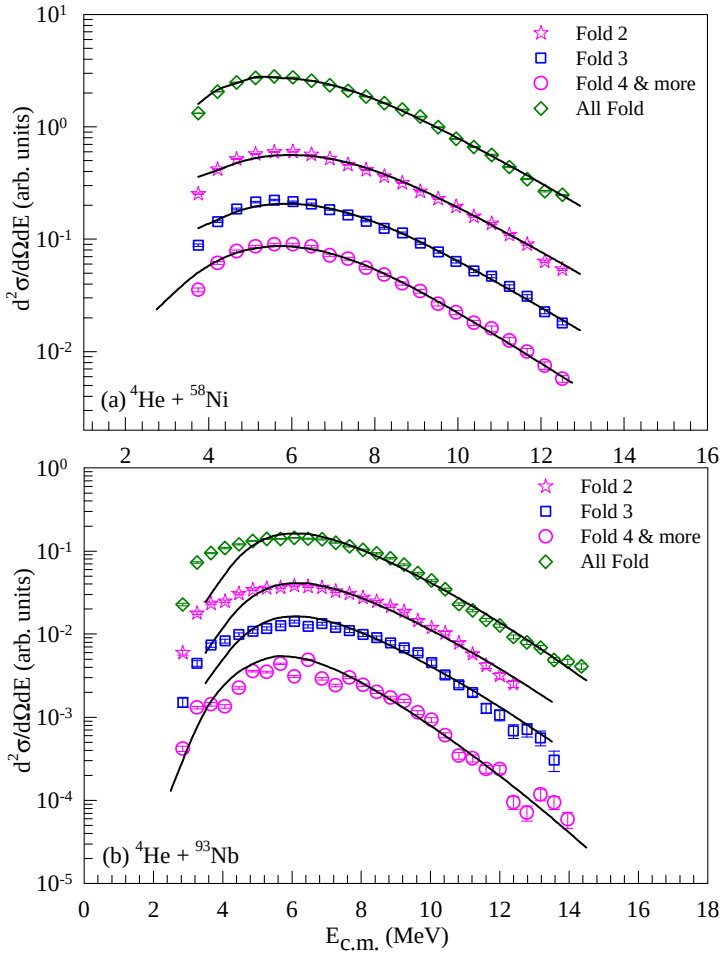

Figure 2.22: *Same as Fig. 2.21 but for protons.*

effect of δ_1 and δ_2 in the *all fold* (inclusive) α-particle spectra for ^{4}He + ^{58}Ni, and ^{4}He + ^{93}Nb reaction. The shape of α-particle spectra for the ^{4}He + ^{93}Nb reaction remains almost same as the deformability parameter were changed from δ_1=6.6×10^{-6}, and δ_2=9.7×10^{-9} (values calculated using rotating liquid drop model (RLDM) [82]), to δ_1=6.6×10^{-4}, and δ_2=9.7×10^{-6}. However, the shape of α-particle spectra for the ^{4}He + ^{58}Ni reaction showed significant change as the deformability parameters were changed from its RLDM values (δ_1=3.9×10^{-5}, and δ_2=4.5×10^{-8}). It was possible to fit the α-particle spectra in this case with much higher values of the deformability parameters (δ_1=3.9×10^{-4}, and δ_2=5.5×10^{-6}). In fixing the δ values for the ^{4}He + ^{58}Ni reaction, the level density parameter was taken as $a = A/9$; this has been fixed by fitting the neutron and the proton spectra, where the spectra were only sensitive to

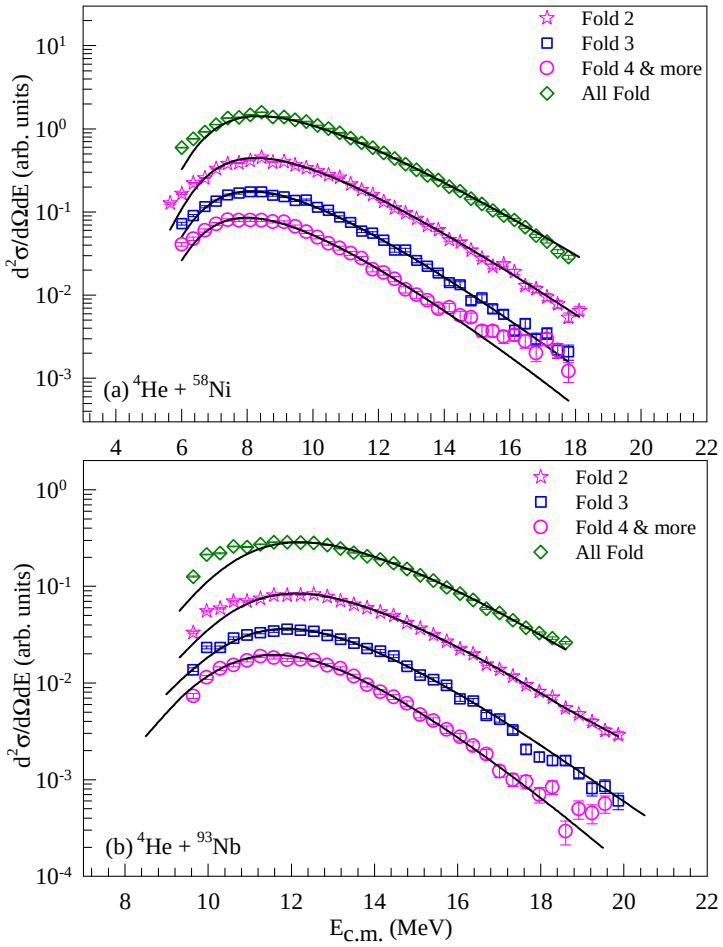

Figure 2.23: *Same as Fig. 2.21 but for α-particles.*

a. For the ^{4}He + ^{93}Nb reaction the RLDM values of δ_1 and δ_2, were used. For the analysis of the fold gated spectra further variation of δ_1 and δ_2 could not explain the experimental data. Thus during the analysis of the particle spectra with different fold gating, all parameters other than the level density parameter were kept fixed to its *all fold* value. The inverse level density parameter *k*, were varied to get the best fit to the experimental data for different folds. Optimum (best fit) values of the inverse level density parameters were obtained from the experimental data by the χ^2 minimization technique. The χ^2-values as a function of the inverse level density parameter obtained form the inclusive neutron spectra for the two reactions are shown in Fig. 2.25. The error (δk) in the fitted *k* values are obtained using the prescription of Ref. [83]. The best fit values of the inverse level density parameter as obtained from the theoretical fits to

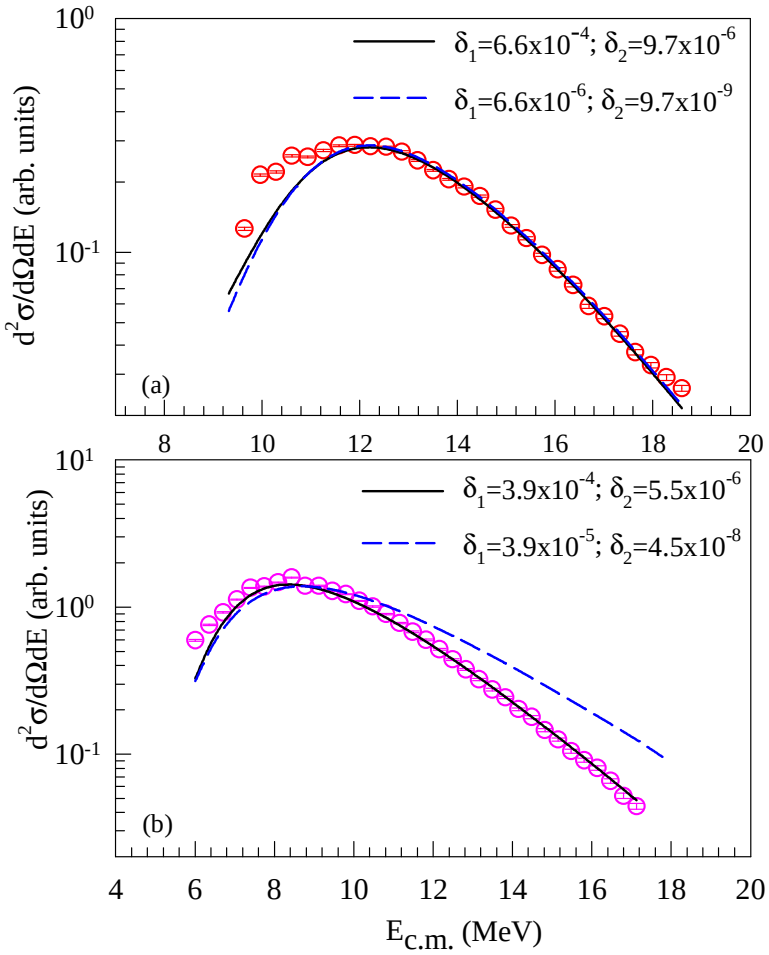

Figure 2.24: *Effect of deformability parameters (δ_1, δ_2) in determining the shape of the a-particle spectra for the (a) ^{4}He + ^{93}Nb and (b) ^{4}He + ^{58}Ni reactions.*

the experimental neutron, proton and α-particle energy spectra, for different folds are given in Table 2.2. The average angular momenta corresponding to different folds are also given in the table. It can be seen that the fitted inverse level density parameters for the *all fold* (inclusive) *n*, *p*, and α-particle spectra are nearly same. However the fold gated values differs significantly among the three types of emissions. In principle the level density is a global parameter in the statistical model of compound nuclei and as such it should not depend on which type of particle is emitted. Thus the three energy spectra (neutrons, protons, and α-particles) should be fitted with only one common level density parameter. This is nearly the case for the inclusive particle spectra. The observed differences in the fold gated *k*-values for different particle spectra could be

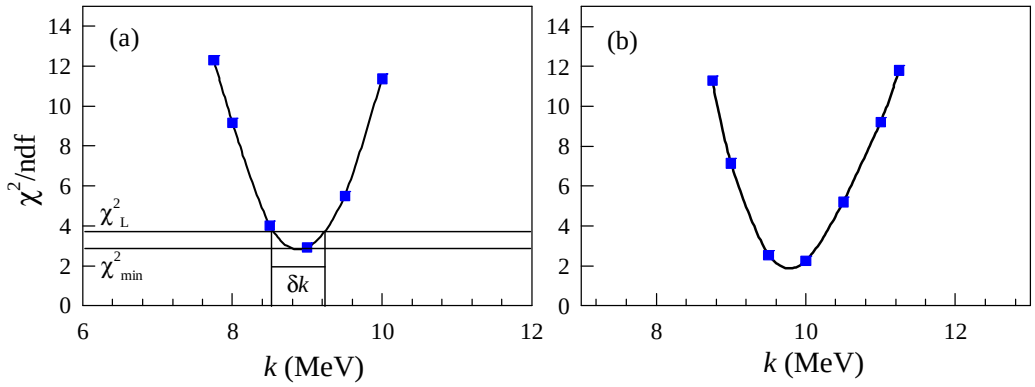

Figure 2.25: *χ^2 distribution for inclusive neutron spectra in case of (a) ^{4}He + ^{58}Ni and (b) ^{4}He + ^{93}Nb reactions. The error in k, i.e. δk, is defined as the intercept of the parabola with the selected number χ^2_L [83].*

Table 2.1: *Average angular momenta and inverse level density parameters for different γ-folds.*

Reaction	Fold	<J>($\hbar$)	k from neutron spectra (MeV)	k from proton spectra (MeV)	k from α spectra (MeV)
^{4}He + ^{93}Nb	All	18.0 ± 5.9	9.9 ± 0.1	9.3 ± 0.3	10.7 ± 0.3
"	2	15.7 ± 5.7	9.7 ± 0.1	9.7 ± 0.8	10.4 ± 0.4
"	3	18.8 ± 5.9	9.5 ± 0.2	9.4 ± 1.1	8.4 ± 0.6
"	≥4	22.5 ± 6.7	8.2 ± 0.2	7.1 ± 1.4	6.0 ± 0.7
^{4}He + ^{58}Ni	All	16.0 ± 5.4	8.9 ± 0.4	9.0 ± 0.1	8.8 ± 0.4
"	2	13.5 ± 4.7	8.0 ± 0.5	9.3 ± 0.2	8.0 ± 0.5
"	3	15.8 ± 4.9	7.0 ± 0.7	8.8 ± 0.4	6.5 ± 0.5
"	≥4	18.8 ± 5.5	6.0 ± 0.8	8.2 ± 0.5	5.6 ± 0.7

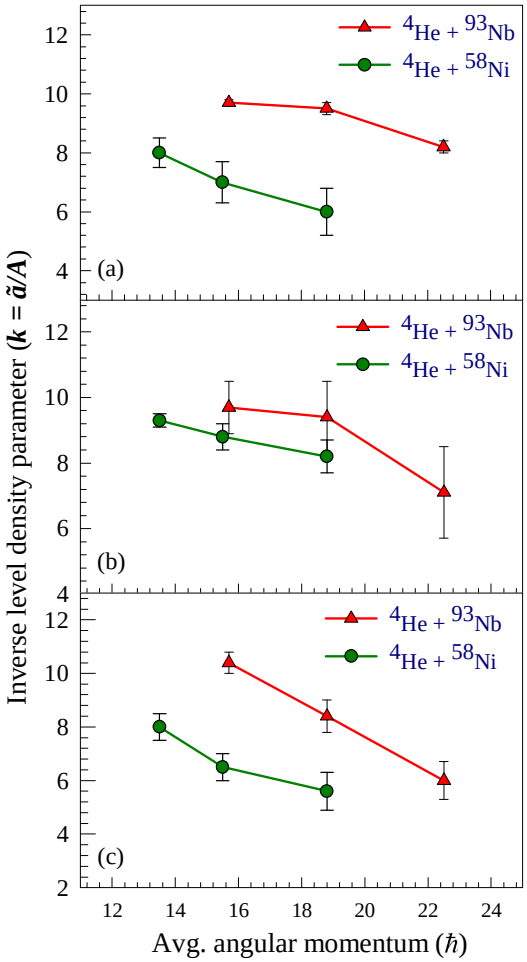

Figure 2.26: *Extracted inverse level density parameters at different angular momentum region as obtained from the analysis of (a) neutron spectra, (b) proton spectra, and (c) α-particle spectra.*

associated with the fact that different particles are emitted at different stages of the compound nuclear decay and they populate different evaporation residues at different temperatures. In case of inclusive measurement, the observed particle spectrum is an average of contributions coming from different spin windows (also at different E^* window, as the different J windows are associated with different E_{rot}). Furthermore, the inclusive spectrum is mostly dominated by the low spin contributions as one can expect from the (E^*,J) phase space diagram. On the other hand, the exclusive particle spectra are associated with a particular region of (E^*,J) phase space. Therefore, the observed values of fold gated level density parameters may not necessarily same.

Measured inverse level density parameters at different γ-folds are plotted as a function of the corresponding average angular momenta in Fig. 2.26. It can be observed from the figure, that the *k*-value decreases consistently with increasing *J* for all three types of particle emissions. The experimental trends are similar for both the reactions. Present observation on the angular momentum dependence of the level density parameter is in accordance with the earlier study of angular momentum gated neutron energy spectra for ^{4}He + ^{115}In system [55].

The angular momentum dependence in NLD is generally taken care of through the rotational energy E_{rot} where the effect of angular momentum dependent deformation on the decay is introduced by the effective moment of inertia ($\Im_{eff}$). The deformability parameters (δ_1 and δ_2), which are generally adjusted to take care of the angular momentum dependent deformation, failed to reproduce the fold gated particle spectra. It may be noted here that in the present theoretical analysis only the single particle level density [$\rho_{int}(E^*, J)$] has been considered. However, there can be additional contributions in NLD due to collective excitations (Eqn. 1.25). The collective enhancement factors have been estimated using the prescription of Hansen and Jensen [84]. The collective enhancement factors primarily depend on the value of quadrupole deformation parameter (β_2). For the present systems having quite small β_2 values, the calculated collective enhancement factors were found to be negligible. Moreover, as per the present formulations the collective enhancement factor does not depend on angular momentum explicitly, though there may be some weak dependence on angular momentum through the temperature. Therefore, it is evident from the present analysis that the phenomenological NLD model with RLDM prescription for spin dependence as well as consideration of collective enhancement as per exiting formulations, could not explain the general trend of the current data. The results suggest additional spin dependence in NLD which was reflected through the variation of the level density parameter with angular momentum.

Chapter 3

Excitation energy dependence of the level density parameter

3.1 Introduction

In the last chapter, we have presented the results of our investigation on the spin dependence of NLD, where a strong variation of the level density parameter with angular momentum was observed from the analysis of angular momentum gated particle evaporation spectra. The observed variation was in contrast to the existing theoretical formulation, where the level density parameter is not expected to vary explicitly with angular momentum. On the other hand, the level density parameter is known to exhibit interesting variation with excitation energy (temperature). The excitation energy dependence of a is highly sensitive to the shell structure of atomic nuclei (particularly at low excitations). A Strong departure of the level density parameter from its standard low energy value of $\sim A/8$, is very well known for nuclei in the vicinity of closed shells (as shown in Fig. 1.8). The shell structure in atomic nuclei is a manifestation of the nuclear mean field which assumes that nucleons move quasi-independently from one another inside a nucleus because of Pauli's principle. So, shell effects are

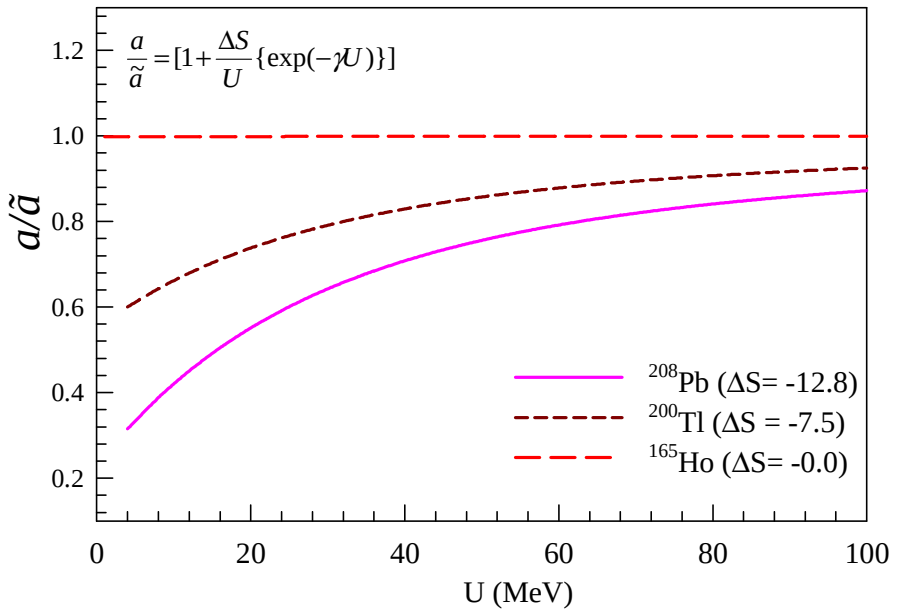

Figure 3.1: *Variation of the level density parameter with excitation energy as per Ignatyuk's prescription.*

strongly excitation energy dependent, expected to be damped and finally washed out at higher excitation energies due to the gradual weakening of the nuclear mean field itself. Consequently, at high excitation energies, the level density parameter reaches an asymptotic value ($\tilde{a}$), which varies smoothly with mass number; not depending on the specific shell structure of the individual nucleus. It is possible to represent the level density parameter as a combination of two parts; a smoothly varying (with nucleon number) part ($\tilde{a}$), and an oscillatory or fluctuating part (a_{osc}) reflecting the effect of shell structure of nuclei,

$$a = \tilde{a}\,[1 + a_{osc}] \tag{3.1}$$

The variation of a_{osc} with excitation energy due to energy dependent shell effect can be described mathematically in an elegant manner using the excitation energy dependent parametrization of the level density parameter, as suggested by Ignatyuk *et al.* [17],

$$a_{osc} = [\frac{\Delta S}{U} exp(-\gamma U)] \tag{3.2}$$

The significance of a_{osc} increases with increasing shell correction (ΔS). This is demonstrated in Fig. 3.1 where the value of $a/\tilde{a}$ has been plotted as a function of the thermal

excitation energy (U) in the case of three nuclei having widely different ΔS values. It can be seen from the figure that for the mid-shell ^{165}Ho nucleus for which ΔS = 0, the level density parameter is determined by its asymptotic value only. In the case of doubly magic ^{208}Pb having large shell correction value (ΔS = -12.8 MeV) the level density parameter is significantly lower than its asymptotic value at low energies. Theoretically, the Ignatyuk formulation is quite useful as it is easy to handle (compared to the direct enumeration of NLD through microscopic calculations using shell model single particle level schemes) and is applicable for almost all nuclei in the nuclear chart. In the Ignatuyk's formulation, the depletion of shell effect with excitation energy is determined by the value of the shell damping factor (γ). Although there have been a few early theoretical estimates on the value of γ [17, 85], experimental information is quite limited. Experimental information on the variation of shell effect in NLD over a wide excitation range can be obtained by measuring particle evaporation spectra from the excited compound nucleus at sufficiently low energies where it (shell effect) has a significant contribution. However, populating nuclei at such low excitation energies through the fusion reactions is difficult due to the entrance channel coulomb barrier. This difficulty has been overcome to an extent in a recent study by Rout *et al.* where the authors have measured neutron evaporation spectra followed by transfer induced fusion of ^{7}Li on ^{205}Tl populating particle unbound states in ^{208}Pb [61]. Another possible solution to the problem of producing low excitation energy can be through the use of light ion beams such as protons or α-particles for which the Coulomb barriers are relatively small. The later method is cleaner over the earlier method in which there may be uncertainty due to the contributions coming from different direct processes. Additionally, in the second case (complete fusion) there is no uncertainty in determining the excitation energy of the compound nucleus as compared to the case of the transfer induced fusion, where the excitation energy is determined by putting an energy gate (of width ~1 - 2 MeV) in the measured outgoing particle energy spectrum. In the work of Rout *et al.* [61] the shell damping parameter has been determined in the vicinity of doubly magic ^{208}Pb nucleus. However, the extracted γ-value ($0.060^{+0.01}_{-0.02}$

MeV^{-1}) differs somewhat from the value (0.079 ± 0.007 MeV^{-1}) extracted earlier from the neutron resonance data [86]. The difference might be attributed to the differences in the angular momentum states sampled in the two works.

At this point it is interesting to note that, apart from the discussed variation of the level density parameter with excitation energy due to the shell effects (important for $T \lesssim 0.5$ MeV or so), the asymptotic (or smooth) part of the LDP ($\tilde{a}$) also shows interesting variation with excitation energy (temperature) [*i.e.* $\tilde{a} = \tilde{a}(U)$ *or* $\tilde{a}(T)$]. A reduction in the value of asymptotic level density parameter with increasing temperature, from $\sim A/8$ (at $T \approx 0$) to $\sim A/13$ (at $T \approx 5$ MeV) was reported in several experimental studies, particularly in the $A \approx 160$ mass region [58, 59, 87, 88, 89]. It has been recognized that the observed temperature dependence of the level density parameter can be accounted for, to a good extent by taking into account the effects of the temperature dependence of the effective nucleon mass [90, 91, 92, 93, 94]. In a simplified calculation under the Thomas-Fermi approach (TFA) including the finite size effects (effects due to surface and curvature), the momentum and frequency dependence of the effective mass, and the effects of continuum, the temperature variation of the smooth part of the level density parameter was reported for several nuclei by Shlomo and Natowitz [90]. Fineman *et al.* [95] showed that the spectral shape of light particles emitted from ^{193}Tl and ^{213}Fr compound systems could be explained very well by using a modest excitation energy dependent parameterization of $\tilde{a}$, based on the work of Shlomo and Natowitz [90]. However, in the same work, a stronger dependence of $\tilde{a}$ was required to explain the data in case of ^{224}Th nucleus. A very strong energy dependence of $\tilde{a}$ (from $A/8$ at low temperature to $A/12$ at $T \sim 2.5$ MeV) has been reported by Fabris *et al.* from the measurement of α-particle emission in ^{19}F + ^{181}Ta fusion-evaporation reactions [60]. However, such strong dependence was not supported by later measurement for the same ^{19}F + ^{181}Ta system by Caraley *et al.* [96]. In the case of lighter systems, a constant nature or rather weak dependence of $\tilde{a}$ on T compared to the observations in A ~ 160 region or to the predictions of Shlomo and Natowitz [90] were reported in many cases [97, 98, 99].

It is, therefore, evident from the above discussion that several interesting studies have been carried out in recent years to investigate the temperature dependence of the level density parameter as well as the role of shell effects and its damping on NLD. For the later, measurements are very few and new measurements will be useful to substantiate the earlier results. On the other hand, results of different measurements on the temperature dependence of the level density parameter are so diverse that it is difficult to arrive at a definite conclusion. Therefore, we planned to study the energy dependence of the level density parameter and the damping of shell effects with excitation energy in the $A \sim 210$ region using light ion induced reactions, which has several advantages; some of them have already been discussed at the beginning. In the present case, the most significant advantage of using light-ion beam is to be able to populate the nuclei at low excitation energies in an efficient manner. Moreover, as the angular momenta populated are much less compared to those in heavy-ion (HI) induced reactions, the thermal excitation energy can be determined with much less uncertainty, and any significant modification in the LDP due to angular momentum effects is less likely to occur in this case. Thus the present study is likely to extend (and improve) the available information on the shell damping and temperature dependence of the level density parameter for systems close to the doubly magic ^{208}Pb nucleus. With this aim, we have carried out the present measurement, in which neutron evaporation spectra have been measured from two different compound nuclei ^{212}Po and ^{213}At populated through the reactions,

$$^{4}\mathrm{He} + {}^{208}\mathrm{Pb} \longrightarrow {}^{212}\mathrm{Po}^{*} \ (\mathrm{Q} = -8.95 \ \mathrm{MeV})$$
$$^{4}\mathrm{He} + {}^{209}\mathrm{Bi} \longrightarrow {}^{213}\mathrm{At}^{*} \ (\mathrm{Q} = -9.25 \ \mathrm{MeV})$$

in the excitation range E^{*} ~18 - 50 MeV. The choice of the current reactions was particularly useful to produce low excitations as both the reactions have large negative Q-values.

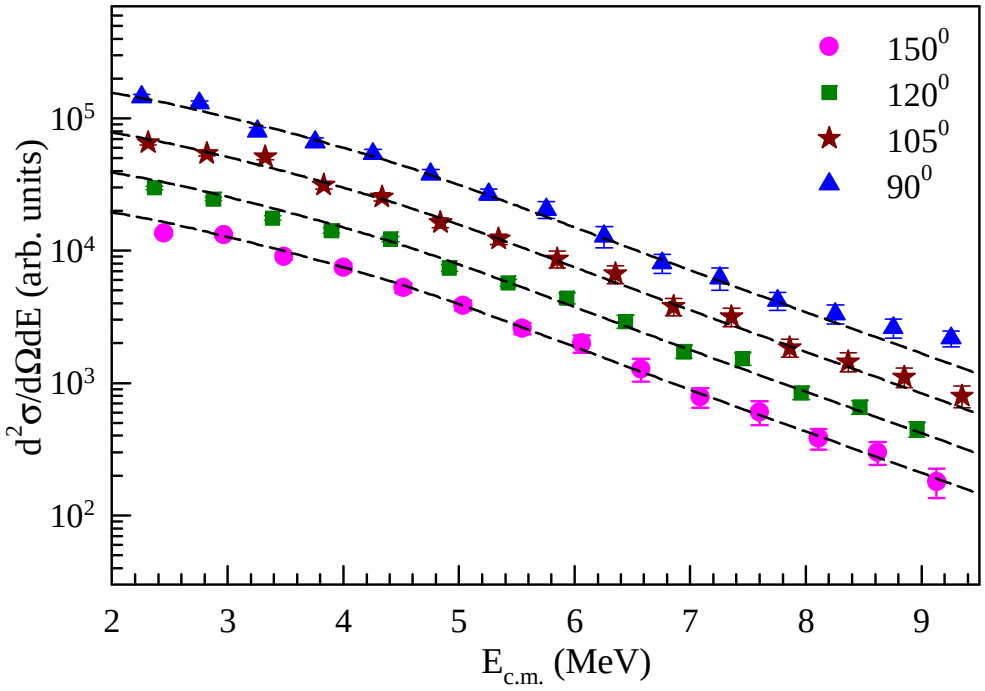

Figure 3.2: *The experimental neutron energy spectra (symbols) at different laboratory angles in the center of mass frame for the* ^{4}*He +* ^{208}*Pb system at 60 MeV incident energy. The corresponding SM predictions are shown by the dashed lines. The individual spectrum has been scaled for better visualization.*

3.2 Experimental Details

The experiment was carried out using the ^{4}He-ion beams of incident energies 28, 31, 35, 40 and 60 MeV from the K130 cyclotron at VECC. In the experiment two self-supporting foils of ^{208}Pb (enriched to > 99%, thickness ~ 4 mg/cm^2) and ^{209}Bi (100% natural abundance, thickness ~ 1.5 mg/cm^2) were used as targets. The emitted neutrons were detected using four liquid scintillator detectors placed at the laboratory angles of 90°, 105°, 120° and 150°, kept at a distance of 1.5 m from the target. Details of the experimental setup and the data analysis technique have already been described in section 2.2.

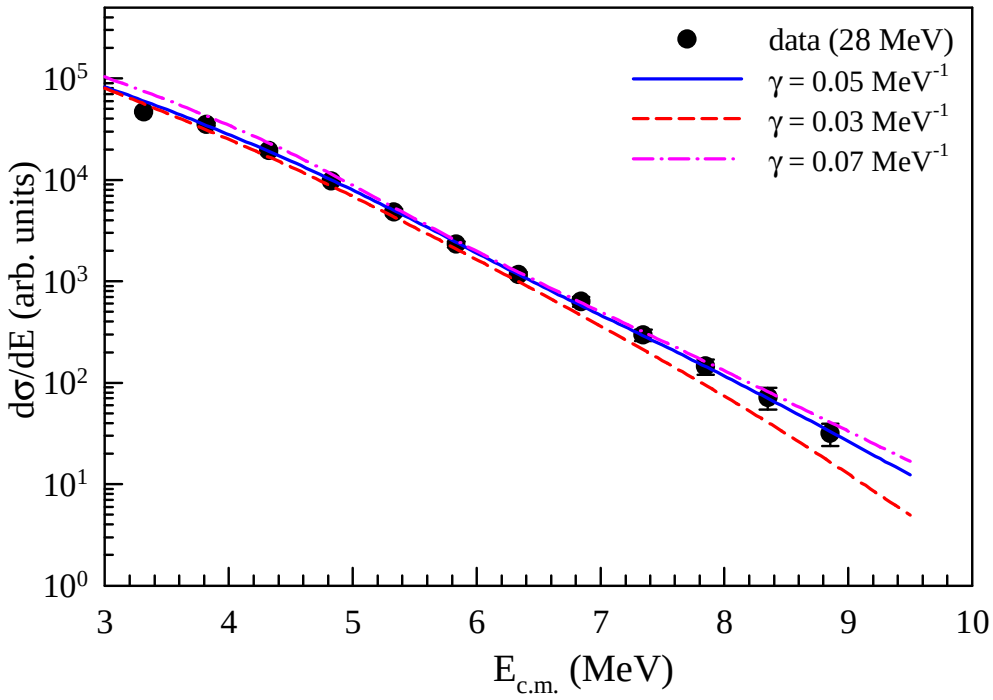

Figure 3.3: *The experimental neutron spectrum (symbols) along with the SM calculations (lines) using three γ-values (see text) for the* $^{4}He + {}^{208}Pb$ *system at 28 MeV incident energy.*

3.3 Results and Discussions

The extracted neutron kinetic energy spectra at different laboratory angles were converted to the center of mass frame; the spectral shapes were found to be almost overlapping (Fig. 3.2), indicating that they have originated from an equilibrated compound nucleus. The neutron data at the most backward angle (150°), were used for further analysis. The experimental neutron energy spectra were compared with the theoretical calculations performed with the statistical model (SM) code CASCADE [72]. In the CASCADE calculation, level densities have been calculated using the phenomenological back-shifted Fermi gas formula. The shell correction in the level density parameter was incorporated using Ignatyuk's prescription (Eqn. 1.33). Complete detail of the SM calculation has been described in section 2.4.

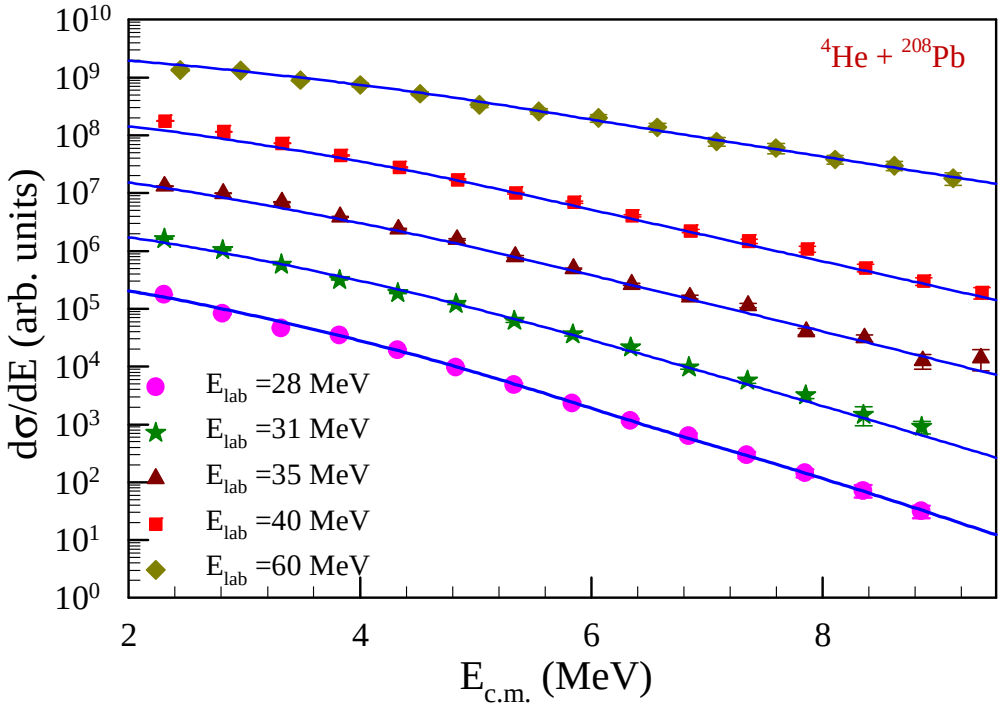

Figure 3.4: *Experimental neutron energy spectra (symbols) at different energies alongwith the statistical model fits (continuous lines) for the* ^{4}*He +* ^{208}*Pb system. The individual spectra have been scaled for better visualization.*

3.3.1 Determination of the shell damping parameter

The value of shell damping parameter was extracted from the lowest energy data (U ~17 MeV), which has the highest sensitivity (as compared to higher energy data) for this parameter. At the lowest excitation energy both the compound nuclei ^{212}Po and ^{213}At decay predominately through 1n and 2n channels populating ^{211,210}Po and ^{212,211}At as evaporation residues (ER) respectively in the energy range E^{*}_{ER} ~2 - 12 MeV. Over this E^{*}_{ER} range, the level density parameter is expected to show significant variation due to the damping of the shell effect. The ground state shell corrections (ΔS), which are determined from the difference between the experimental and liquid drop masses, have the values ~ -11 MeV for the present isotopes [100]. Fig. 3.3 shows the measured neutron energy spectrum along with the SM predictions for the ^{4}He + ^{208}Pb reaction at the 28 MeV incident energy. The calculated spectra are shown for the three

γ-values 0.03, 0.05 and 0.07 MeV^{-1}. The value of $\tilde{a}$ was taken as $A/8$ while extracting the value of γ. This is justified from the observed temperature dependence of the inverse level density parameter (shown in the next section) which suggests a value of k close to 8 at low energies. However, the data could also be fitted by simultaneous variation of both $\tilde{a}$ and γ. In that case one could get more than one set of $\tilde{a}$ and γ values which could equally describe the experimental data. In principle the $\tilde{a}$ and γ values are not completely independent as suggested by Schmidt *et al.* [85]. Similar result has also been reported by Rout *et al.* [61], where an acceptable range of simultaneous $\tilde{a}$ and γ values has been presented. Here we have extracted a reasonable value of the shell damping factor considering one particular value of $\tilde{a}$ (= A/8, frequently used value at low energy) for two nearby systems in the A$\sim$210 region. Now it can be clearly seen from Fig. 3.3 that γ = 0.05 describes the shape of the spectra reasonably well compared to the other two γ values. The optimum γ-values were extracted for the two reactions by χ^2 minimization and found to be 0.052 ± 0.018 MeV^{-1}(for ^{4}He + ^{208}Pb) and 0.054 ± 0.020 MeV^{-1}(for ^{4}He + ^{209}Bi). The measured values are consistent with the theoretical estimates of ref. [17] and ref. [85] and also matches with the measured value of ref. [61]. Measurements at further lower excitation energies will be useful to constrain the value of the shell damping parameter to a narrower range. The spectral shapes at higher energies (for $E_{lab} \geq 31$ MeV) for the current study observed to have very little sensitivity on the variation of γ indicating the weakening of the influence of shell effects at these energies.

3.3.2 Temperature dependence of $\tilde{a}$

The excitation energy (temperature) dependence of the asymptotic part of the level density parameter has also been investigated by fitting the experimental spectra at different excitation energies (shown in Fig. 3.4 and Fig. 3.5 by varying the inverse level density parameter k ($k = A/\tilde{a}$). The statistical temperature *(T)* can be obtained from

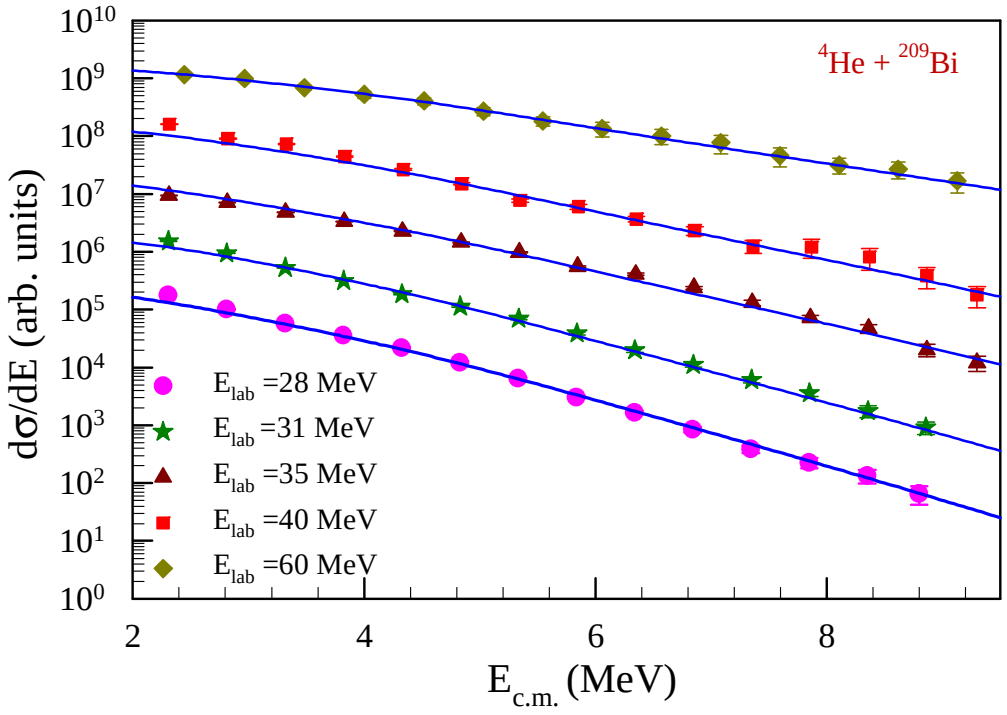

Figure 3.5: *Same as Fig. 3.4 for the ^{4}He + ^{209}Bi system.*

the relation

$$T = \sqrt{\frac{U}{a}} \tag{3.3}$$

However, in the measured neutron spectra there may be contributions coming from neutrons emitted from different stages of the decay. So, the measured spectra are fitted with the Maxwellian function $\sqrt{E}\ exp(-E/T_{app})$ to estimate the average experimental temperatures also called the apparent temperatures (T_{app}). The extracted k values along with the corresponding thermal excitation energies and temperatures are given in Table 3.1. It can be seen from the table that the extracted temperatures from Eqn. 3.3 (T) and those from the Maxwell fitting (T_{app}) are close to each other. However, the temperatures extracted from the fitting are consistently lower than that obtained from Eqn. 3.3, and the difference is maximum at the highest excitation energy. This clearly reflects the fact that in the measured spectra there are contributions of the neutrons emitted at later stages of the decay corresponding to lower U values than those used in Eqn. 3.3. Although the temperature defined through Eqn. 3.3 and T_{app} are not exactly the same quantity they are closely correlated and should carry same physical informa-

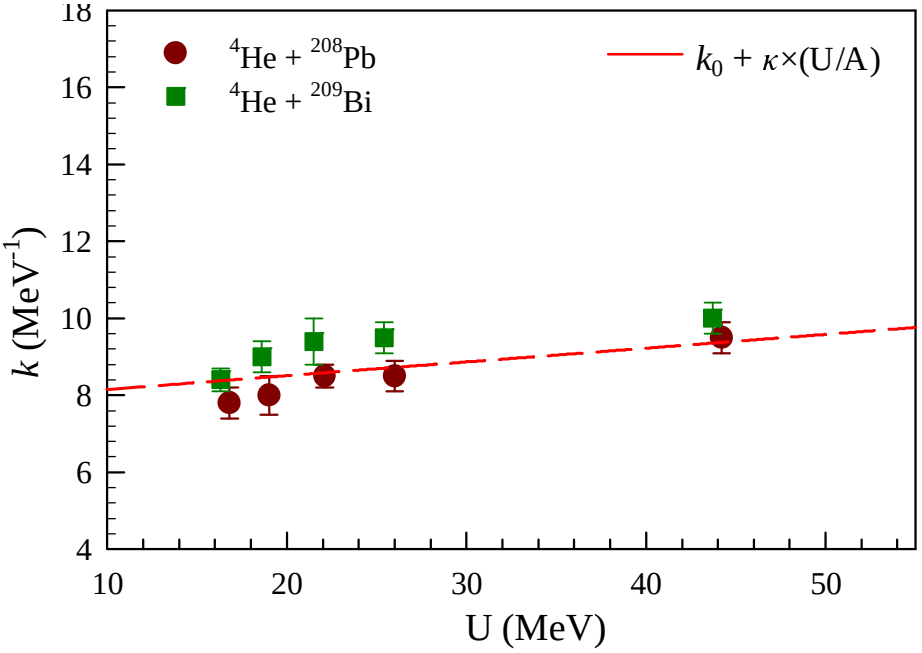

Figure 3.6: *Excitation energy dependence of the inverse level density parameter. The experimental data (symbols) are compared with the prediction of Eqn. 3.4 (red dashed line).*

tion. An overall increase of the inverse level density parameter with increasing thermal excitation energy is observed for both the reactions. The variation of k with U has been shown in Fig. 3.6 for the two reactions. It is observed that the experimental trend can be very well represented by an empirical relation (shown by the red dashed line in Fig. 3.4),

$$k(U) = k_0 + \kappa\frac{U}{A}, \tag{3.4}$$

as used in the past by several authors to reproduce the spectral shapes of light charged particles emitted in different heavy-ion reactions in a wide excitation energy range [95, 96, 62]. The average variation of k with U, in the current study can be explained by Eqn. 3.4, with $k_0 = 7.8$ and $\kappa = 7.5$. The value of κ, which basically decides the rate of increase of k with U, is predicted to depend strongly on nuclear mass number and has been parametrized as a function of the mass number [62],

$$\kappa(A) = 0.00517exp^{(0.0345A)}. \tag{3.5}$$

Table 3.1: *Extracted inverse level density parameters and temperatures.*

System	E_{lab} (MeV)	E^* (MeV)	U (MeV)	k (MeV)	T (MeV)	T_{app} (MeV)
^{4}He + ^{208}Pb	28	18.5	16.6	7.8 ± 0.4	0.78	0.70 ± 0.03
^{4}He + ^{208}Pb	31	21.5	18.8	8.0 ± 0.5	0.84	0.77 ± 0.05
^{4}He + ^{208}Pb	35	25.4	21.9	8.5 ± 0.3	0.94	0.84 ± 0.04
^{4}He + ^{208}Pb	40	30.3	25.8	8.5 ± 0.4	1.02	0.92 ± 0.03
^{4}He + ^{208}Pb	60	49.9	44.0	9.5 ± 0.4	1.41	1.25 ± 0.04
^{4}He + ^{209}Bi	28	18.2	16.3	8.3 ± 0.3	0.81	0.72 ± 0.04
^{4}He + ^{209}Bi	31	21.2	18.6	9.0 ± 0.4	0.89	0.80 ± 0.05
^{4}He + ^{209}Bi	35	25.0	21.5	9.4 ± 0.6	0.97	0.92 ± 0.03
^{4}He + ^{209}Bi	40	30.0	25.5	9.5 ± 0.4	1.04	0.99 ± 0.04
^{4}He + ^{209}Bi	60	49.6	43.7	10.0 ± 0.4	1.43	1.28 ± 0.04

The extracted value of κ in the current study is in close agreement with the prediction of Eqn. 3.5. The temperature dependence of the asymptotic level density parameter has been is plotted in Fig. 3.7. The observed temperature dependence of $\tilde{a}$ has been compared with the theoretical prediction of Shlomo and Natowitz [90] performed under the Thomas-Fermi approach for a nucleus with A = 210 (continuous line in Fig. 3.7). It can be seen from Fig. 3.7 that the average trend of the data is similar to that of the TFA prediction; both of which show a reduction in the $\tilde{a}$ value with increasing temperature. However, the experimental values of $\tilde{a}$ decrease at a slightly faster rate than the theoretical prediction. It may be mentioned here that the reduction in the value of the asymptotic level density parameter with excitation energy can mainly be accounted for, by the temperature dependence of the frequency and momentum dependent effective mass [90] of the nucleons inside the nucleus which is different from their free or bare mass. It may be remembered that the level density parameter is directly proportional to the density of single-particle states, g(ϵ) (Eqn. 1.18), which in turn is proportional to

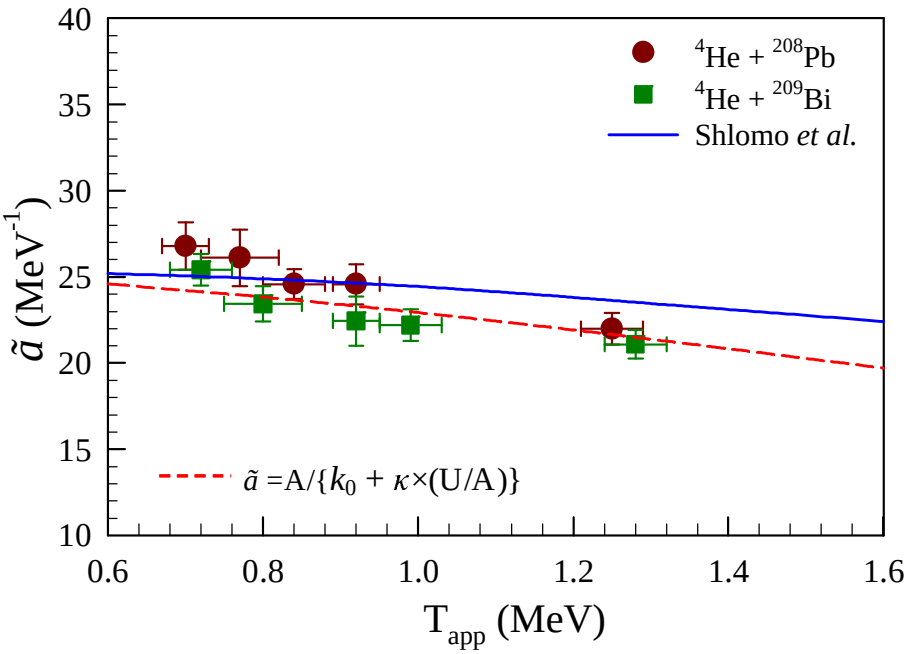

Figure 3.7: *Temperature (T_{app}) dependence of the asymptotic level density parameter. The experimental data (symbols) are compared with the prediction of Eqn. 3.4 (dashed line) and the TFA calculations (continuous line) of ref. [90] (see text).*

the effective mass (m^*) of the nucleon. This can easily be understood from the simple examples (Fig. 3.8) of (i) infinite square well (SW) potential and (ii) one dimensional harmonic oscillator (HO) potentials. The energy eigen values in the case of SW potential of width 'a' is given by

$$E_n = \frac{n^2h^2}{8m^*a^2}, \tag{3.6}$$

and in the case of HO potential the energy eigen value is given by

$$E_n = (n + \frac{1}{2})\,\hbar\omega \tag{3.7}$$

where $\omega = \sqrt{K/m^*}$. Therefore, in case of both these simple potentials the spacing between the energy levels (ΔE_n) decreases as the mass increases, so that, the density of levels increases (or decreases) with increasing (or decreasing) effective nucleon mass. This behavior is true for any general potential. Under the Thomas-Fermi approximation of a finite nucleus one can write [91]

$$\tilde{a}(T) = \frac{\pi^2}{4}\sum_{q=1,2}\int \frac{\rho_q(r)}{\hbar^2k_q^2(r)/2m_q^*(r,T)}dr \tag{3.8}$$

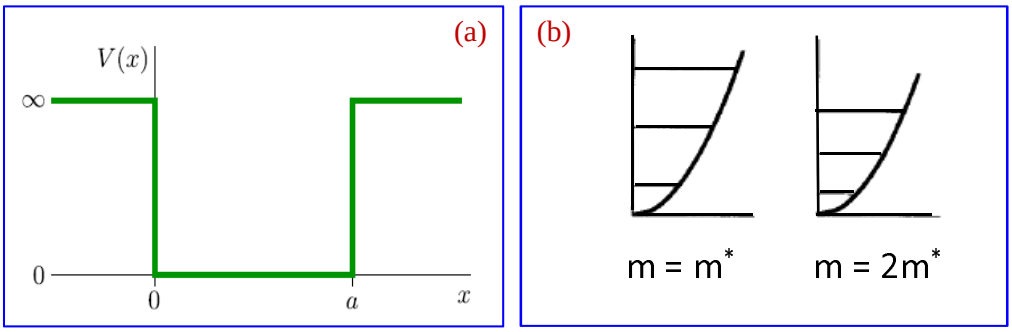

Figure 3.8: *(a) Infinite square well potential (b) one dimensional harmonic oscillator potential*

The summation index q = 1(2) refers to neutrons (protons), ρ_q(r) is the corresponding nucleon density, k_{Fq}(r) the local Fermi momentum and $m_q^*(r,T)$ is the temperature dependent effective mass of a nucleon inside the nucleus. The effective nucleon mass has two components a momentum dependent part, m_k, and a frequency dependent part, m_ω, thus $(m^*) = ((m_k \times m_\omega)/m)$, where m is the free nucleon mass. The temperature dependence of the effective mass can be calculated microscopically (*e.g.* using temperature dependent Hatree-Fock calculations [101, 102]), however, simplistic phenomenological parametrization given by,

$$\left\langle \frac{m_\omega(T)}{m} \right\rangle = 1 + 0.4\, exp\left(\frac{-T}{4}\right)^2 \tag{3.9}$$

$$\left\langle \frac{m_k(T)}{m} \right\rangle = 1 - 0.2\,(1 - 0.005\,T^2) \tag{3.10}$$

is observed to provide equivalent results [91]. The temperature dependence of the effective mass as obtained using Eqns. 3.9 & 3.10 has been shown in Fig. 3.9. It can be seen that the effective mass has the maximum value m^* =1.12 at T =0 and reduces to a minimum around T ~6 MeV after that it slowly increases again. The reduction in the effective mass with temperature is because of the frequency dependent part whereas the momentum dependent part always increases slowly with temperature. The frequency dependence of the effective mass, which reflects the effects of correlations, considerably enhances the surface contribution to $\tilde{a}$ at low energies (through Eqn. 3.8) bringing it close to the observed value (~A/8) compared to the Fermi-gas prediction (~A/15) [91]. However, the effect of correlation dies out with the increase in excitation

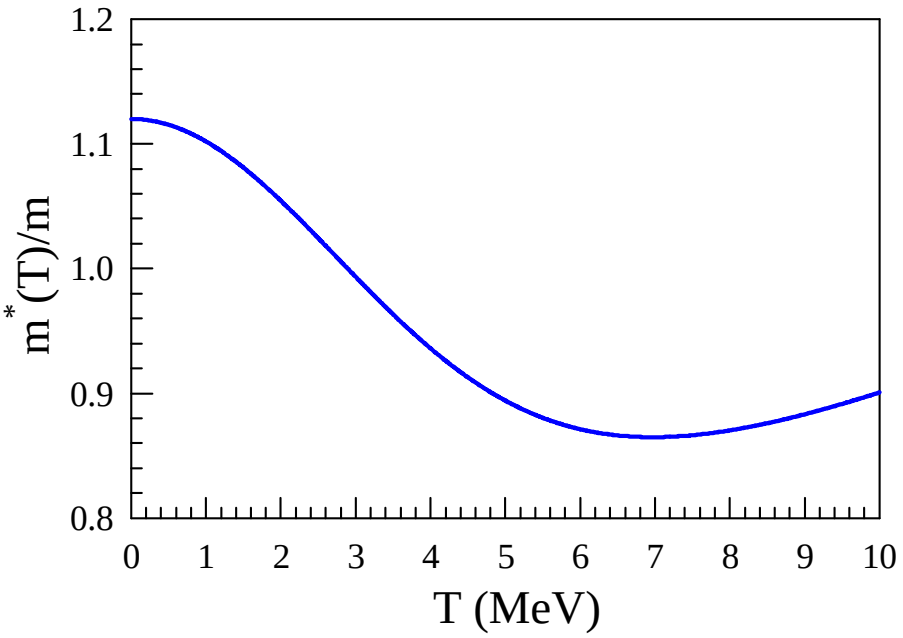

Figure 3.9: *Temperature dependence of the effective mass.*

energy and the value of $\tilde{a}$ approaches its Fermi gas limit [101].

The effect of correlation has another significant effect in NLD. Apart from increasing the value of LDP at lower energies, the long-range correlations can also cause an enhancement of the FG level density which is known as the collective enhancement (section 1.5.2). A variation of the level density parameter (with energy) can be observed as a manifestation of the excitation energy dependence of the collective enhancement factor (as discussed in the following chapter). However, in the current study all the nuclei being close to the Z = 82 and N = 126 shell closure, are spherical in their ground-state. So, the rotational enhancement factor, $K_{rot} \approx 1$ [84]. Besides, the estimated vibrational enhancement factors are also quite small (1 - 10) for current nuclei of interest [103]. Therefore the contribution of the collective enhancement in the present study can safely be neglected. Although the current experiment could not go up to very high excitation energies as compared to the earlier results of similar measurements on the temperature dependence of the level density parameter, a clear trend could be established from the experimental data because of the precise determination of level density parameter.

Chapter 4

Collective enhancement and its fadeout

4.1 Introduction

Nuclei that are not too far from the closed shell configuration can reasonably be described using shell model which assumes the independent particle motion of the nucleons in an average field. However, signatures of coherent or collective motion of many nucleons beyond the independent particle picture can be found in a number of nuclear properties particularly in the case of nuclei away from the closed shells. The existence of low-lying first excited 2^+ state, observation of large quadrupole moment over the single-particle predictions for many nuclei provide such signatures of the collective motion in the nucleus. Collective excitations are expected to have important consequences in NLD too. An additional contribution to NLD beyond the independent particle motion may arise from the collective rotation and/or vibration which involve coherent excitations of the nucleons. In this case, the two properties (single-particle and collective) can be closely interlinked. It was predicted both phenomenologically as well as microscopically [84, 104, 105, 106], that there should be an enhancement of

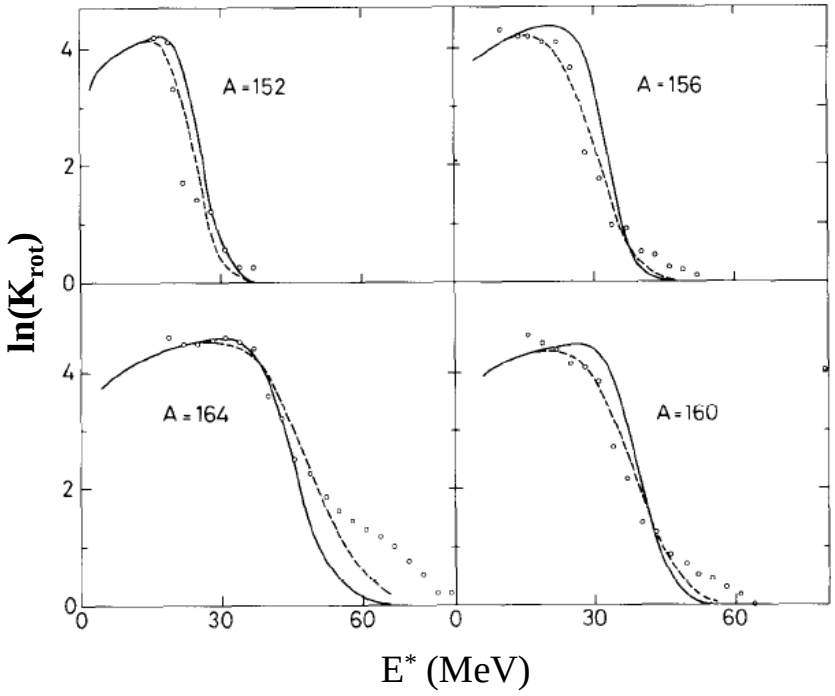

Figure 4.1: *Energy dependence of the rotational enhancement factor [84]. The open circles are results of microscopic calculations, the lines represents different empirical parametrization.*

NLD over its single-particle value due to collectivity, that is conventionally described in terms of the collective enhancement factor, K_{coll} (Eqn. 1.25) which is a product of rotational (K_{rot}) and vibrational (K_{vib}) enhancement factors. For nuclei with appreciable ground-state deformation, the significant contribution to the collective enhancement comes from the rotational excitations, whereas in the case of spherical nuclei, the collective enhancement is likely to be due to vibrational excitations. The collective enhancement is expected to be damped at higher excitation (finally vanishes beyond a critical energy) due to the gradual damping of long-range correlations, which are mainly responsible for the collective enhancement in NLD. This is termed as the fadeout of collectivity which implies $K_{coll} = 1$. Björnholm, Bohr and Mottleson [107] have suggested a critical temperature T_c, beyond which the fadeout is expected. T_c is given by,

$$T_c = \hbar\omega_0\beta_2 \sim 40A^{-1/3}\beta_2 \text{ MeV}, \tag{4.1}$$

where, ω_0 is the mean oscillation frequency, and β_2 is the ground state nuclear

quadrupole deformation parameter. The excitation energy dependence of the rotational enhancement factor was studied by Hansen and Jensen using microscopic SU(3) model in the case of a number of deformed nuclei [84] which is shown in Fig. 4.1. A transition from axial (deformed) to spherical level density at higher excitation implying the fadeout of collectivity was reported. The transition energy was found to be closely related to the ground-state deformation. A simple phenomenological parametrization of the excitation energy dependence of the rotational enhancement factor

$$K_{rot}(E^*) = \begin{cases} (\sigma^2 - 1) f(E^*) & \sigma^2 > 1 \\ \\ 1 & \sigma^2 \leq 1. \end{cases} \tag{4.2}$$

was suggested by Hansen and Jensen that reproduces their SU(3) model calculations. Here, $\sigma = \sqrt{\frac{IT}{\hbar^2}}$ is the spin-cutoff factor, $I = 2/5 m_0 A R^2 (1 + \beta_2/3)$, is the rigid body moment of inertia perpendicular to the symmetry axis, A is the mass number, R is the radius, T is the temperature of the nucleus and m_0 is the nucleon mass. The fadeout of $K_{rot}(E^*)$ with excitation energy has been represented by the Fermi function $f(E^*) = \left\{1 + exp(\frac{E^* - E_{cr}}{d_{cr}})\right\}^{-1}$, where E_{cr} (= $120\beta_2^2 A^{1/3}$ MeV) and d_{cr} (= $1400\beta_2^2/A^{2/3}$ MeV) gives the deformation dependent critical energy and width, respectively. Typically, $K_{rot}(E^*)$ rises sharply at low excitation energy to reach a near-plateau (slowly increasing with energy) and then falls off (fadeout transition) at $E \sim E_{cr}$ with a slope decided by d_{cr}. The results obtained from the empirical parametrization given by Eqn. 4.2 are shown by the continuous lines in Fig. 4.2. The vibrational enhancement factor for nuclei which are known to be good vibrators can be obtained in the adiabatic limit [107, 108] as,

$$K_{vib}^{ad} = \left(1 - exp\left(\frac{-E_1(2^+)}{T}\right)\right)^{-5} \tag{4.3}$$

where $E_1(2^+)$ is the energy of the first excited 2^+ level of the nucleus and T is the nuclear temperature. The vibrational enhancement is generally smaller (often by an order of magnitude) than the rotational enhancement for deformed nuclei.

Recent microscopic shell model Monte Carlo (SMMC) calculations on rare earth nuclei [109] has elucidated the close link between level density and collectivity. A

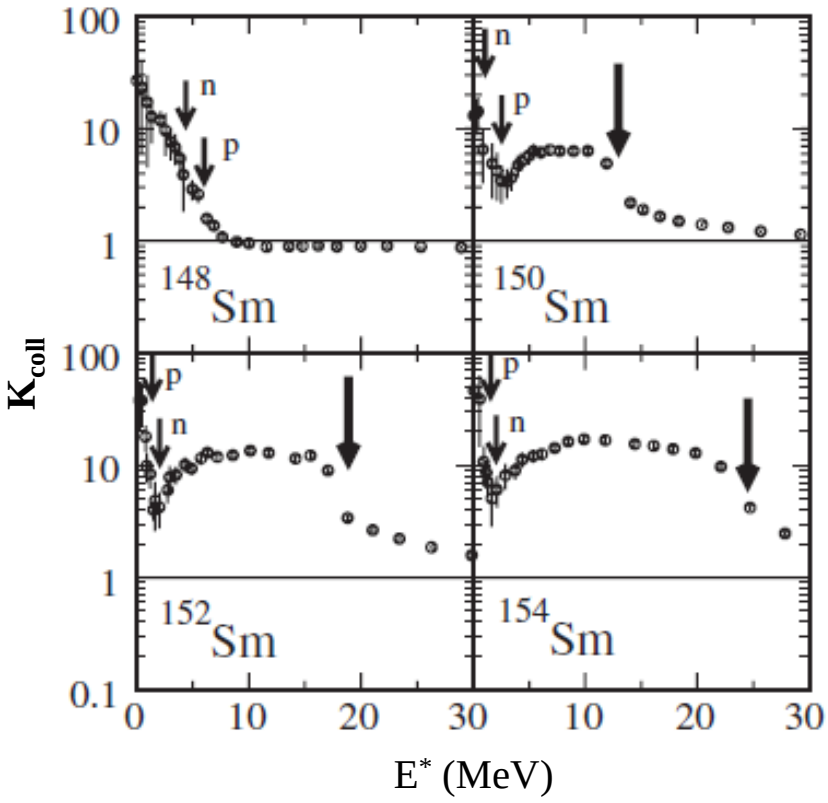

Figure 4.2: *Total collective enhancement factor K_{coll} in the even-even $^{148-154}$Sm isotopes as a function of excitation energy [109].*

crossover from vibrational to rotational collectivity emerges as one moves from the nearly spherical to the deformed nuclei. The vibrational collectivity decays at very low excitation energy (typically $\lesssim$2 - 3 MeV), which can be correlated with the pairing phase transition. On the other hand, the rotational collectivity which is appreciable for the mid-shell nuclei having finite ground-state deformation is also observed to vanish typically around 15 - 25 MeV excitation energy. The disappearance of the rotational collectivity was predicted to be due to the shape phase transition of the nucleus, which becomes spherical from deformed ground state and can no longer support rotational bands. The transition energy (shown by the thick arrows in Fig. 4.2 which shows the variation of K_{coll} with excitation energy for the samarium isotopes) was observed to increase with increasing ground state deformation of the nuclei [109]. Various other finite temperature microscopic calculations (e.g., Hartree-Fock-Bogoliubov

cranking [110], Auxiliary field Monte Carlo [111]) have also indicated the occurrence of such a shape transition in deformed nuclei in the vicinity of the excitation energy where the damping of rotational collectivity takes place. In the case of light *sd* and *pf* shell nuclei also, recent shell model calculation has clearly demonstrated the link between nuclear deformation and collective enhancement of NLD and hinted at the possibility of a deformed to spherical shape transition [106].

On the experimental front, only a few attempts have been made in the recent past to look for the collective enhancement in nuclear level density and its subsequent fadeout at higher excitation energy. Junghans *et al.* [108] studied the yields of nuclei produced in the fragmentation of relativistic Pb and U projectiles. They observed that the yields of the projectile-like fragments near N=126 magic number did not comply with the predicted stabilization against fission due to shell effect. Assuming that the neutralization of shell effect was due to collective enhancement in level density (all these fragments were highly deformed in the ground state), they concluded that the fadeout of collectivity is independent of the ground state deformation, which is in contrast to the existing theoretical predictions. The authors could reasonably explain their experimental data using E_{cr} =40 and d_{cr} =10 MeV. On the other hand, Komarov *et al.* [112] attempted to extract information on collective enhancement and its fadeout by studying α-particle evaporation from the highly deformed ^{178}Hf compound nucleus produced in heavy-ion fusion reaction. However, they did not find any convincing evidence of the existence of collective enhancement and its fadeout in their data. Therefore, it is evident that the interrelationship between collective excitations and nuclear level density as a function of excitation energy (or temperature) is yet to be resolved on the observational ground. The scarcity of experimental data and the nature of the controversy among the existing results warrants new measurements to independently verify the status of collective enhancement. So, with this aim, we have carried out two new experiments where neutron evaporation spectra have been measured from a number of compound nuclei producing evaporation residues which have large ground-state deformations. A nearly spherical system (^{201}Tl*) has also been studied for the sake of comparison. In

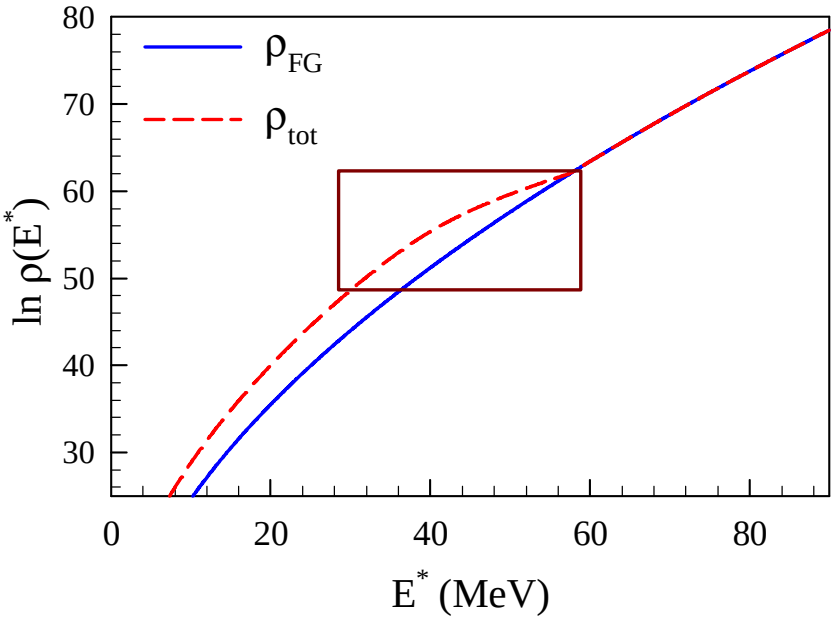

Figure 4.3: *Variation of nuclear level density with energy, continuous line represents the FG level density whereas the red dashed line gives the total level destiny (see text)*

the first experiment three compound nuclei $^{169}Tm^{*}$, $^{185}Re^{*}$, and $^{201}Tl^{*}$; out of which the first two have large deformations (so that the corresponding daughter nuclei produced after neutron emission are also deformed), have been populated at two excitation energies (~26 and 37 MeV) near the predicted fadeout region. As earlier, light particle (^{4}He) induced reactions were chosen to keep the input angular momenta at low values (~15 $\hbar$) and also to limit the number of effective decay channels, so that the level density information is not averaged over too many evaporation residues. For the present systems, the shell corrections were small enough that they are not expected to affect the signature of collective enhancement (if any). The experiment provided a positive signature (as shown in the following sections) towards the existence of collective enhancement at low energies for the deformed systems, though proper identification of the transition zone (fadeout) could not be possible due to the limited range of the data. Therefore, to understand the phenomenon in more detail the study has been extended by performing a second experiment in which three compound nuclei $^{173}Lu^{*}$, $^{185}Re^{*}$, and $^{201}Tl^{*}$ have been populated in a wider excitation energy range (~22 - 55 MeV)

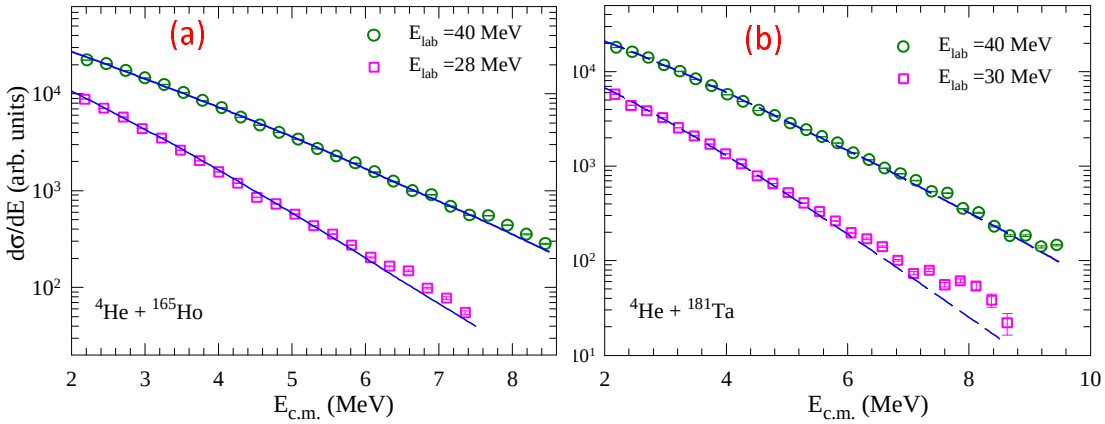

Figure 4.4: *Measured neutron energy spectra (symbols) for the (a)* $^{4}He + {}^{165}Ho$*, and (b)* $^{4}He + {}^{181}Ta$ *systems along with the statistical model predictions (lines) at two bombarding energies.*

in small energy intervals. The prime objective of the present experiments was to observe the variation of the level density parameter a with excitation energy which can provide imprints of the existence of collective enhancement and its fadeout in nuclear level density. As the shape of the kinetic energy spectrum (particularly the exponential tail) is highly sensitive to the rate of change of level density any significant variation in the value of K_{coll} and thus in ρ should be exhibited in the slope of the kinetic energy spectra of the evaporated particles. Around the fadeout region where the collective enhancement factor is predicted to drop by a factor of ~100 to 1 within a small energy interval, the level density is expected to show a kink or at least a plateau at this energy of transition. This is demonstrated in Fig. 4.3 where the variation of intrinsic (single-particle) level density given by the Fermi gas formulation (ρ_{FG}), and total level density ρ_{tot} ($= K_{coll}(E) \times \rho_{FG}$) with excitation energy has been plotted for a typical nucleus with $A = 160$, where K_{coll} has been evaluated using the prescription of Hansen and Jensen [84] considering $\beta = 0.28$. In Fig. 4.3 the fadeout region has been shown by the red box where the change in the slope of $ln(\rho)$ can be clearly visible. Such a variation of level density should be reflected in the value of the level density parameter which is determined by fitting the high energy part of the evaporation spectrum.

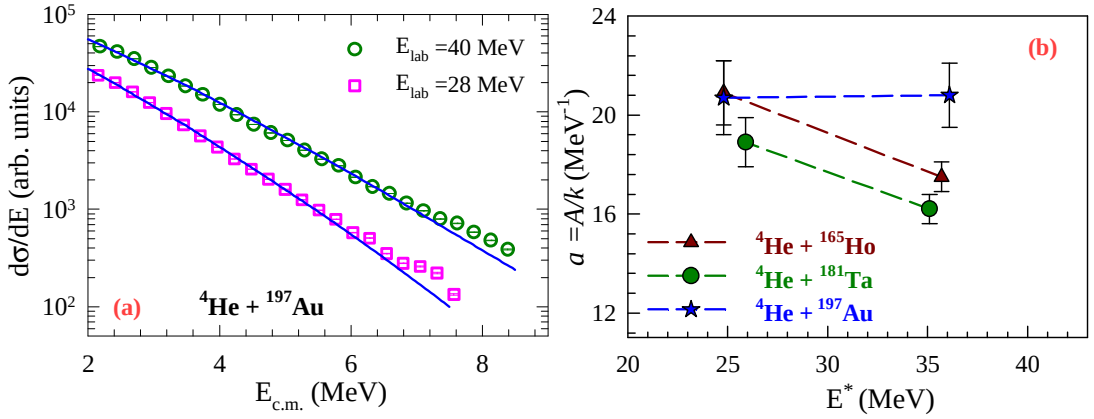

Figure 4.5: *(a) Same as fig. 4.4 for the $^{4}He + ^{197}Au$ system (b) extracted level density parameter at the two excitation energies*

4.2 Experimental Details

The experiments have been performed using ^{4}He ion beams from the K130 cyclotron facility at the Variable Energy Cyclotron Centre, Kolkata. The first experiment was carried out at two bombarding energies E_{lab}= 40, and 28 MeV (40 MeV and 30 MeV for ^{181}Ta target). Self-supporting foils of ^{181}Ta, ^{165}Ho (thicknesses ~1 mg/cm^2) and, ^{197}Au (thickness ~500 μg/cm^2) were used as targets. The compound nuclei ^{201}Tl* (^{4}He + ^{197}Au), ^{185}Re* (^{4}He + ^{181}Ta) and ^{169}Tm* (^{4}He + ^{165}Ho) were populated by the complete fusion reactions at the excitation energies, E^* ~26 and 37 MeV. The second experiment was performed using ^{4}He ion beams of several incident energies in the range of 26 - 60 MeV. Self-supporting foils of ^{169}Tm (thickness ~ 1.15 mg/cm^2), ^{181}Ta (thickness ~1.3 mg/cm^2) and ^{197}Au (thickness ~3.1 mg/cm^2) were used as targets to populate the compound nuclei ^{173}Lu*(β ~0.286), ^{185}Re* (β ~0.221) and ^{201}Tl* (β ~0.044), respectively, in the excitation energy range ~22 - 55 MeV. The emitted neutrons were detected at the backward angles (90°, 105°, 120° and 150°) using four liquid-scintillator (BC501A) based detectors. Details of the experimental setup are already described in Section 2.2.

Table 4.1: *Fitted inverse level density parameter for different systems.*

System	U (MeV)	Fitted inverse level density parameter (k)	T (MeV)	T_c (MeV) (from Eq. 4.1)
^{4}He + ^{165}Ho	35.7	9.5 ± 0.3	1.37	2.06
"	24.8	8.0 ± 0.5	1.03	"
^{4}He + ^{181}Ta	35.1	11.2 ± 0.4	1.40	1.62
"	25.9	9.7 ± 0.5	1.11	"
^{4}He + ^{197}Au	36.1	9.5 ± 0.6	1.26	0.30
"	24.8	9.6 ± 0.7	1.03	"

4.3 Results and discussions

The neutron kinetic energy spectra (Figs. 4.4 & 4.5(a)) were obtained from the corresponding time of flight spectra, after correcting for the background. Statistical model analysis (Section 2.4) of the experimental data was carried out; the shapes of the neutron energy spectra were found to be mostly determined by the value of level density parameter. The optimum values of the inverse level density parameter (k) extracted by fitting the experimental neutron spectra using the χ^2 minimization technique have been tabulated in Table 4.1. It is observed that the best-fit values of the inverse level density parameter decrease from 9.5 ± 0.3 to 8.0 ± 0.5 for ^{4}He + ^{165}Ho system as the thermal excitation energy decreases from 35.7 to 24.8 MeV. Similar change (decrease) in k value from 11.2 ± 0.4 to 9.7 ± 0.5 has also been observed for ^{4}He + ^{181}Ta system at the same excitation energy range. On the contrary, the k value remained almost same (9.5 ± 0.6 and 9.6 ± 0.7) at both excitation energies in case of the ^{4}He + ^{197}Au system. The level density parameter $\tilde{a}$ (=A/k) has been plotted as a function of excitation energy for the three systems in Fig. 4.5(b); a sharp increase of the LDP for the ^{4}He + ^{165}Ho and ^{4}He + ^{181}Ta reactions can clearly be visible. The above observation (the increment of $\tilde{a}$) suggests that there has been a relative enhancement in nuclear level density at lower excitation energy for the first two systems, whereas for the third system no such variation has been observed. It should be noted, that the level density

expression used in the present analysis (Eq. 2.15) is based on the Fermi gas model, which is purely single particle in nature. Therefore the observed variation in k (or $\tilde{a}$) may be a manifestation of the collective contributions to NLD through the relation [62],

$$\rho_{tot}(E^*) = K_{coll}(E^*)\,\rho_{FG}(E^*, \tilde{a}) = \rho_{FG}(E^*, \tilde{a}_{eff}), \tag{4.4}$$

where $\tilde{a}_{eff}$ is the effective or enhanced level density parameter required to account for the collective contribution in ρ. The nature of variation as seen above may be directly linked with the deformation of the respective systems. The dominant daughter nuclei produced in ^{4}He + ^{165}Ho and ^{4}He + ^{181}Ta are ^{166,167}Tm and ^{182,183}Re, respectively; the corresponding ground state deformations (β_2) are 0.28 and 0.24 [100] which are significantly higher than those produced in ^{4}He + ^{197}Au reaction ($\beta_2 \sim 0.044$ for ^{198,199}Tl). The collective enhancement factors calculated using Eqn. 4.2 for these systems indicate that there should be an appreciable collective enhancement in the two deformed systems (K_{coll} ~80) as compared to the nearly spherical third system (K_{coll} ~1). So, the observed variation of inverse level density parameter with excitation energy for the deformed systems is a signature of collectivity induced modification (enhancement) of the level density, which is absent in the case of nearly spherical system (^{4}He + ^{197}Au).

Although the current data provides a clear signature of the existence of the collective enhancement for the deformed systems at the lower energy, it is difficult to make any conclusion on the fadeout region due to the limited energy range of the data. The difficulty has been overcome by performing the second experiment where the neutron evaporation spectra from the three compound nuclei (^{173}Lu*, ^{185}Re* and ^{201}Tl*) were measured in a wide excitation energy range (~22 - 55 MeV). The measured neutron energy spectra along with the corresponding statistical model fits for the three reactions are shown in Figs. 4.6, 4.7 & 4.8, respectively. The best-fit values of k for all three systems at various excitation energies have been shown in Fig. 4.9. It is evident from the figure that, the overall energy dependence of the inverse level density parameter can reasonably be described by the standard empirical relation $k(U) = k_0 + \kappa(U/A)$ (shown by the blue dashed line in Fig. 4.9), as discussed in the last chapter (Eqn. 3.4). In the present case the k_0 values are in the range of 9 - 10 for the three systems whereas

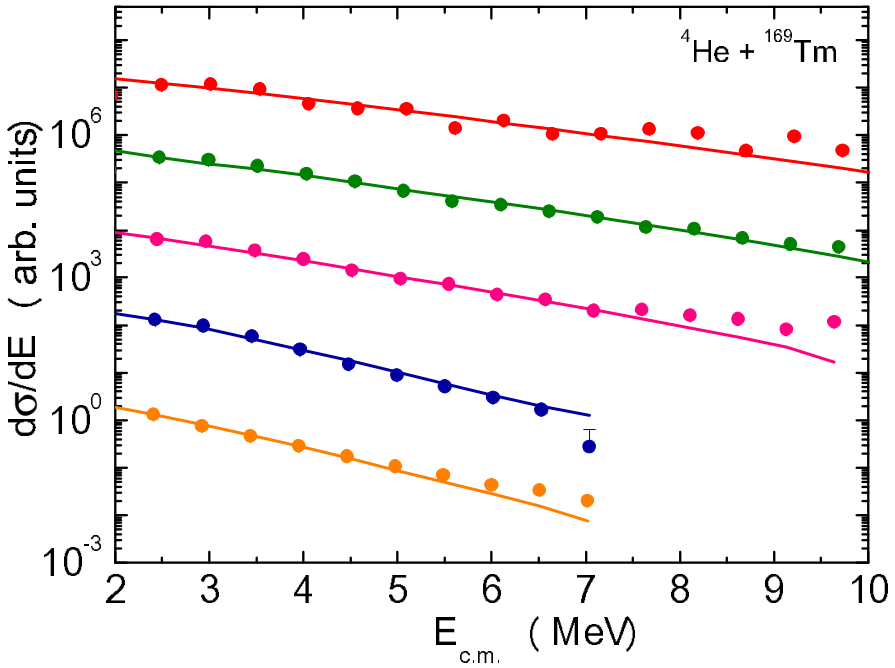

Figure 4.6: *Measured neutron energy spectra (symbols) at different incident energies (26, 30, 40, 50, and 60 MeV, serially up from bottommost) shown along with the respective statistical model fits (lines). The individual spectrum has been scaled for better visualization.*

the values of κ have been obtained from Eqn. 3.5 (κ = 1.95, 2.95, and 5.13 for the ^{173}Lu*, ^{185}Re* and ^{201}Tl* systems, respectively). Although the general trend of the data can be explained by the energy systematic, there is a sharp change (reduction) in the value of *k* around excitation energy ~30 MeV. No such sharp variation of *k* is observed in the case of the nearly spherical ^{201}Tl system. Any sharp variation in the *k* value corresponds to a sudden change in level density which is expected around the fade-out region that is clearly reflected trough the transition behavior *k* around the E^{*} ~30 MeV (shown by the shaded region in Fig. 4.9) for the deformed systems. Interestingly, though the two systems were having different ground state deformations ($\beta_2 \approx 0.286$ and 0.221 for the Lu and Re isotopes, respectively), the transition seems to occur at nearly similar excitation energy (temperature). This is in qualitative agreement with the conjecture made earlier by the Junghans *et al.* though the energy region of transition observed in the present experiment (U ~30 - 35 MeV which correspond to an excitation energy range 15 - 21 MeV in the daughter nuclei) is somewhat lower than

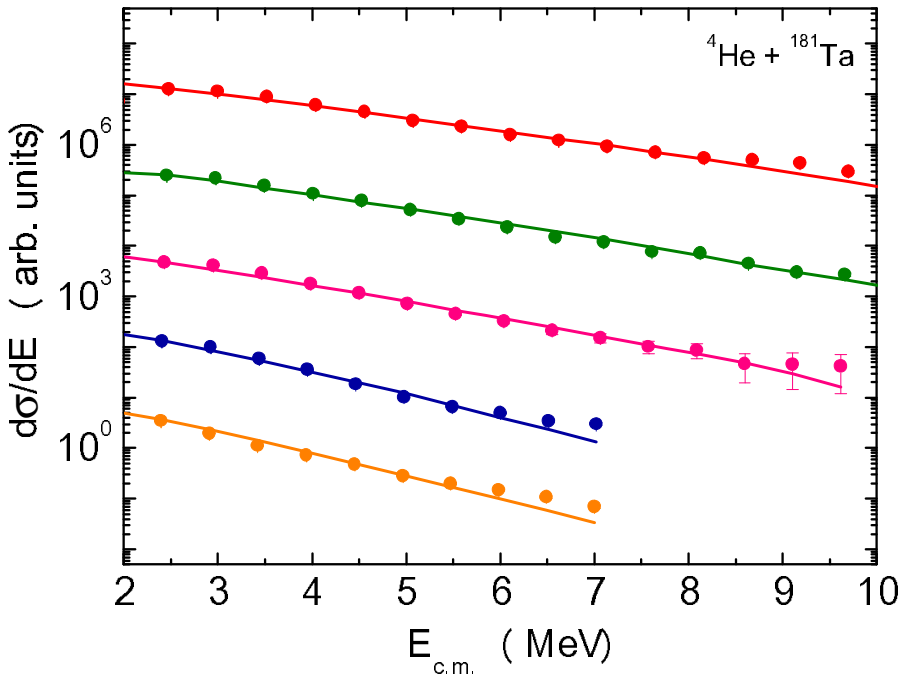

Figure 4.7: *Same as Fig. 4.6 for the ^{4}He + ^{181}Ta reaction.*

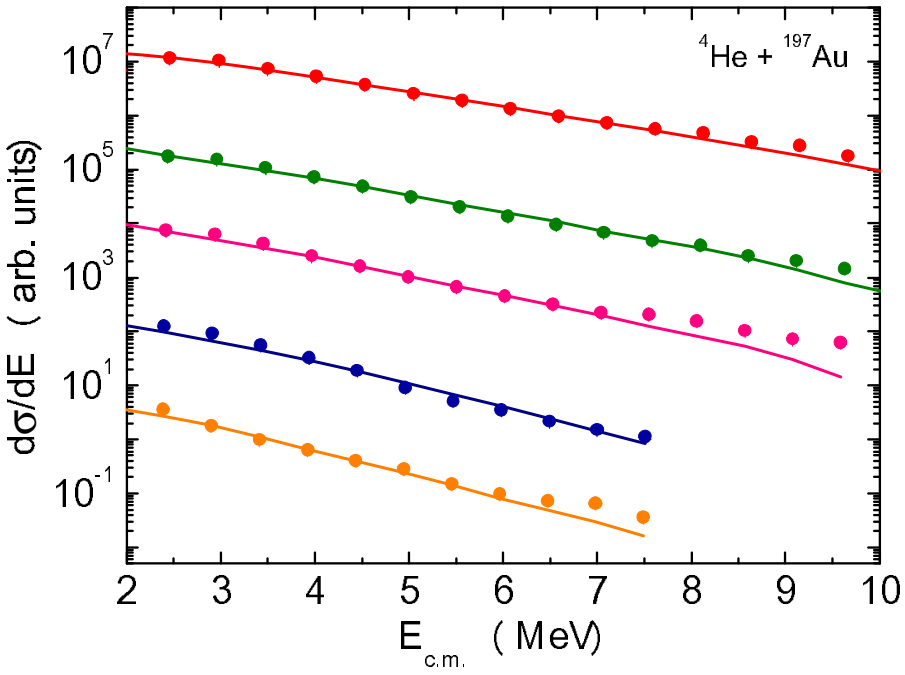

Figure 4.8: *Same as Fig. 4.6 for the ^{4}He + ^{197}Au reaction*

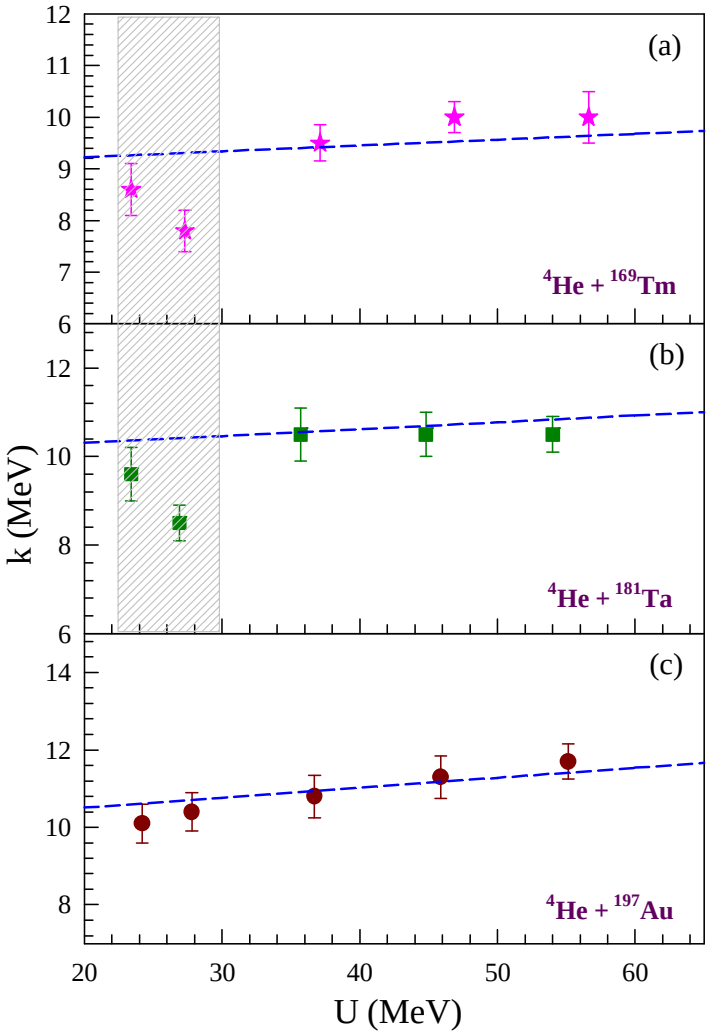

Figure 4.9: *Inverse level density parameter plotted as a function of excitation energy. Experimental points are shown in symbols, lines represent systematics (see text)*

their predicted value (40 MeV). The microscopic origin of the fade-out of collectivity can be connected to a shape transition (from deformed to spherical) at finite temperature. Microscopic calculations using *e.g.* as Finite Temperature Density Functional Theory (FT-DFT) [113, 114, 115, 116], and/or macroscopic-microscopic shape phase transition model (MMSTM) [117, 118, 119] may be useful to confirm the existence of such shape transition for the current systems.

Chapter 5

Summary, conclusion and future outlook

5.1 Summary and conclusion

The aim of the thesis was to extend and improve experimental information on the dependence of nuclear level density on key factors such as excitation energy, angular momentum, and collectivity using light-particle evaporation as a probe. Although the evaporation process doesn't provide an absolute measure of level density, it provides crucial information on the variation of NLD with excitation energy and/or angular momentum. Other frequently used experimental methods such as study of neutron (and charged particle) resonances, inelastic scattering, primary γ-ray spectrum, excitation function of isolated levels *etc.* also provide information about NLD, but the applicability of each of these methods is mostly limited to a very narrow range of E^* and J. Therefore, the study of particle evaporation has been the most widely used technique to investigate the properties of NLD over a wide range of E^* and J. On the theoretical front, even after substantial theoretical efforts, it has not been possible yet to have a complete microscopic solution including all known nuclear effects that can lead to a

closed analytical form of NLD. This is primarily because of the complicated nature of the exact nuclear potential as well as due to the inherent difficulty in solving many body problems itself. Simplistic nuclear models such as the Fermi gas model has been employed to get an analytic expression for nuclear level density and important factors due to the shell, pairing, and collective effects are incorporated as phenomenological corrections. Therefore, in the absence of complete microscopic solutions, one has to heavily rely on these phenomenology based semi-empirical formulations of NLD which is used as the essential input in various nuclear reaction calculations carried out under the framework of statistical model. Thus it is of extreme importance and fundamental interest to investigate experimentally the variation of NLD over a broad window of excitation energy and angular momentum. A series of experiments have been performed under the present thesis work using ^{4}He-ion beams having specific advantages. Evaporation spectra of charged particles and/or neutrons were measured from a number of compound nuclei populated at different excitation energies. The experimental results were compared with theoretical predictions obtained using the statistical model code CASCADE to understand the dependence of NLD on the key nuclear factors.

The first experiment has been performed to understand the angular momentum dependence of NLD. In this experiment, the kinetic energy spectra of the evaporated neutrons, protons, and α-particles have been measured at backward angles in coincidence with the multiplicity of low energy γ-rays in the case of ^{4}He + ^{93}Nb, and ^{4}He + ^{58}Ni reactions at E^{*} $\sim$35 MeV. Different angular momentum regions in the residual nuclei were selected experimentally by measuring the γ-ray fold distributions using the BaF_2 detector array. The experimental kinetic energy spectra of neutron, proton and α-particles were measured for different folds where a high fold event corresponds to a high J populated in the final nucleus. The analysis of γ-ray fold gated particle spectra have been carried out using the statistical model code CASCADE. The spin dependence of NLD was incorporated through the spin and deformation dependent rotational energy. It is observed that the shapes of the fold gated particle spectra could not be explained by the standard level density formulation; so additional spin

dependence was suggested which was reflected through the variation of the level density parameter with angular momentum. From the present analysis, it is observed that the inverse level density parameter decreases significantly with the increase in $< J >$ for all three emissions, although there are some differences in the absolute values of the inverse level density parameter extracted from different particle spectra. The observed variation of k (or a) with angular momentum is in contrast with the existing picture where the level density parameter is not expected to vary explicitly with spin or deformation. The decrease of k at higher J is indicative of the fact that there is a relative increase of NLD at higher angular momentum. Shape change at higher angular momentum based on RLDM as well as the concept of collective enhancement as per the existing formulations have failed to explain the observed variation of NLD with J. Microscopic calculations for the specific systems will be useful in order to understand the observed phenomenon in more detail.

In the second experiment, the energy spectra of the neutrons emitted in the decay of $^{212}Po^{*}$ and $^{213}At^{*}$ formed by the reactions of ^{4}He on the ^{208}Pb and ^{209}Bi targets, respectively, have been measured at backward angles at the projectile energies E_{lab} = 28, 31, 35, 40 and 60 MeV, and compared with the statistical model calculations. In the present case, the compound nuclei, as well as the residual nuclei formed after neutron emission, are in the vicinity of Z = 82 and N = 126 shell closure, have large ground-state shell corrections. Therefore, the level density of these nuclei is expected to strongly influenced by the shell structure, particularly at low energies. Use of light ion induced reactions has enabled us to populate these nuclei at sufficiently low excitation energies where the damping of shell effect with excitation energy can be studied. In the statistical model calculations, the shell effect has been incorporated by using the energy and shell correction dependent parametrization of the level density parameter. The value of the shell damping factor has been extracted from the lowest energy data (having the highest sensitivity over this parameter) and found to be $\gamma = 0.052 \pm 0.018$ and 0.054 ± 0.020 MeV^{-1} in case of ^{4}He + ^{208}Pb and ^{209}Bi reactions, respectively. The measured γ values are in good agreement with the available theoretical estimates as

well as the recent measurement for the similar system. The excitation energy (temperature) dependence of the asymptotic part of the level density parameter has also been extracted and compared with the Thomas-Fermi (TF) model calculations. An overall reduction in the value of the LDP with increasing temperature in the range of T ~0.7 - 1.4 MeV is observed in qualitative agreement with the TF model calculation. However, the experimental rate of reduction of $\tilde{a}$ with temperature was found to be little more than the corresponding theoretical prediction. It was argued that the observed variation of the LDP with temperature can primarily be accounted for by the temperature dependence of the effective nucleon mass. The experimental results were also showed to follow a simple empirical relation, k(U)= 7.8 + 7.4 (U/A), where k is the inverse level density parameter.

The collective enhancement and its variation with excitation energy has been investigated in a couple of experiments that had been described in the third part of the thesis. The collective excitations are expected to cause an enhancement in NLD (compared to its single-particle estimates) which is described in terms of the collective enhancement factor (K_{coll}), which is predicted to be damped at higher excitations. In one of the present experiments, the backward angle neutron evaporation energy spectra from the deformed ^{185}Re*, ^{169}Tm*, and nearly spherical ^{201}Tl* compound nuclei, have been measured at ~26 and 37 excitation energies. All the compound nuclei at these excitation energies decay predominantly via 2n and 3n emission channels populating evaporation residues that have ground-state deformations similar to those of the corresponding compound nuclei. The statistical model analysis of the experimental data has been carried out to extract the value of inverse level density parameter. It has been observed that, for the deformed systems (^{185}Re*, and ^{169}Tm*), there was significant reduction in the k value at lower excitation energy; however, no such variation of k was observed for near spherical ^{201}Tl* system. The decrease in k (or increase in a) at lower excitation for the deformed systems is suggestive of a relative increase in level density which provide a strong signature of the collective enhancement. To understand the phenomena in more detail the investigation has been extended in a wider excitation

energy range (~ 22 - 56 MeV), where the neutron evaporation spectra have been measured from the deformed ^{173}Lu* (^{4}He + ^{169}Tm), ^{185}Re* (^{4}He + ^{181}Ta) and the nearly spherical ^{201}Tl* (^{4}He + ^{197}Au) systems. Excitation energy dependence of the inverse level density parameter has been obtained from the statistical model analysis of the experimental neutron spectra. It is found that the energy dependence of k can be reasonably described by the empirical relation k(U)= k_0 + κ(U/A), where the value of k_0 ranges between 9 - 10, and the value of κ is in agreement with Eqn. 3.5 for the three systems. Although the general trend of the data matches with the energy systematic, there is transition behavior (reduction from the systematic) in the k-value observed for the two deformed systems compared to the near spherical system around E^{*} ~30 MeV. The observation confirms the existence of collective enhancement at low excitation energies which is expected for the deformed systems due to the collective rotation. The data also shows that for E^{*} $\gtrsim$40 MeV the k-value increases smoothly with excitation energy as per the systematic signifying a fadeout of the collective effects which were present at lower energies. The fadeout indicates a shape transition from deformed to spherical around the transition energy.

5.2 Future outlook

The present thesis provides important information on several aspects of NLD addressed through the measurement of light-particle evaporation spectra. Exclusive measurement with respect to angular momentum in case of the ^{4}He + ^{58}Ni, and ^{93}Nb reactions have shown that the shapes of the fold (angular momentum) gated particle spectra could not be explained by the standard phenomenological formulation of nuclear level density. A strong variation (decrease) of the inverse level density parameter with J was observed from the statistical model analysis of the data in the angular momentum range of ~10 - 25 $\hbar$. It will be interesting to extend these studies to higher angular momentum regions which are possible by using heavy ion beams. It will also be interesting to carry out similar measurements in other mass regions to see whether the

observation is generic or specific to some mass regions.

In the present thesis, the shell damping parameter has been measured experimentally for systems close to the doubly magic ^{208}Pb nucleus. However, the uncertainty in the measured γ-value is quite large (~35%). This γ-value could be constrained into a narrower range by performing measurements at further low excitation energy (where the sensitivity of γ increases) with improved statistics. The measurement of nuclear shell effect can be extended to other doubly magic nucleus (^{132}Sn) and the to nuclei where the shell effect is sizable. It is also of current interest to study the variation of shell effect with excitation energy for nuclei having a proton (neutron) number close to a magic number and a neutron (proton) number far enough from a magic number. This is particularly encouraging in view of the recent combinatorial level density calculation [8] which showed that for such a system the variation of shell effect with energy can be complicated and one should use different damping parameters for proton and neutron shells (*i.e.* $\gamma_p \neq \gamma_n$). Temperature dependence of the asymptotic part of the level density parameter has also been investigated in the same experimental study in a temperature range of T ~0.7 - 1.4 MeV. Extension of this measurement to higher temperature will be interesting as the current data indicated some deviation in the rate of change of the level density parameter from the corresponding theoretical prediction towards the higher temperatures.

Some of the very recent and interesting topics that can also be addressed using particle evaporation as a probe are (i) iso-spin dependence of level density and (ii) pairing re-entrance in NLD. Understanding the level distribution of the exotic nuclei is extremely important from the points of view of both nuclear structure and nuclear astrophysics. The iso-spin (N-Z) effects in NLD come from the iso-spin distribution of the nuclear states and also from the symmetry energy. A reduction of level density with increasing $|T_3|$ (T_3 =N-Z/2) is predicted [120]. However, very little information is available on the N-Z dependence of NLD. Measurements of energy spectra of *xp* (for proton-rich nuclei) or *xn* (for neutron rich nuclei) channels along with the evaporation residue yields can provide useful information on the iso-spin dependence of NLD.

Another interesting area that has emerged very recently is the *pairing re-entrance* in NLD. Recent, microscopic shell model Monte Carlo (SMMC) calculation for N = 40 isotones showed the phenomenon of pairing re-entrance in rotating hot nucleus through an anomalous behaviour of specific heat and also in the level density [121, 122]. Bardeen-Cooper- Schriefer (BCS) based quasiparticle calculation for ^{60}Ni, ^{72}Ge nuclei also showed the pairing re-entrance in the heat capacity and a rather weak signature in level density [123]. The phenomenon of pairing re-entrance is predicted to occur at high frequencies but at low temperatures. A detailed experimental investigation is required particularly in the open-shell nuclei at finite temperature and high angular momentum where both the pairing and rotation plays a crucial role in the occurrence of the pairing re-entrance which is predicted to be observed through the variation in specific heat and level density.

Appendices

Appendix A

Pulse height calibration of the neutron detector

An accurate pulse height calibration of a neutron detector is essential when neutron energy is determined by the spectral unfolding technique. In case the neutron energies are determined by the time of flight, pulse height calibration is required in order to set an appropriate and uniform threshold to different detectors. Since no monoenergetic neutron source is available for laboratory use, the pulse height calibration was performed using standard γ-ray sources. In liquid scintillators, the major interaction process for γ-rays is Compton scattering for γ-ray energies up to 3 MeV. The sharp upper edge of the well known Compton distribution (Compton Edge) is used for energy calibration. But due to multiple scattering effects and pulse height resolution of the detector, the theoretical shape of the Compton edge is modified (Fig. A.1(a)). So, determination of the exact position of the Compton edge (L_C) becomes tricky. The relative position of the Compton edge (L_C) with respect to the position of the maximum (L_{max}), indicated by the ratio L_{max}/L_C, is observed to influenced strongly by the pulse height resolution and detector dimension. A value of $L_{max}/L_C \approx 0.9$ is suggested to give better estimation [124] for the type of detectors used in the present experimental study. So, in the current analysis, the position of the Compton edge is taken at the point

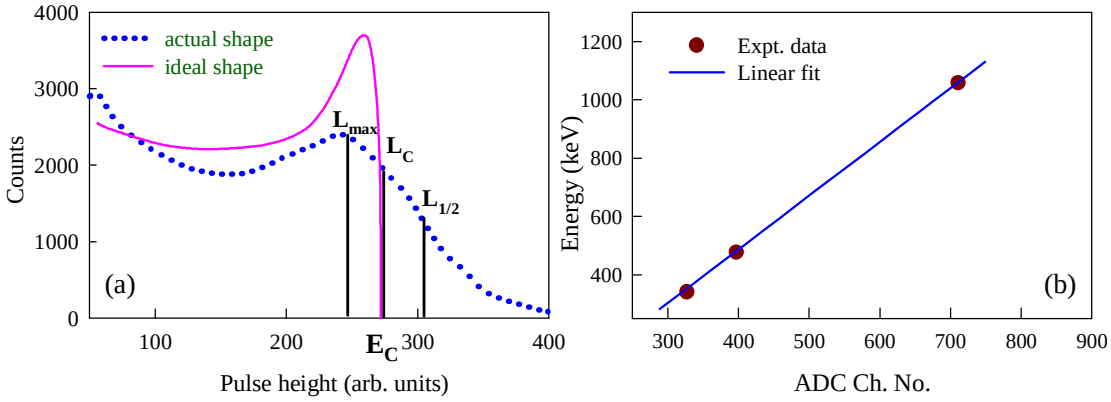

Figure A.1: *(a) Ideal and actual Compton spectra, (b) pulse height calibration using γ-ray sources.*

Table A.1: *Data for PH calibration of a typical neutron detector.*

SL. No.	Source	E_γ (keV)	E_C (keV)	Ch. No.
1	^{22}Na	511	341	327
2	^{137}Cs	662	477	387
3	^{22}Na	1274	1058	711

where the maximum value falls to its 90%. The expression for the Compton edge in terms of the energy of the γ-ray (E_γ) is given by,

$$E_C = \frac{2E_\gamma^2}{m_e c^2 + 2E_\gamma}. \qquad \text{(A.1)}$$

Here m_e is the rest mass of the electron. The energy calibration is performed using two standard γ-ray sources: ^{137}Cs and ^{22}Na. The γ-ray energies of ^{137}Cs and ^{22}Na and corresponding E_C values calculated using Eqn. A.1 are shown in Table A.1. The pulse height calibration of a typical neutron detector is shown in Fig. A.1(b).

Bibliography

[1] *Nuclear Dynamics in the Nucleonic Regim*, D Durand, E Suraud, and B Tamain, CRC press (Nov. 2000).

[2] J. R. Huizenga and L. G. Moretto, Annu. Rev. Nucl. Sci., **22**, (1972) 427 and references therein.

[3] Bernard Pichon, Nuclear Physics **A 568**, (1994) 553-571.

[4] Nicolas Cerf, Phys. Rev. **C 50**, 836 (1994).

[5] S. Hilaire, J. E Delaroche, A. J. Koning, Nuclear Physics **A 632**, (1998) 417-441.

[6] S. Hilaire, J. P. Delaroche, and M. Girod, Eur. Phys. J. **A 12**, 169-184 (2001).

[7] R. Pezer, A. Venturab, D. Vretenar, Nuclear Physics **A 717** (2003) 21-43.

[8] S. Hilaire, Physics Letters **B** 583 (2004) 264-268.

[9] S. Hilaire, S. Goriely, Nuclear Physics **A 779** (2006) 63-81.

[10] H. Uhrenholta, S. Aberga, A. Dobrowolskib, Th. Døssingc, T. Ichikawad, P. Möller, Nuclear Physics **A 913** (2013) 127-156.

[11] A. Bohr and B. R. Mottleson, Nuclear Structure (Benjamin, New York, 1975), Vol. I.

[12] H. A. Bethe, Phys. Rev. **50**, 332 (1936); Rev. Mod. Phys. **9**, 69 (1937).

[13] T. Ericson, Advan. Phys. **9**, 425 (1960).

[14] A. Gilbert and A. G. W. Cameron, Canadian Journal of Physics, **43** (1965) 1446.

[15] L. G. Moretto, R. Stella and V Caramella Crespi, Energia Nucleare **17**, 436 (1970).

[16] R. Capote *et al.* Nucl. Data Sheets **110**, (2009) 3107.

[17] A.V. Ignatyuk, G.N. Smirenkin and A.S. Tishin, Sov. J. Nucl. Phys. **21**, 255

(1975).

[18] A. A. Katsanos, J. R. Huizenga, and H. K. Vonach, Phys. Rev. **141**, 1053 (1966).

[19] A. A. Katsanos and J. R. Huizenga, Phys. Rev. **159**, 931 (1967).

[20] S. Raman *et al.* Phys. Rev. **C 43**, 521 (1991).

[21] V. Mishra, N. Boukharouba, C. E. Brient, S. M. Grimes, and R. S. Pedroni, Phys. Rev. **C 49**, 750 (1994).

[22] T. D. Newton, Can. J. Phys. **34**, 804 (1956).

[23] A. G. W. Cameron, Can. J. Phys. **36**, 1040 (1958).

[24] J. E. Lynn, The Theory of Neutron Resonance Reactions. (Oxford: Clarendon, New York, 1968)

[25] U. Facchini, E. Saetta-MenichelIa, Energ. Nucl. **15**, 54 (1968).

[26] F. Gunsing *et al.* Phys. Rev. **C 85**, 064601 (2012).

[27] P. M. Endt, C. Van der Leun, Nucl. Phvs. **A 105**, 1 (1967).

[28] J. R. Huizenga, H. K. Vonach, A. A. Katsanos, A. J. Gorski, and C. J. Stephan, Phys. Rev. **182**, 149 (1969).

[29] S. M. Grimes, J. D. Anderson, J. W. McClure, B. A. Pohl, C. Wong, Phys. Rev. **C 3**, 645 (1971).

[30] S. M. Grimes, J. D. Anderson, B. A. Pohl, J. W. McClure, C. Wong, Phys. Rev. **C 4**, 607 (1971).

[31] A. A. Katsanos, R. W. Jr. Shaw, R. Vandenbosch, D. Chamberlin, Phys. Rev. **C 1**, 594 (1970).

[32] E. Gadioli, and L. Zetta, Phys. Rev. **167**, 1016 (1968).

[33] H. K. Vonach, J. R. Huizenga, Phys. Rev. **B 138**, 1372 (1965).

[34] A. Richter, W. von Witsch, P. von Brentano, O. Haeusser, T. MayerKuckuk, Phys. Lett. **14**, 121 (1965).

[35] A. Schiller, L. Bergholt, M. Guttormsen, E. Melby, J. Rekstad, and S. Siem, Nucl. Instrum. Methods Phys. Res. **A 447**, 498 (2000).

[36] M. Guttormsen, T. Ramsoy, and J. Rekstad, Nucl. Instrum. Methods Phys. Res. **A 255**, 518 (1987).

[37] L. Henden, L. Bergholt, M. Guttormsen, J. Rekstad, and T.S. Tveter, Nucl. Phys. **A 589**, 249 (1995).

[38] A. Spyrou *et al.* Phys. Rev. Lett. **113**, 232502 (2014).

[39] M. Guttormsen *et al.* Phys. Rev. **C 90**, 044309 (2014).

[40] T. G. Tornyi *et al.* Phys. Rev. **C 89**, 044323 (2014).

[41] A. C. Larsen *et al.* Phys. Rev. **C 87**, 014319 (2013).

[42] M. Guttormsen *et al.* Phys. Rev. **C 88**, 024307 (2013).

[43] H. T. Nyhus, S. Siem, M. Guttormsen, A. C. Larsen, A. Burger, N. U. H. Syed, H. K. Toft, G. M. Tveten, and A. Voinov, Phys. Rev. **C 85**, 014323 (2012).

[44] A. C. Larsen *et al.* Phys. Rev. **C 83**, 034315 (2011)

[45] A. Schiller *et al.* Phys. Rev. **C 63**, 021306 (R) (2001).

[46] V. F. Weisskopf and D. H. Ewing, Phys. Rev. **57** (1940) 472.

[47] D. R. Chakrabarty, V. M. Datar, Suresh Kumar, E. T. Mirgule, H. H. Oza, and U. K. Pal Phys. Rev. **C 51**, 2942 (1995).

[48] U. K. Pal, D. R. Chakrabarty, V. M. Datar, Suresh Kumar, E. T. Mirgule, and H. H. Oza, J. Phys. **G 25**, 1671 (1999).

[49] D. R. Chakrabarty, V. M. Datar, Suresh Kumar, E. T. Mirgule, A. Mitra, and H. H. Oza, Nucl. Phys. **A 712**, 23 (2002).

[50] A. P. D. Ramirez, A. V. Voinov, S. M. Grimes, A. Schiller, C. R. Brune, and T. N. Massey, and A. Salas-Bacci, Phys. Rev. **C 88**, 064324 (2013).

[51] A. Mitra, D. R. Chakrabarty, V. M. Datar, Suresh Kumar,E. T. Mirgule, H. H. Oza, Nucl. Phys. A **707**, (2002) 343.

[52] A. Mitra, D. R. Chakrabarty, V. M. Datar, Suresh Kumar, E. T. Mirgule, V. Nanal and P. C. Rout, J. Phys. **G 36**, (2009) 095103.

[53] Y. K. Gupta, Bency John, D. C. Biswas, B. K. Nayak, A. Saxena, R. K. Choudhury, Phys. Rev. **C 78**, 054609 (2008).

[54] Y. K. Gupta, D. C. Biswas, Bency John, B. K. Nayak, A. Saxena, and R. K. Choudhury, Phys. Rev. **C 80**, 054611 (2009).

[55] K. Banerjee, S. Bhattacharya, C. Bhattacharya, M. Gohil, S. Kundu, T. K. Rana, G. Mukherjee, R. Pandey, P. Roy, H. Pai, A. Dey, T. K. Ghosh, J. K. Meena, S. Mukhopadhyay, D. Pandit, S. Pal, and S. R. Banerjee, Phys. Rev. C **85**, 064310 (2012).

[56] M. Gohil, Pratap Roy, K. Banerjee, C. Bhattacharya, S. Kundu, T. K. Rana, T. K. Ghosh, G. Mukherjee, R. Pandey, H. Pai, V. Srivastava, J. K. Meena, S. R. Banerjee, S. Mukhopadhyay, D. Pandit, S. Pal, and S. Bhattacharya, Phys. Rev.

C **91**, 014609 (2015).

[57] Balaram Dey, Deepak Pandit, Srijit Bhattacharya, K. Banerjee, N. Quang Hung, N. Dinh Dang, Debasish Mondal, S. Mukhopadhyay, Surajit Pal, A. De, and S. R. Banerjee, Phys. Rev. **C 91**, 044326 (2015).

[58] K. Hagel, D. Fabris, P. Gonthier, H. Ho, Y. Lou, Z. Majka, G. Mouchaty, M. N. Namboodiri, J. B. Natowitz, G. Nebbia, R. P. Schmitt, G. Viesti, R. Wada, and B. Wilkins, Nucl. Phys. **A 486**, 429 (1988).

[59] M. Gonin, L. Cooke, K. Hagel, Y. Lou, J. B. Natowitz, R. P. Schmitt, S. Shlomo, B. Srivastava, W. Turmel, H. Utsunomiya, R. Wada, G. Nardelli, G. Nebbia, G. Viesti, R. Zanon, B. Fornal, G. Prete, K. Niita, S. Hannuschke, P. Gonthier, and B. Wilkins, Phys. Rev. C **42**, 2125 (1990).

[60] D. Fabris, E. Fioretto, G. Viesti, M. Cinausero, N. Gelli, K. Hagel, F. Lucarelli, J. B. Natowitz, G. Nebbia, G. Prete, and R. Wada, Phys. Rev. C **50** 1261(R), (1994).

[61] P. C. Rout, D. R. Chakrabarty, V. M. Datar, Suresh Kumar, E. T. Mirgule, A. Mitra, V. Nanal, S. P. Behera and V. Singh, Phys. Rev. Lett. **110**, 062501 (2013).

[62] R. J. Charity, Phys. Rev. C **82**, 014610 (2010), and references therein.

[63] S. Cohen, F. Plasil and W. J. Swiatechi, Ann. Phys. (NY) **82**, 557 (1974).

[64] M. Aggarwal and S. Kailas Phys. Rev. C **81**, 047302 (2010).

[65] Deepak Pandit, S. Mukhopadhyay, Srijit Bhattacharya, Surajit Pal, A. De, S. R. Banerjee, Nucl. Instr. Meth. A **624**, 148 (2010).

[66] *http* : *//www.mesytec.com/products/nuclear − physics/MPR* − 16.*html*

[67] *http* : *//www.mesytec.com/products/nuclear − physics/MSCF* − 16*_F_V.html*

[68] *http* : *//www.mesytec.com/products/nuclear − physics/MPD* − 4.*html*

[69] James F. Zieglera, M.D. Zieglerb and J.P. Biersackc, NIM **B 268**, (2010) 1818.

[70] D.G. Madland and J.R.Nix, Nucl. Sci. and Eng. **81**, 213 (1982).

[71] G. Dietze, H. Klein, PTB-ND-22 Report, 1982.

[72] F. Puhlhofer, Nucl. Phys. A **280**, 267 (1976).

[73] Niels Bohr, Nature **137**, (1936) 344.

[74] W. Hauser and H. Feshbach, Phys. Rev. **87** (1952) 366.

[75] S. Fernbach, R. Serber, and T. B. Taylor, Phys. Rev. **75**, 1352 (1949).

[76] P. E. Hodgson, *The Optical Model of Elastic Scattering* (Oxford University

Press, Oxford, 1963)

[77] H. Feshbach, C. E. Porter, and V. F. Weisskopf, Phys. Rev. **96**, 448 (1954).

[78] D. Wilmore and P. E. Hodgson, Nucl. Phys. **55**, 673 (1964); P .E. Hodgson, Ann. Rev. Nucl. Sci **17**, 1 (1967).

[79] F. G. Perey, Phys. Rev. **131**, 745 (1963).

[80] J. R. Huizenga and G. Igo, Nucl. Phys. **29**, 462 (1961)

[81] C. Kalbach, Phys. Rev. **C 37**, 2350 (1988).

[82] Arnold. J. Sierk, Phys. Rev. C **33**, 2039 (1986).

[83] D. Cline and P. M. S. Lesser, Nucl. Inst. and Meth. **82**, (1970) 291.

[84] G. Hansen and A. S. Jensen, Nucl. Phys. **A 406**, 236 (1983).

[85] K. H. Schmidt, H. Delagrange, J.P. Dufour, N. Cgtrjan, and A. Fleury, Z. Phys. **A 308**, 215-225 (1982).

[86] S. F. Mughabghab and C. Dunford, Phys. Rev. Lett. **81**, 4083 (1998).

[87] G. Nebbia, K. Hagel, D. Fabris, Z. Majka, J. B. Natowitz, R.P. Schimitt, B. Sterling, G. Mouchaty, G. Berkowitz, K. Strozewski, G. Viesti, P. L. Gonthier, B. Wilkins, M. M. Namboodiri, H. Ho, Phys. Lett. B **176**, 20 (1986).

[88] M. Gonin, L. Cooke, K. Hagel, Y. Lou, J. B. Natowitz, R. P. Schmitt, B. Srivastava, W. Turmel, H. Utsunomiya, R. Wada, B. Fornal, G. Nardelli, G. Nebbia, G. Viesti, R. Zanon, G. Prete, P. Gonthier, and B. Wilkins, Phys. Lett. **B 217**, 406 (1989).

[89] R. Wada, D. Fabris, K. Hagel, G. Nebbia, Y. Lou, M. Gonin, J. B. Natowitz, R. Billerey, B. Cheynis, A. Demeyer, D. Drain, D. Guinet, C. Pastor, L. Vagneron, K. Zaid, J. Alarja, A. Giorni, D. Heuer, C. Morand, B.Viano, C. Mazur, C. Ngo, S. Leray, R. Lucas, M. Ribrag, and E. Tomasi, Phys Rev. **C 39**, 497 (1989).

[90] S. Shlomo and J. B. Natowitz, Phys. Rev. **44**, 2878, (1991).

[91] M. Prakash, J. Wambach and Z.Y. Ma Phys. Lett. **B 128**, 141 (1983).

[92] R. W. Hasse, P. Schuck, Phys. Lett. **B 179**, 313 (1986).

[93] S. Shlomo and J. B. Natowitz, Phys. Lett. **B 252**, 187 (1990).

[94] J. N. De, S. Shlomo, and S. K. Samaddar Phys. Rev. **C 57**, 1398 (1998).

[95] B. J. Fineman, K. T. Brinkrnann, A. L. Caraley, N. Gan, R. L. McGrath, and J. Velkovska, Phys. Rev. **C 50**, 1991 (1994).

[96] A. L. Caraley, B. P. Henry, J. P. Lestone, and R. Vandenbosch, Phys. Rev. **C 62**,

054612 (2000).

[97] A. Chbihi, L. G. Sobotka, N. G. Nicolis, D. G. Sarantites, D. W. Stracener, Z. Majka, D. C. Hensley, J. R. Beene, and M. L. Halbert, Phys Rev. **C 43**, 666 (1991).

[98] G. Nebbia, D. Fabris, A. Perin, G. Viesti, F. Gramegna, G. Ptete, L. Fiore, V. Paticchio, F. Lucatelli, B. Chambon, B. Cheynis, D. Drain, A. Giorni, A. Lleres, J.B. Viano, Nucl. Phys. **A 578** (1994) 285.

[99] K. Yoshida, J. Kasagi, H. Hama, M. Sakurai, M. Kodama, K. Furutaka, K. Ieki, W. Galster, T. Kubo, M. Ishihara and A. Galonsky, Phys. Rev. **C 46**, 964 (1992).

[100] P. Moller, J. R. Nix, W. D. Myers, W. J. Swiateki, Atomic Data and Nuclear Data Tables **59**, 185 (1995).

[101] P. F. Bortingnon, C. H. Dasso, Phys. Lett. **B 189**, 381 (1987).

[102] D. Vautherin and N. Vin Mau, Orsay report/PNO/TH 87-03 (1987).

[103] V.A. Plujko, O.M. Gorbachenko and I.M Kadenko, International Journal of Modern Physics **E 16**, 570 (2007)

[104] A. V. Ignatyuk, K. K. Istekov, and G. N. Smirenkin, Sov. J. Nucl. Phys. **29**, 450 (1979).

[105] C. Ozen, Y. Alhassid and H. Nakada Phys. Rev. Lett. **110**, 042502 (2013).

[106] S. Karampagia and V. Zelevinsky, Phys. Rev. **C 94**, 014321 (2016).

[107] S. Björnholm, A. Bohr and Mottelson, in Proceedings of the International Conference on the Physics and Chemistry of Fission, Rochester, New York, 1973 (IAEA, Vienna, 1974) Vol. **1**, p. 367.

[108] A. R. Junghans, M. de Jong, H. G. Clerc, A. V. Ignatyuk, G. A. Kudyaev, K. H. Schmidt, Nucl. Phys. **A 629**, 635 (1998).

[109] C. O. Zen, Y. Alhassid and H. Nakada, Phys. Rev. Lett. **110**, 042502 (2013)

[110] Alan L. Goodman, Phys. Rev. **C 35**, 2338(R) (1978).

[111] Y. Alhassid, C. N. Gilbreth and G. F. Bertsch, Phys. Rev. Lett. **113**, 262503 (2014).

[112] S. Komarov, R. J. Charity, C. J. Chiara, W. Reviol, D. J. Sarantites, L. G. Sobotka, A. L. Caraley, M. P. Carpenter, D. Seweryniak, Phys. Rev. **C 75**, 064611 (2007).

[113] J. L. Egido, L. M. Robedo and V. Martin, Phys. Rev. Lett. **85**, 26 (2000).

[114] J. C. Pei, W. Nazarewicz, J. A. Sheikh, A. K. Kerman, Phys. Rev. Lett. **102**,

192501 (2009).

[115] J. D. McDonnell, W. Nazarewicz, J. A. Sheikh, A. Staszczac and M. Warda Phys. Rev. **C 90**, 021302(R) (2014).

[116] N. Schunck, D. Duke, H. Carr, Phys. Rev. **C 91**, 034327 (2015).

[117] Y.Alhassid et al, Nuclear Physics **A 469**, 205 (1987).

[118] N. Dubrey, J. Dudek and A. Maj, Acta Physica Polonica **B 36** (2005) 1161.

[119] Deepak Pandit et al., Phys. Rev. **C 81**, 061302(R) (2010).

[120] H. Feshbach *Theoretical Nuclear Physics-Nuclear Reactions,* J. Wiley 1992.

[121] K. Langanke,D. J. Dean and W. Nazarewicz, Nucl. Phys. **A 757**, (2005) 360.

[122] D. J. Dean, K. Langanke, H. Nam and W. Nazarewicz, Phys. Rev. Lett. **105** (2010) 212504.

[123] N. Quang Hung, N. Dinh Dang, Phys. Rev. **C 84** (2011) 054324.

[124] G. Dietze and H. Klein, Nucl. Inst. Meth. **193**, (1982) 549.

Publication list

(A) Publications relevant to the thesis:

1. *"Angular-momentum-gated light-particle evaporation spectra from $^{97}Tc^{*}$ and $^{62}Zn^{*}$ systems"*,

   Pratap Roy, K. Banerjee, S. Bhattacharya, C. Bhattacharya, S. Kundu, T. K. Rana, T. K. Ghosh, G. Mukherjee, R. Pandey, J. K. Meena, M. Gohil, H. Pai, V. Srivastava, A. Dey, Deepak Pandit, S. Mukhopadhyay, S. Pal, and S. R. Banerjee, Phys. Rev. **C 86**, 044622 (2012).

2. *"Effect of collectivity on the nuclear level density"*,

   Pratap Roy, K. Banerjee, M. Gohil, C. Bhattacharya, S. Kundu, T. K. Rana, T. K. Ghosh, G. Mukherjee, R. Pandey, H. Pai, V. Srivastava, J. K. Meena, S. R. Banerjee, S. Mukhopadhyay, D. Pandit, S. Pal, and S. Bhattacharya, Phys. Rev. **C 88**, 031601(**R**) (2013).

3. *"Excitation energy dependence of the level density parameter in the doubly magic ^{208}Pb region"*,

   Pratap Roy, K. Banerjee, C. Bhattacharya, R. Pandey, A. Sen, S. Manna, S. Kundu, T. K. Rana, T. K. Ghosh, G. Mukherjee, T. Roy, A. Dhal, A. Dey, J. K. Meena, S. Mukhopadhyay, Deepak Pandit, and S. Bhattacharya, Phys. Rev. **C 94**, 064607 (2016).

(B) Other publications:

1. *"Survival of cluster correlation in dissipative binary breakup of $^{24,25}Mg^{*}$"*,

   S. Manna, T. K. Rana, C. Bhattacharya, S. Bhattacharya, S. Kundu, K. Banerjee, **Pratap Roy**, R. Pandey, Vishal Srivastava, A. Chaudhuri, T. Roy, T. K. Ghosh, G. Mukherjee, J. K. Meena, S. K. Pandit, K. Mahata, A. Shrivastava, and V. Nanal, Phys. Rev. **C 94**, 051601(**R**) (2016).

2. *"Exclusive measurement of isospin mixing at high temperature in ^{32}S"*,
   Debasish Mondal, Deepak Pandit, S. Mukhopadhyay, Surajit Pal, Srijit Bhattacharya, A. De, Soumik Bhattacharya, S. Bhattacharyya, Balaram Dey, **Pratap Roy**, K. Banerjee, S.R. Banerjee, Physics Letter **B 763**, (2016) 422.

3. *"Fission fragment mass distributions in reactions populating ^{200}Pb"*,
   A. Chaudhuri, A. Sen, T. K. Ghosh, K. Banerjee, Jhilam Sadhukhan, S. Bhattacharya, **P. Roy**, T. Roy, C. Bhattacharya, Md. A. Asgar, A. Dey, S. Kundu, S. Manna, J. K. Meena, G. Mukherjee, R. Pandey, T. K. Rana, V. Srivastava, R. Dubey, Gurpreet Kaur, N. Saneesh, P. Sugathan, and P. Bhattacharya, Phys. Rev **C 94**, 024617 (2016).

4. *"Fission dynamics study in ^{243}Am and ^{254}Fm"*,
   K. Banerjee, T. K. Ghosh, **P. Roy**, S. Bhattacharya, A. Chaudhuri, C. Bhattacharya, R. Pandey, S. Kundu, G. Mukherjee, T. K. Rana, J. K. Meena, G. Mohanto, R. Dubey, N. Saneesh, P. Sugathan, R. Guin, S. Das and P. Bhattacharya, Phys. Rev **C 93**, 064602 (2016).

5. *"Experimental investigation of T = 1 analog states of ^{26}Al and ^{26}Mg"*,
   Vishal Srivastava, C. Bhattacharya, T. K. Rana, S. Manna, S. Kundu, S. Bhattacharya, K. Banerjee, **P. Roy**, R. Pandey, G. Mukherjee, T. K. Ghosh, J. K. Meena, T. Roy, A. Chaudhuri, M. Sinha, A. K. Saha, Md. A. Asgar, A. Dey, Subinit Roy, and Md. M. Shaikh Phys. Rev. **C 93**, 044601 (2016).

6. *"No influence of a N = 126 neutron-shell closure in fission-fragment mass distributions"*,
   A. Chaudhuri, T. K. Ghosh, K. Banerjee, S. Bhattacharya, Jhilam Sadhukhan, S. Kundu, C. Bhattacharya, J. K. Meena, G. Mukherjee, A. K. Saha, Md. A. Asgar, A. Dey, S. Manna, R. Pandey, T. K. Rana, **P. Roy**, T. Roy, V. Srivastava, P. Bhattacharya, D. C. Biswas, B. N. Joshi, K. Mahata, A. Shrivastava, R. P. Vind, S. Pal, B. R. Behera and Varinderjit Singh, Phys. Rev. **C 92**, 041601(**R**) (2015).

7. *"Fusion-fission dynamics studies using mass distribution as a probes"*,
   T K Ghosh, A Chaudhuri, K Banerjee, S Bhattacharya, C Bhattacharya, S Kundu, G Mukherjee, R Pandey, T K Rana, **P Roy**, T Roy, V Srivastava, P Bhattacharya, Pramana **85**, 291 - 301 (2015).

8. *"Experimental study of ^{26}Al through the 1n pick-up reaction ^{27}Al(d,t)"*,
   Vishal Srivastava, C. Bhattacharya, T. K. Rana, S. Manna, S. Kundu, S. Bhattacharya, K. Banerjee, **P. Roy**, R. Pandey, G. Mukherjee, T. K. Ghosh, J. K. Meena, T. Roy, A. Chaudhuri, M. Sinha, A. Saha, Md. A. Asgar, A. Dey, Subinit Roy and Md. M. Shaikh, Phys Rev. **C 91**, 054611 (2015).

9. *"Direct evidence of "washing out" of nuclear shell effects"*,
   A. Chaudhuri, T. K. Ghosh, K. Banerjee, S. Bhattacharya, Jhilam Sadhukhan, C. Bhattacharya, S. Kundu, J. K. Meena, G. Mukherjee, R. Pandey, T. K. Rana, **P. Roy**, T. Roy, V. Srivastava and P. Bhattacharya, Phys Rev. **C 91**, 044620 (2015).

10. *"Angular momentum dependence of the nuclear level density in the A ~170 - 200 region"*,
    M. Gohil, **Pratap Roy**,* K. Banerjee, C. Bhattacharya, S. Kundu, T. K. Rana, T. K. Ghosh, G. Mukherjee, R. Pandey, H. Pai, V. Srivastava, J. K. Meena, S. R. Banerjee, S. Mukhopadhyay, D. Pandit, S. Pal, and S. Bhattacharya, Phys Rev. **C 91**, 014609 (2015).

11. *"Decay of Hoyle state"*,
    S Bhattacharya, T K Rana, C Bhattacharya, S Kundu, K Banerjee, T K Ghosh, G Mukherjee, R Pandey and **P Roy**, Pramana -journal of physics **83** (2014) 673 - 682.

12. *"MONSTER: a TOF Spectrometer for β-delayed Neutron Spectroscopy"*,
    T. Martinez *et al*. Nuclear Data Sheets **120** (2014) 78 - 80.

13. *"Estimation of direct components of the decay of the Hoyle state,"*,
    T. K. Rana, S. Bhattacharya, C. Bhattacharya, S. Kundu, K. Banerjee, T. K.

Ghosh, G. Mukherjee, R. Pandey, **P. Roy**, V. Srivastava, M. Gohil, J. K. Meena, H. Pai, A. K. Saha, J. K. Sahoo, and R. M. Saha, Phys. Rev. **C 88**, 021601(R) (2013).

14. *"Projectile structure effects in multi-nucleon and cluster transfers in* $^{16,18}O + {}^{164}Dy, {}^{208}Pb$ *reactions"*,
D.C. Biswas, **Pratap Roy**, Y.K. Gupta, B. N. Joshi, B.K. Nayak, L.S. Danu, B.V. John, R.P. Vind, N. Deshmukh, S. Mukherjee, A.K. Jain and R.K. Choudhury, Journal of Physics: Conference Series **381** (2012) 012091.

15. *"Variation of nuclear level density with angular momentum"*,
K. Banerjee, S. Bhattacharya, C. Bhattacharya, M. Gohil, S. Kundu, T. K. Rana, G. Mukherjee, R. Pandey, **P. Roy**, H. Pai, A. Dey, T. K. Ghosh, J. K. Meena, S. Mukhopadhyay, D. Pandit, S. Pal, and S. R. Banerjee, Phys. Rev. **C 85**, 064310 (2012).

16. *"Systematic study of projectile structure effect on fusion barrier distribution"*,
Pratap Roy, A. Saxena, B. K. Nayak, E. T. Mirgule, B. John, Y. K. Gupta, L. S. Danu, R. P. Vind, Ashok Kumar, and R. K. Choudhury, Phys. Rev **C 84**, 011602(**R**) (2011).

17. *"Pulse height and timing characteristics of CsI(Tl)-Si(PIN) detector for gamma-rays and fission fragments"*,
Y.K. Gupta, D.C. Biswas, **P. Roy**, B.K. Nayak, R.G. Thomas, A.L. Inkar, R.P. Vind, B. John, A. Saxena, R.K. Choudhury, Nucl. Instr. and Meth. **A 629** (2011) 149.